



THE HONG KONG  
POLYTECHNIC UNIVERSITY

香港理工大學

Pao Yue-kong Library

包玉剛圖書館

---

## Copyright Undertaking

This thesis is protected by copyright, with all rights reserved.

**By reading and using the thesis, the reader understands and agrees to the following terms:**

1. The reader will abide by the rules and legal ordinances governing copyright regarding the use of the thesis.
2. The reader will use the thesis for the purpose of research or private study only and not for distribution or further reproduction or any other purpose.
3. The reader agrees to indemnify and hold the University harmless from and against any loss, damage, cost, liability or expenses arising from copyright infringement or unauthorized usage.

### IMPORTANT

If you have reasons to believe that any materials in this thesis are deemed not suitable to be distributed in this form, or a copyright owner having difficulty with the material being included in our database, please contact [lbsys@polyu.edu.hk](mailto:lbsys@polyu.edu.hk) providing details. The Library will look into your claim and consider taking remedial action upon receipt of the written requests.

**INVESTIGATION OF THE SUBSTRATE RECOGNITION  
MECHANISMS OF BOTULINUM NEUROTOXIN AND ITS  
APPLICATION IN DETECTION AND THERAPY  
DEVELOPMENT**

**by**

**JIUBIAO GUO**

**Ph.D**

**THE HONG KONG POLYTECHNIC UNIVERSITY**

**2015**

**THE HONG KONG POLYTECHNIC UNIVERSITY**

**Department of Applied Biology & Chemical Technology**

**Investigation of the Substrate Recognition Mechanisms of  
Botulinum Neurotoxin and Its Application in Detection and  
Therapy Development**

**by**

**Jiubiao Guo**

**A thesis submitted in partial fulfillment of the requirements for  
the degree of Doctor of Philosophy**

**April, 2015**

## **CERTIFICATE OF ORIGINALITY**

**I hereby declare that this thesis is my own work and that, to the best of my knowledge and belief, it reproduces no material previously published or written, nor material that has been accepted for the award of any other degree or diploma, except where due acknowledgement has been made in the text.**

\_\_\_\_\_ (Signed)

\_\_\_\_\_ **Jiubiao Guo** \_\_\_\_\_ (Name of student)

## Abstract

Botulinum Neurotoxin (abbreviated as BTX or BoNT), produced by *Clostridium botulinum*, can lead to clinical syndrome of botulism by specifically targeting and blocking the release of neurotransmitter at nerve terminals. Among the 7 unambiguously identified serotypes (designated as BoNT/A, /B, /C, /D, /E, /F, and /G), BoNT/A, /B, /E, and /F (rarely) mainly cause human botulism, and BoNT/C and /D infect animals. Even though BoNTs are considered as the most potent protein toxins, they are approved by FDA as effective therapies for numerous neuronal disorders and cosmetics. No effective antitoxins or inhibitors, however, are available to date. A better understanding of the mechanism of substrate recognition and cleavage by BoNTs is the prerequisite to develop inhibitors or antidotes for BoNTs intoxication, novel therapeutic applications and rapid detection system. This thesis focuses on the investigation of the substrate recognition mechanisms employed by BoNT/D, /F5 and /F7 to dissect their step by step substrate binding and cleavage. In addition, based on previous understanding and comparison of the substrate recognition mechanisms utilized by BoNT/B and Tetanus Neurotoxins (TeNT), a BoNT/B derivative was engineered with elevated substrate cleavage activity, with the hope to minimize the immunoresistance impact from patients during BoNT/B therapy. As an extension of this work, a FRET peptide (designated as FVP-B) was synthesized to develop a rapid and sensitive detection assay for BoNT/B detection. In the last part of the thesis, a set of potent peptide inhibitors were developed to inhibit BoNT/A activity both in vitro and in murine model. In summary, the research works in this study will provide useful information for the development effective countermeasures to combat BoNT intoxication and for the development of novel BoNT based therapies.

## Publications arising from the thesis

**Chapter Two**—This chapter is a version of a manuscript by **Guo J**, Pan X, Zhao Y, Chen S. entitled “Engineering Clostridia Neurotoxins with elevated catalytic activity” published in *Toxicon*. 2013 Nov;74:158-66.

**Chapter Three**—This chapter is a version of a manuscript by **Guo J**, Xu C, Li X, Chen S. entitled “A simple, rapid and sensitive FRET assay for botulinum neurotoxin serotype B detection” published in *PLoS One*. 2014 Dec 1;9(12):e114124.

**Chapter Four**—This chapter is a version of a manuscript by **Guo J**, Chen S. entitled “Unique substrate recognition mechanism of the botulinum neurotoxin D light chain” published in *J Biol Chem*. 2013 Sep 27;288(39):27881-7.

**Chapters Five, Six and Seven**—These chapters will be published soon.

### Additional publications

1. Jingyu Shi, **Jiubiao Guo**, *et al.* (2014) A graphene oxide based fluorescence resonance energy transfer (FRET) biosensor for ultrasensitive detection of botulinum neurotoxin A (BoNT/A) enzymatic activity. *Biosensors and Bioelectronic*, 2014 Oct 23;65C:238-244.
2. Lin D, Chen K, Li R, Liu L, **Guo J**, Yao W, Chen S. (2014) Selection of target mutation in rat gastrointestinal tract E. coli by minute dosage of enrofloxacin. *Front Microbiol*. 5:468.
3. Weiwei Ye, **Jiubiao Guo**, Sheng Chen and Mo Yang. (2013) Nanoporous membrane based impedance sensors to detect the enzymatic activity of botulinum neurotoxin A. *J. Mater. Chem. B*, 1, 6544.
4. **Jiubiao Guo**; Jinglin Wang; Edward Wai Chi Chan, and Chen S. (2015) Exploration of endogenous substrate cleavage by various forms of Botulinum Neurotoxins. *Toxicon*. 2015 Apr 22; 100: 42-45.

5. **Guo J**, Chen S. (2015) Expression and biochemical characterization of light chains of Botulinum neurotoxin subtypes F5 and F7. *Protein Expression and Purification*. 2015 Jul; 111: 87-90.
6. Chun-Yu Chan, **Jiubiao Guo** *et al.* (2015) A reduced graphene oxide-Au based electrochemical biosensor for ultrasensitive detection of enzymatic activity of botulinum neurotoxin A. *Sensors and Actuators B: Chemical*. December 2015, 220:131-137.

## Acknowledgments

Without the help and support from the following many individuals, this dissertation could not be completed in time, and thanks so many wonderful people I have worked with or will continuing work with in the future. My life has enriched both as a scientist and as a person. To this end, I would like to try to thank them here.

Firstly, my eternal gratefulness and thankfulness go to my supervisor, Dr. Chen Sheng. Without his instructions I cannot achieve this and I have learned so much from him, besides scientific researches. I will try best to emulate his leadership skills and be a qualified scientist and a more nice person in my future career.

I would like to thank Dr. Edward Waichi Chan for his critical reading of some of the chapters in the dissertation and some of my manuscripts for publication. I would also like to thank Dr. Jiachi Chiou and Mr. Marcus Ho Yin Wong for the helpful discussions and suggestions of the dissertation and manuscripts. In addition, a great thanks go to Mr. Ka Chi HUI and Miss Echo Hoi Ying WAN for their help in some experiments of the dissertation and thanks all the other members of the Sheng's laboratory for their help.

Next I would like to thank the two external examiners, Prof. Jiang XIA and Prof. Quan Hao for their agreements to comment and attend my oral defense and thanks all the members of Board of Examiners for their participations in my thesis defense. I would also like to thank all the staffs, scientific officers, technicians in the Department of Applied Biology and Chemical Technology and staffs from Departmental Research Committee for their help in the preparation, review of the dissertation and oral examination.

Last but certainly not least, I need to thank my family for their unconditional love, support, and encouragement during the past years. We finally made it!

# Table of contents

<b>ABSTRACT</b> .....	<b>III</b>
<b>PUBLICATIONS ARISING FROM THE THESIS</b> .....	<b>IV</b>
<b>ACKNOWLEDGMENTS</b> .....	<b>VI</b>
<b>TABLE OF CONTENTS</b> .....	<b>VII</b>
<b>LIST OF FIGURES</b> .....	<b>XI</b>
<b>LIST OF TABLES</b> .....	<b>XIII</b>
<b>LIST OF SYMBOLS, ABBREVIATIONS AND NOMENCLATURE</b> .....	<b>XIV</b>
<b>CHAPTER ONE: INTRODUCTION</b> .....	<b>1</b>
1.1 NEUROTOXIN.....	1
1.2 CLOSTRIDIA.....	2
1.3 BOTULISM.....	3
1.4 SNARE COMPLEX AND EXOCYTOSIS.....	4
1.5 BOTULINUM NEUROTOXINS.....	6
<i>1.5.1 Structure of Botulinum Neurotoxins</i> .....	8
<i>1.5.2 Mode of action</i> .....	10
1.5.2.1 Intestine uptake.....	11
1.5.2.2 Double receptor anchorage and endocytosis.....	12
1.5.2.3 Neuron cytosol translocation of LC.....	14
<i>1.5.3 SNARE substrate recognition and cleavage</i> .....	15
1.5.3.1 Identification of CNT substrates.....	15
1.5.3.2 CNT need extended substrate region for efficient cleavage .....	16
1.5.3.3 Mode of SNAP-25 recognition by BoNTs.....	18
1.5.3.4 Mode of VAMP-2 recognition by CNTs.....	20
1.5.3.5 Substrate recognition by CNTs.....	22
1.5.3.6 BoNT antitoxin development.....	24
1.5.3.7 Detection of CNT.....	25
1.6 PHARMACEUTICAL APPLICATIONS OF BOTULINUM NEUROTOXINS .....	26
1.7 SUMMARY AND OBJECTIVES OF THE THESIS .....	26
<b>CHAPTER TWO: ENGINEERING CLOSTRIDIA NEUROTOXINS WITH ELEVATED CATALYTIC ACTIVITY*</b> .....	<b>29</b>
2.1 ABSTRACT.....	29
2.2 INTRODUCTION.....	29

2.3 EXPERIMENTAL SECTION.....	31
2.3.1 Plasmid construction for protein expression .....	31
2.3.2 Linear velocity and kinetic constant determinations for VAMP -2 cleavage by LC/B and LC/T.....	32
2.3.3 Compensatory assay.....	32
2.3.4 LC crystallization and structure determination.....	33
2.3.5 Cleavage of endogenous VAMP of Neuro2A cell by recombinant LC/T, LC/B and their derivatives.....	33
2.4 RESULTS.....	33
2.4.1 Optimization of LC/T and LC/B S1' pockets enhanced their catalytic activities.....	35
2.4.2 Optimization of LC/T S1' pocket regained optimal recognition of P2' site .....	36
2.4.3 Optimization of S1' and S1 substrate recognition pockets further enhanced LC/T activity .....	37
2.4.4 Side chain positioning of L230 of LC/T affects its optimal recognition of both P1' and P2' sites.....	38
2.4.5 Activities of LC/B, LC/T and their derivatives on endogenous VAMP-2 .....	40
2.5 DISCUSSION .....	42
<b>CHAPTER THREE: A SIMPLE, RAPID AND SENSITIVE FRET ASSAY FOR BOTULINUM NEUROTOXIN SEROTYPE B DETECTION*</b> .....	<b>44</b>
3.1 ABSTRACT.....	44
3.2 INTRODUCTION.....	44
3.3 EXPERIMENTAL SECTION.....	46
3.3.1 BoNT LCs Recombinant Proteins .....	46
3.3.2 Fluorogenic Peptide design .....	46
3.3.3 Fluorogenic Peptide synthesis.....	47
3.3.4 Proteolytic activity of LC/B and other LCs .....	48
3.3.5 LC/MS analysis of the FVP-B cleavage by LC/B.....	48
3.4 RESULT .....	49
3.4.1 LC/B specificity of FVP-B.....	49
3.4.2 FVP-B assay for LC/B activity detection.....	51
3.4.3 FVP-B as LC/B inhibitor screening assay.....	54
3.5 DISCUSSION .....	54
<b>CHAPTER FOUR: UNIQUE SUBSTRATE RECOGNITION MECHANISM OF BOTULINUM NEUROTOXIN D LIGHT CHAIN*</b> .....	<b>57</b>
4.1 ABSTRACT.....	57
4.2 INTRODUCTION.....	57
4.3 MATERIALS AND METHODS .....	59
4.3.1 Molecular Modelling.....	59
4.3.2 Plasmids Construction and Protein Expression.....	59

4.3.3 VAMP-2 and LC/D mutagenesis.....	59
4.3.4 Linear velocity and kinetic constants.....	59
4.3.5 Trypsin digestion of LC/D and its derivatives.....	60
4.3.6 Far UV-Circular dichroism analysis.....	60
4.4 RESULTS.....	60
4.4.1 Recognition of P2' site of VAMP-2, S <sup>61</sup> by the S2' pocket of LC/D.....	61
4.4.2 Dual recognition of VAMP-2, P1' site by S1' pocket of LC/D.....	64
4.4.3 S3 pocket residue of LC/D interacts with the VAMP-2 P3 (D <sup>57</sup> ).....	65
4.4.4 Main chain of P <sup>64</sup> of LC/D interacts with P1 site, K <sup>59</sup> of VAMP-2.....	65
4.4.5 Substrate binding and recognition distal to the active site of LC/D.....	65
4.4.5.1 Recognition of VAMP-2, V <sup>53</sup> by LC/D B1 binding site.....	65
4.4.5.2 Recognition of VAMP-2, N <sup>49</sup> by LC/D B2 binding site.....	66
4.4.5.3 Recognition of VAMP-2, M <sup>46</sup> by LC/D B3 binding site.....	66
4.4.5.4 Recognition of VAMP-2, V <sup>42</sup> by LC/D B4 binding site.....	67
4.4.5.5 Recognition of VAMP-2, V <sup>39</sup> by LC/D B5 binding site.....	67
4.5 DISCUSSION.....	67

## **CHAPTER FIVE: DISTINCT EVOLUTIONARY ROUTES OF BOTULINUM**

### **NEUROTOXIN SUBTYPES F1 AND F7 FEATURING DIFFERENTIAL SUBSTRATE**

#### **RECOGNITION AND CLEAVAGE MECHANISMS\* .....71**

5.1 ABSTRACT.....	71
5.2 INTRODUCTION.....	71
5.3 MATERIALS AND METHODS.....	73
5.3.1 Plasmid Construction and Protein Purification.....	73
5.3.2 Molecular Modeling.....	73
5.3.3 LC/F7 and VAMP-2 Derivatives Generation and purification.....	73
5.3.4 Standard Linear Velocity Reaction.....	73
5.3.5 Kinetic Parameters Determination.....	73
5.3.6 Far-UV Circular Dichroism Analysis.....	74
5.4 RESULTS.....	74
5.4.1 VAMP-2 regions mapping analysis for efficient cleavage by LC/F7.....	74
5.4.2 Contribution of individual residues of VAMP-2 on LC/F7 cleavage.....	74
5.4.3 CD analysis of LC/F7 and derivatives.....	75
5.4.4 LC/F7 active site substrate recognition.....	77
5.4.4.1 Triple recognition between the P1' (K <sup>59</sup> ) of VAMP-2 and the S1' pocket of LC/F7.....	77
5.4.4.2 Salt bridge mediates the interaction between the P2 (D <sup>57</sup> ) of VAMP-2 and the S2 pocket of LC/F7.....	79
5.4.5 LC/F7 binding pockets interactions with VAMP-2.....	80
5.4.5.1 LC/F7 B2&B3 pockets.....	80
5.4.5.2 LC/F7 B1 pocket.....	81
5.5 DISCUSSION.....	82

<b>CHAPTER SIX: THE MOST DIVERSE SUBTYPE BOTULINUM NEUROTOXIN F5 WITH UNIQUE SUBSTRATE RECOGNITION MECHANISM*</b> .....	<b>85</b>
6.1 ABSTRACT.....	85
6.2 INTRODUCTION.....	85
6.3 MATERIALS AND METHODS .....	87
6.3.1 <i>Construct design and cloning</i> .....	87
6.3.2 <i>Protein expression and Purification</i> .....	87
6.3.3 <i>Molecular Modeling</i> .....	87
6.3.4 <i>Standard Linear Velocity Reaction</i> .....	87
6.3.5 <i>Kinetic Parameters Determination</i> .....	88
6.3.6 <i>Far-UV Circular Dichroism Analysis</i> .....	88
6.4 RESULTS.....	88
6.4.1 <i>LC/F5 active site substrate recognition</i> .....	91
6.4.2 <i>LC/F5 binding pockets interactions with VAMP-2</i> .....	92
6.5 DISCUSSION .....	95
<b>CHAPTER SEVEN: SUBSTRATE-BASED INHIBITORS EXHIBITING EXCELLENT PROTECTIVE AND THERAPEUTIC EFFECTS AGAINST BOTULINUM NEUROTOXIN A INTOXICATION*</b> .....	<b>98</b>
7.1 ABSTRACT.....	98
7.2 INTRODUCTION.....	99
7.3 MATERIALS AND METHODS .....	100
7.3.1 <i>Plasmid construction and proteins purification</i> .....	100
7.3.2 <i>Development of high affinity peptides for LC/A</i> .....	100
7.3.3 <i>Development of potential LC/A inhibitors with high inhibition efficiency</i> .....	101
7.3.4 <i>Cell-based inhibition of potential peptide-based inhibitors</i> .....	101
7.3.5 <i>Evaluation of selected peptide inhibitors in mouse model</i> .....	102
7.4 RESULTS.....	102
7.4.1 <i>Screening for SNAP25 sites that contribute to higher binding to LC/A</i> .....	103
7.4.2 <i>Development of inhibitors using SNAP25 based peptides with enhanced affinity</i> .....	105
7.4.3 <i>Inhibition of LC/A by SNAP25 based inhibitors in cell model</i> .....	108
7.4.4 <i>Full protection of BoNT/A intoxication by SNAP25 inhibitors in mice</i> .....	109
7.5 DISCUSSION .....	110
<b>CHAPTER EIGHT: CONCLUSION AND SUMMARY</b> .....	<b>112</b>
<b>REFERENCES</b> .....	<b>114</b>

## List of Figures

Figure 1. 1 Mechanism of BoNTs neurotoxins. ....	1
Figure 1. 2 A photomicrograph of <i>Clostridium botulinum</i> stained with Gentian violet. ....	3
Figure 1. 3 The different locations of <i>v</i> -SNAREs and <i>t</i> -SNAREs. ....	4
Figure 1. 4 The locations of R- and Q-SNAREs in the layers of synaptic core SNARE complex. ....	5
Figure 1. 5 Percent identities at both nucleotide and amino acid levels between subtypes within different serotypes. ....	8
Figure 1. 6 The di-chain structure of BoNT/A. ....	9
Figure 1. 7 The three resolved crystal structure of Botulinum Neurotoxin holotoxins. ....	9
Figure 1. 8 Molecular architecture of progenitor toxin complexes and structural comparison between BoNT/A and NTNHA-A. ....	10
Figure 1. 9 A proposed transit mechanism of BoNT through the intestinal epithelial barrier. ....	12
Figure 1. 10 Schematic illustration of the trafficking pathways of BoNT and TeNT in neurons. ....	13
Figure 1. 11 Schematic illustration of neuron cellular intoxication by BoNT. ....	15
Figure 1. 12 Multistep recognition and cleavage of SNAP25 by LC/A. ....	20
Figure 1. 13 Molecular mechanisms of substrate recognition by LC/B & LC/T and LC/F. ....	22
Figure 1. 14 Substrate recognition and cleavage by the CNTs. ....	23
Figure 2. 1 Schematic illustration of S2', S1' and S1 pockets, their constituent residues in LC/T and LC/B and their recognition of different VAMP-2 P sites. ....	34
Figure 2. 2 Different catalytic activities of LC/T, LC/B and their derivatives to substrate VAMP-2. ....	36
Figure 2. 3 Different positioning of S1' residue of LC/B, LC/T and LC/T(K <sup>168</sup> E, L <sup>230</sup> T). ...	39
Figure 2. 4 Different distances between the residues in S1' and S2' pockets. ....	41
Figure 2. 5 Cleavage of endogenous VAMP-2 by recombinant LC/B, LC/T and their derivatives. ....	41
Figure 3. 1 Spectral properties of EDANS-Dabcyl pair (247) and the flowchart of the experimental design. ....	47
Figure 3. 2 The specificity of the synthesized FVP-B. ....	50
Figure 3. 3 LC/MS analysis of specific cleavage of FVP-B by LC/B. ....	51
Figure 3. 4 The feasibility of the synthesized FVP-B and our developed assay. ....	52
Figure 3. 5 Optimization of the developed assay system. ....	53

Figure 3. 6 Limit of detection of the developed LC/B detection system. ....	53
Figure 3. 7 The inhibitory effect of EDTA on LC/B.....	54
Figure 4. 1 The overall view of the modeled LC/D-VAMP-2 complex structure.....	62
Figure 4. 2 CD spectroscopy analysis of LC/D and its derivatives.....	62
Figure 4. 3 The specific recognition of VAMP-2 by LC/D pockets.....	63
Figure 4. 4 Mechanism of substrate recognition by LC/D.....	69
Figure 5. 1 Hydrolysis comparison of LC/F and LC/F7 on the cleavage of VAMP-2 and its derivatives. ....	75
Figure 5. 2 Overall view of the modeled LC/F7-VAMP-2 complex structure and aligned interactions between LC/F7 and VAMP-2.....	76
Figure 5. 3 CD spectroscopy analysis of LC/F7 and its derivatives. ....	76
Figure 5. 4 Recognition specificity of VAMP-2 by LC/F7 pockets. ....	78
Figure 5. 5 Schematic representation of interactions between LC/F-VAMP-2 and LC/F7-VAMP-2.....	84
Figure 6. 1 Hydrolysis analysis LC/F5 on the cleavage of VAMP-2 and derivatives. ....	89
Figure 6. 2 Overall view of the modeled LC/F5-VAMP-2 complex structure.....	90
Figure 6. 3 Circular Dichroism spectroscopy analysis of LC/F5 derivatives.....	91
Figure 6. 4 Specific interactions and recognition between VAMP-2 and LC/F5.....	94
Figure 6. 5 Overall comparison of the N-terminal shifted $\alpha$ -helix in the modeled VAMP-2. ....	97
Figure 7. 1 The two examples illustrate the enhanced interactions between SNAP25 and LC/A.....	105
Figure 7. 2 Molecular interactions of the modeled complex structure of inhibitor and LC/A. ....	108
Figure 7. 3 Neuro-2a cell based <i>in vivo</i> inhibition effect of inhibitors. ....	109
Figure 7. 4 Protection of mice against dosages of BoNT/A challenge by SNAP25-based inhibitor.....	110

## List of Tables

Table 1. 1 Discovery time-line of all the eight serotypes of BoNTs.....	7
Table 1. 2 The corresponding binding sites between CNT and dual receptors. ....	14
Table 1. 3 Identified SNARE substrate and cleavage site of the CNTs. ....	16
Table 1. 4 The current pharmaceutical applications of BoNT and relative products. ....	28
Table 2. 1 Kinetic constants of LC/B, LC/T and their derivatives. ....	36
Table 2. 2 Results of a compensatory mutational assay for interactions of LC/T with VAMP-2 and derivatives. ....	37
Table 2. 3 The crystallographic statistics of LC/T (K <sup>168</sup> E, L <sup>230</sup> I). ....	40
Table 4. 1 Efficiency of VAMP-2 hydrolysis and kinetic constants of LC/D and its derivatives. ....	64
Table 5. 1 Efficiency of VAMP-2 hydrolysis and kinetic constants of LC/F7 and derivatives. ....	79
Table 6. 1 Efficiency of VAMP-2 hydrolysis and kinetic constants of LC/F5 and derivatives. ....	95
Table 7. 1 Cleavage of SNAP25 and its derivatives by LC/A (1-425).....	104
Table 7. 2 IC <sub>50</sub> and K <sub>i</sub> of peptide inhibitors of LC/A (1-425). ....	107

## List of Symbols, Abbreviations and Nomenclature

Symbol	Definition
BoNTs/ TeNT	Botulinum Neurotoxins/ Tetanus Neurotoxin
Ach	Acetylcholine
SNARE	Soluble N-ethylmaleimide sensitive fusion protein (NSF) Attachment protein Receptor
C. botulinum/ C. difficile	Clostridium botulinum/ Clostridium difficile
ADP	Adenosine diphosphate
C. perfringens/ C. welchii	Clostridium perfringens/ Clostridium welchii
C. tetani/ C. sordellii	Clostridium tetani/ Clostridium sordellii
SNAP-25	Synaptosomal-associated membrane protein of 25 kDa
SVs	Synaptic vesicles
VAMP-2	Vesicle-associated membrane protein-2
LC/HC	Light chain/ Heavy chain
GI	Gastrointestinal
PTCs	Progenitor toxin complexes
NAPs	Non-toxin neurotoxin-associated proteins
NTNHA/HA	Non-toxic non-hemagglutinin/ Hemagglutinin
L-PTC	Large progenitor toxin complex
CNT	Clostridia Neurotoxin
NMJ	Neuromuscular junction
Cer	Ceramide part of Polysialo-gangliosides
HCC	Receptor-binding domain of heavy chain of CNT
FRET	Förster resonance energy transfer
MBA	Mouse bioassay
ELISA	Enzyme-linked immunosorbent assay
GE	Genome equivalent
MS	Mass spectrometry
IPTG	Isopropyl 1-thio- $\beta$ -D-galactopyranoside

# Chapter One: Introduction

## 1.1 Neurotoxin

The medical definition of neurotoxin is "a poisonous protein complex that acts on the nervous system". In a broader sense, any substance that is poisonous or destructive to nerve tissue can be defined as neurotoxins, such as lead, drinking alcohol, glutamate, nitric oxide, Botulinum Neurotoxins (BoNTs), Tetanus Neurotoxin (TeNT) and tetrodotoxin. However, some substances, nitric oxide and glutamate, for example, only exert adversely neurotoxic effects at excessive concentrations, under normal condition, they are essential for body to function properly.

According to the activity mechanisms of neurotoxins, they either interfere with the controlling of ion concentrations across cell membrane by neuron or inhibit the communication between neurons across synapse by blocking the release of neurotransmitters. The former type of neurotoxins normally play a role as membrane channel inhibitors, such as Na channel inhibitor (tetrodotoxin) (1), K channel inhibitor (tetraethylammonium) (2), Cl channel inhibitor (chlorotoxin) (3), and Ca channel inhibitor (conotoxin) (4). A typical representative of the neurotransmitters release blocker is BoNTs which can inhibitor the release of acetylcholine (ACh) by specifically targeting and degrading the SNARE (Soluble N-ethylmaleimide sensitive fusion protein (NSF) Attachment protein Receptor) proteins at the neuromuscular junction, resulting in botulism (**Figure 1.1**). With a high similarity in structure and origin, TeNT functionally reduces inhibitory transmissions in the nervous system resulting in muscular tetany.

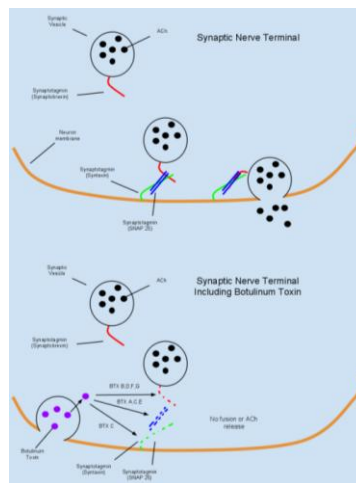


**Figure 1. 1 Mechanism of BoNTs neurotoxins.**

Image adapted from Wikipedia.

## 1.2 Clostridia

Based on the realization that infectious diseases was caused by microbial agents, the idea that bacteria could produce poisonous substances was raised. As early as 19<sup>th</sup> century, Klebs firstly suggested the presence of toxic molecules from staphylococci and then pioneering works done by Koch and Loeffler on cholera (*Vibrio cholerae*) and diphtheria (*Corynebacterium diphtheriae*) infections respectively.

The *Clostridia* are a highly polyphyletic class of Firmicutes, including *Clostridium* which are obligate anaerobes, Gram-positive and spore-forming species (5). *Clostridium* is originated from Greek *kloster* or spindle, the individual cell of *Clostridium* is rod-shaped (**Figure 1.2**). Traditionally, the genus of *Clostridium* was defined by its rod-shaped characteristics; however, many species have been reclassified into other genera. *Clostridium botulinum* is widely distributed in soil, sediments of lakes, ponds and decaying vegetation. More than 100 species of *Clostridium* have been identified, including common free-living bacteria and pathogens. There are five main species that responsible for human diseases.

*C. botulinum* produces BoNTs, which can cause botulism from food or wounds infection. Honey that contains spores of *C. botulinum* may cause human infant (one year old and younger) botulism (6), but cannot infect adult or older children in that they cannot compete with the dominant bacteria present in gastrointestinal tract.

*C. difficile* can cause antibiotic-associated diarrhea under which situation other bacteria in the gut are killed by antibiotic therapy, thus leading to pseudomembranous colitis. Some virulence factors, such as glucosyltransferase toxins and ADP-ribosylating binary toxin are involved in the infections caused by *C. difficile*(7).

*C. perfringens* (formerly named *C. welchii*) produces about 12 different toxins and causes a wide range of symptoms, such as enterotoxemia in sheep and goats. The produced cytolytic  $\alpha$ -toxin can hydrolyze phosphatidylcholine and sphingomyelin and lead to cell death (8).

*C. tetani* is the causative organism of tetanus by producing the TeNT which can specifically inhibit neurotransmission at the central nervous system, leading to spastic paralysis and potentially to death (9).

In addition, *C. sordellii* is one pathogen that can cause even rare, fatal infection. Since the year of 2000, less than one case was reported per year (10).

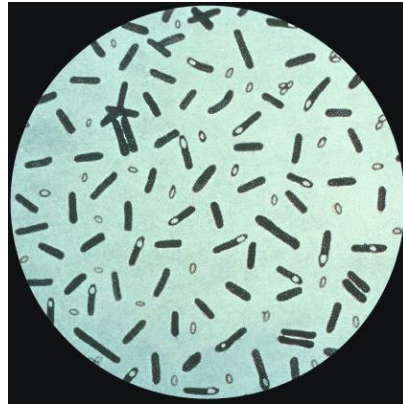


**Figure 1. 2 A photomicrograph of *Clostridium botulinum* stained with Gentian violet.**

Image adapted from <http://www.ppdictionary.com/bacteria/gpbac/botulinum.htm>.

### **1.3 Botulism**

Botulism was named after the Latin word “*botulus*” for sausage in that it was firstly described by Justinus Kerner after a food poisoning outbreak that followed the ingestion of blood sausages (11). Human botulism is serious and fatal. After 12-36 hours exposure, early symptoms of botulism will appear with marked fatigue, weakness and vertigo, usually followed by trouble seeing, swallowing and speaking. If prompt diagnosis and immediate treatment are not given, the mortality rate of botulism is really high, with 5-10% cases are fatal, even though the incidence of botulism is low, and thus early detection and diagnosis is the key in preventing botulism. There are four main causes of botulism (12). Foodborne botulism occurs when *Clostridium botulinum* grows and produces toxins in food prior to consumption. Due to the anaerobic characteristics of *Clostridium botulinum*, foodborne botulism is often associated with lightly preserved foods and in inadequately processed, home-canned or home-bottled substances and fermented uncooked dishes. Infant botulism, which mostly occurs in infants under six months of age, is the most common form in Western countries. By lacking of the competition from other dominant bacteria that are existed in older children and adults, *Clostridium botulinum* will be easily colonize in the gut of infants and then release toxins into the intestine, which is then absorbed into the bloodstream (13). Spore-contaminated honey has been reported to associate with a number of cases though there are several possible sources of infection of infant botulism. Wound botulism is another cause which mainly resulted from wound contamination by *Clostridium botulinum*. Even though wound botulism is rare, increasing cases were reported in intravenous drug users, especially people using black tar heroin (13). Inhalation botulism is rare as well and does not happen naturally, it is described after inhalation by laboratory workers and after cosmetic use of inappropriate dose of Botox (13). This type of botulism is

becoming a serious concern from the bioterrorism perspective. Moreover, there are some other types of intoxication, such as waterborne botulism, but the risk is very low in that the common water treatment will destroy the toxin.

## 1.4 SNARE complex and exocytosis

In yeast and mammalian cells, there are more than 60 members of SNAP (Soluble N-ethylmaleimide sensitive fusion protein (NSF) Attachment) Receptor (SNARE) proteins which primarily play roles in mediating vesicle fusion for materials distribution among intracellular organelles and communication (14,15). Divided based on location, SNAREs can be classified into two categories, *vesicle* or *v-SNAREs* and *target* or *t-SNAREs* (**Figure 1.3**), the former type is located into the membranes of transport vesicles during budding and the later one is incorporated into the membranes of target compartments (16). It was reported that the *t-SNAREs* served as a guide for the *v-SNAREs* binding to form a complete SNARE complex (17,18). Recently, several SNARE members were identified to locate on both the vesicle and target membranes, leading to a new classification with the consideration of structural features of SNAREs: R-SNAREs (corresponding to v-SNAREs) and Q-SNAREs (acting as t-SNAREs) which can be further grouped as Qa, Qb and Qc by locations in the four-helix bundle (**Figure 1.4**). In the formed zero ionic layer of assembled core SNARE complex, R-SNAREs (including synaptobrevin) contribute an arginine (R) residue and Q-SNAREs (including syntaxin and synaptosomal-associated membrane protein of 25 kDa (SNAP-25)) contribute a glutamine (Q) residue (19-22).

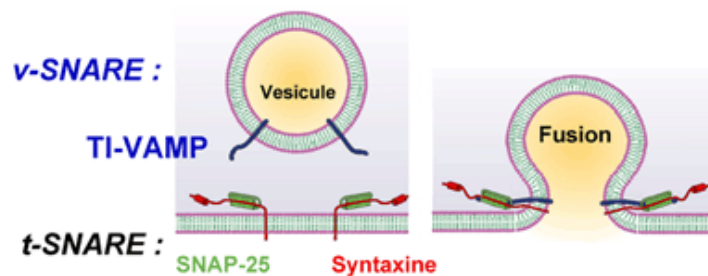


**Figure 1.3** The different locations of *v-SNAREs* and *t-SNAREs*.

Image adapted from (16).

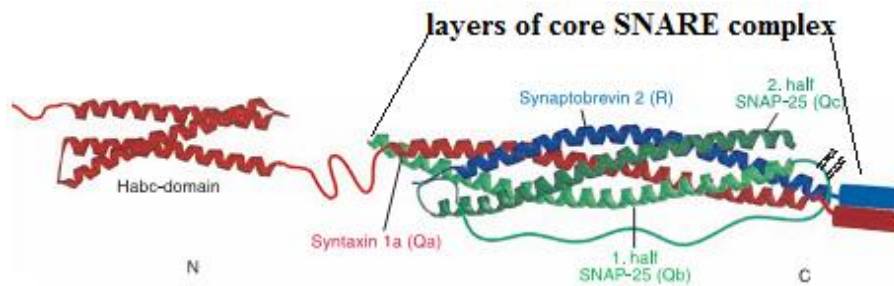


**Figure 1. 4 The locations of R- and Q-SNAREs in the layers of synaptic core SNARE complex.**

In the extended helix bundle structure of SNARE complex, Synaptobrevin 2 (R), Syntaxin 1a (Qa), and two helices of SNAP-25 (Qb and Qc) are illustrated. Image adapted from (22) with modifications.

The SNAREs that mediate docking of synaptic vesicles (SVs) with the presynaptic membrane in neurons were well studied. Located at the end of neuronal axons in presynaptic terminals, the SVs are key organelles of neuronal communication by mainly functioning on concentrating, storing and releasing neurotransmitters into synaptic cleft. During the process of exocytosis and endocytosis, the SVs are in recyclable usage. In the fusion process of SV with presynaptic membrane, the increasing concentration of free  $Ca^{2+}$  in cytoplasmic is important as well (23). On the surface of SV, more than 80 integral membrane proteins have been identified which can be grouped into, in the respect of responsibility, classes for trafficking and for transmitter loading and its modulation. The drive force in vesicular exocytosis is the formation of the core of SNARE complex which consists of vesicular protein synaptobrevin and the preferentially plasma membrane-localized proteins SNAP-25 and syntaxin (21).

Synaptobrevin-2 (or named vesicle-associated membrane protein (VAMP) -2), presenting on secretory vesicles both in or outside the central nervous system, is one of the most abundant proteins on SV (about 70 copies per SV). The VAMPs family proteins are characterized by a C-terminal integral membrane domain and the N-terminus which comprises a SNARE motif for interacting with SNAP-25 and syntaxin faces the cytosol. VAMP-1, the second most abundant VAMP isoform (24,25) and VAMP-4 and VAMP-7/Ti-VAMP were found occurred on SV as well (26). However, the VAMP-2 knockout animals studying indicated that the role played by VAMP-2 in the SNARE core complex formation could not be reconstituted by other isoforms and in addition, the interactions of VAMPs with synaptophysin or the SNARE proteins were mutually exclusive (25,27,28). Besides, there are many other isoforms of VAMP-2 (VAMP-5 and VAMP-8, for example), they locate outside of the central nervous system but play important roles in membrane fusions (29-31).

SNAP-25 is proposed to account for membrane fusion specificity by forming tight interactions with VAMP-2 and syntaxin (32). With the help from palmitoylation side chains covalently bound to the four cysteine residues in between the two SNARE motifs, SNAP-25 can stably anchored to the cytosolic face of membranes (33). The identified two isoforms (mRNA splice variants) of SNAP-25 (labeled as A and B) differed only in nine residues, including a re-localization of one of the four cysteine residues, leading to the diffuse localization of SNAP-25A and SNAP-25B mainly localized to terminals and varicosities (34,35). In addition, SNAP-25A is mainly expressed in embryos and developing neural tissue but not in adult tissue except in pituitary and adrenal gland tissues, in contrast, SNAP-25B is dominantly expressed in adult neural tissue, suggesting the switched expression pattern from A to B after birth (35,36). SNAP-23, -29 and -47 are another membrane-associated isoforms of SNAP-25 but with different locations, functions and resistant to natural BoNTs (37-39).

Syntaxins are a family of Q-SNARE proteins that reside on SV membrane and function in exocytosis process (40). Functionally, syntaxins can be divided into three domains: a single C-terminal transmembrane domain, H3 (SNARE domain) and Habc (N-terminal regulatory domain) which is comprised of three  $\alpha$ -helices (19). In the 'closed' conformation of syntaxin 1a, the H3 domain folds back onto the Habc domain, preventing the H3 domain from interacting with other SNARE components. The 'closed' conformation of syntaxin 1a was found mediated by the binding of Munc 18a (Sec 1) which is a key modulator of exocytosis. Thus, in order to assemble into a SNARE complex, syntaxin 1a must dissociate from Munc 18a and switch to an open conformation in which the H3 domain is free from the Habc domain. However, the binding affinity of Munc 18a with syntaxin 1a is at nanomolar level, therefore the dissociation of the Munc 18a-syntaxin 1a complex is a slow process (41-44). Syntaxin 1b is another closely related isoform of syntaxin 1a, both of which share more than 80% homology in sequence. It was proved that syntaxin 1b overlapped in function with syntaxin 1a (45,46). Syntaxin-3, -4 and -5, which belong to the large syntaxin family, are reported involving in other types of membrane fusion in different cells (40,47,48).

## 1.5 Botulinum Neurotoxins

Botulinum Neurotoxins are the most potent protein neurotoxin identified so far. The dual roles of BoNTs as causative agent of human botulism/biological warfare and most widely used protein therapies for numerous neuromuscular disorders/cosmetic uses make it an extreme hot topic in diverse fields. As listed in **Table 1.1**, since the isolation of BoNT/B, the firstly identified serotype of BoNTs, from salted ham by van Ermengem in 1897 (49), in

the following 73 years (1897-1970), serotypes of BoNT/A, /C, /D, /E, /F and /G were identified successively (50-54). In addition, an eighth serotype, BoNT/H, was reported recently (55), however, some scientists question of the new identification and more experiments need to be performed to further prove it as a new serotype (56). Then bivalent strains which produce 2 toxins with different amounts were identified, including the dual toxicities of Af (1970), Bf (1980), Ab (1983), Ba (1984) and AB (both toxins are produced equally in amounts) (57). Moreover, A(B) strains which are termed as “A silent B” has been identified as well, due to a stop-codon mutation in the additional gene of BoNT/B (58,59). Besides the alphabetically designated toxin serotypes, the host bacterium was grouped as well. Four groups (I-IV) have been described, and recently another two additional groups, Group V and Group VI have been included as well, both of which represent the BoNT/F-producing *C. baratii* strains and the BoNT/E-producing *C. butyricum* strains respectively (60).

With more and more sequences being generated by PCR and sequencing, more variations within the toxin of the existing serotypes has been identified. As defined, if > 2.5% difference in amino acid sequence compared with other strains within a serotype was found, that strain can be defined as a subtype. Till now, about 31 *bont* gene subtypes/variants have been identified within serotypes BoNT/A-F (Figure 1.5) (61-64).

**Table 1. 1 Discovery time-line of all the eight serotypes of BoNTs.**

Serotype	Source	Country	Year
<b>BoNT/B</b>	salted ham	Belgium	1897
<b>BoNT/A</b>	bean salad	Germany	1904
<b>BoNT/C</b>	fly larvae cattle	US, Australia	1924/1926
<b>BoNT/D</b>	cattle	S. Africa	1929
<b>BoNT/E</b>	sprats salmon	US	1936/1938
<b>BoNT/F</b>	duck paste	Denmark	1958
<b>BoNT/G</b>	soil	Argentina	1970
<b>BoNT/H*</b>	feces	US	2014

\* More authentic evidence needed.

		Percent nucleotide identity								
Strain	A1	A2	A3	A4	A5					Accession #
A1	Hall	-----	94.6%	92.0%	94.3%	98.6%				AF488749
A2	Kyoto-F	89.9%	-----	96.4%	93.6%	94.9%				CP001581
A3	Loch Maree	84.6%	93.0%	-----	91.6%	92.3%				DQ185900
A4	Ba 657	89.3%	88.3%	84.4%	-----	93.7%				CP001082
A5	H04402 065	97.1%	90.3%	85.0%	87.4%	-----				EU679004
		B1	B2	B3	B4	B5	B6	B7		
B1	okra	-----	97.5%	97.9%	96.2%	98.0%	97.9%	97.5%		CP000940
B2	213B	95.6%	-----	99.1%	96.2%	97.3%	99.1%	97.7%		EF028395
B3	CDC 795	96.0%	98.4%	-----	96.4%	97.7%	98.9%	97.8%		EF028400
B4	Eklund 17B <sup>1</sup>	93.2%	93.9%	93.7%	-----	96.0%	96.0%	96.3%		EF051570
B5	Ba 657 <sup>2</sup>	96.1%	95.0%	95.4%	92.7%	-----	97.3%	97.1%		EF033130
B6	Osaka05	96.1%	98.4%	98.1%	93.1%	95.4%	-----	97.3%		AB302852
B7	Bac-04-07755	94.7%	95.6%	95.7%	93.6%	94.1%	95.1%	-----		IQ354985
		C1	C/D	D	D/C					
C1	Stockholm	-----	85.3%	68.3%	76.2%					D90210
C/D	003-9	76.0%	-----	80.3%	68.8%					AB200360
D	1873	51.2%	68.7%	-----	85.9%					AB012112
D/C	5995	64.7%	51.9%	76.5%	-----					EF378947
		E1	E2	E3	E4	E5	E6	E7	E8	
E1	Beluga <sup>1</sup>	-----	99.4%	99.3%	98.5%	98.3%	98.5%	99.1%	97.9%	X62089
E2	CDC 5247 <sup>1</sup>	99.0%	-----	98.7%	98.3%	97.9%	98.2%	98.5%	98.5%	EF028404
E3	Alaska E43 <sup>1</sup>	98.2%	97.4%	-----	97.9%	97.6%	98.0%	98.8%	97.6%	EF028403
E4	BL5262 <sup>1,3</sup>	97.3%	97.0%	95.6%	-----	97.2%	98.3%	98.1%	98.0%	ACOM01000005
E5	LCL155 <sup>1,3</sup>	96.8%	96.3%	95.1%	95.0%	-----	97.2%	97.3%	96.9%	AY327861
E6	K35 <sup>1</sup>	96.9%	96.7%	95.8%	96.8%	94.7%	-----	98.2%	98.3%	AM695752
E7	IBCA97E-0192 <sup>1</sup>	97.8%	97.0%	97.3%	96.2%	94.7%	96.2%	-----	98.8%	JN695729
E8	Bac-02-06430 <sup>1</sup>	96.2%	97.0%	95.6%	96.1%	94.0%	96.6%	98.2%	-----	JN695730
		F1	F2	F3	F4	F5	F6	F7		
F1	Langeland	-----	91.2%	91.5%	96.0%	81.5%	93.1%	82.4%		X70821
F2	Bf An436 <sup>2</sup>	83.4%	-----	98.9%	91.9%	84.6%	95.2%	80.2%		EF028397
F3	CDC 54086	83.9%	97.0%	-----	92.1%	84.5%	95.1%	79.6%		GU213218
F4	CDC 54076 <sup>2</sup>	92.2%	83.5%	83.8%	-----	81.9%	93.4%	81.5%		GU213213
F5	CDC 54096 <sup>2</sup>	69.8%	74.0%	74.0%	69.4%	-----	83.8%	75.9%		GU213225
F6	Eklund 202F <sup>1</sup>	87.4%	89.8%	89.8%	86.9%	73.6%	-----	80.2%		M92906
F7	Sullivan <sup>4</sup>	73.7%	68.6%	68.9%	71.9%	63.8%	69.8%	-----		HM746656
		Percent amino acid identity								

**Figure 1. 5 Percent identities at both nucleotide and amino acid levels between subtypes within different serotypes.**

Nucleotide level and amino acid level identities are colored in blue and red respectively. Strains, subtype/variant designation, and their GenBank accession numbers are listed within serotypes A-F. Variants within a serotype are shaded to highlight the pairwise comparisons that show the least or the greatest similarity. 1 nonproteolytic strains; 2 bivalent toxin producing strains; 3 C. butyricum strains; 4 C. baratii strain. Image adapted from (64).

### 1.5.1 Structure of Botulinum Neurotoxins

BoNTs belong to AB toxin family. The holotoxin is a ~ 150 kDa single polypeptide chain which can be functionally divided into two domains: an N-terminal ~ 50 kDa light chain (LC, catalytic domain) and a ~ 100 kDa C-terminal heavy chain (HC) and both of which are covalently linked through a disulfide bond until they encounter reducing conditions in the neuronal cytosol (65). The HC domain is composed of two sub-domains: translocation domain H<sub>N</sub> which mediates translocation of LC across the endosomal membrane, and cell surface receptor-binding domain H<sub>C</sub> (Figure 1.6) (66,67). Till now, three full length BoNTs' crystal structures have been resolved, (Figure 1.7).

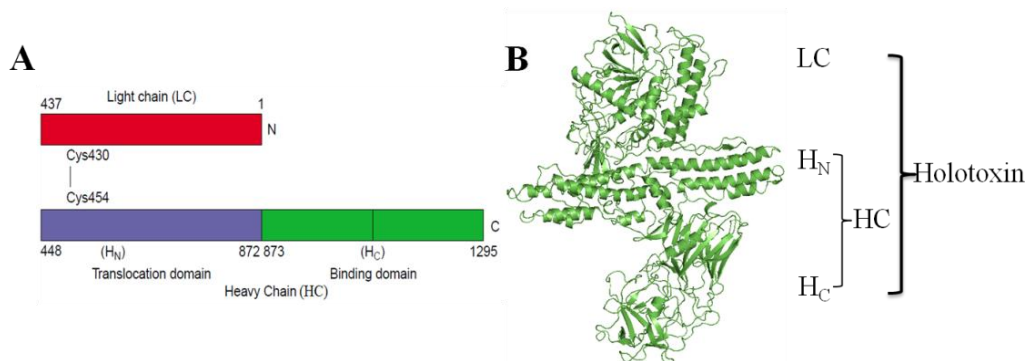


**Figure 1. 6 The di-chain structure of BoNT/A.**

(A) An overall view of the domains organization of BoNT/A, with the locations of LC, HC and disulfide bond illustrated. The image adapted from (66) with modifications. (B) The crystal structure of BoNT/A holotoxin (PDB: 3BTA) prepared by PyMOL.

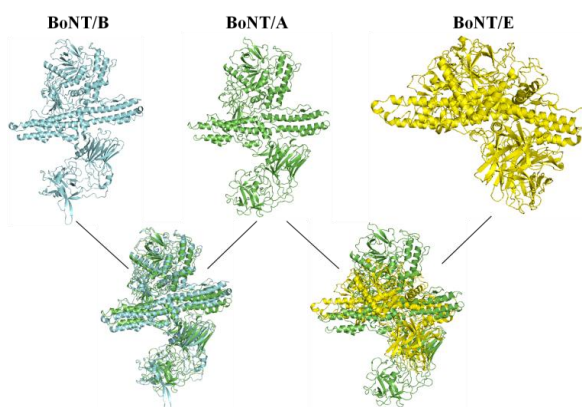


**Figure 1. 7 The three resolved crystal structure of Botulinum Neurotoxin holotoxins.**

The crystal structures of BoNT/A (PDB: 3BTA), BoNT/B (PDB: 1EPW), and BoNT/E (chain A, PDB:3FFZ) were colored in green, cyan and yellow respectively. Images were prepared by PyMOL.

BoNT/A (PDB: 3BTA), BoNT/B (PDB: 1EPW), and BoNT/E (PDB:3FFZ) (67-69), and BoNT/B shares high structural similarity with BoNT/A, but BoNT/E has dramatic difference with BoNT/A. BoNTs are inherently fragile, however, the environment of low pH and rich in proteases in the gastrointestinal (GI) tract is harsh enough to destroy them, so before interacting with host cells and approaching their substrates, what kind strategy of BoNTs utilized to survive such harsh condition and cross the intestinal epithelial barrier to enter the bloodstream. Recently studies suggested that when BoNT is incorporated into progenitor toxin complexes (PTCs), it exhibited greater oral toxicity than the BoNT alone (70). The PTCs are composed of BoNT and several non-toxin neurotoxin-associated proteins (NAPs) (71) which comprise a non-toxic non-hemagglutinin (NTNHA) and three different hemagglutinin proteins (HA-17, HA-33, and HA-70) (**Figure 1.8A and B**). The naturally occurring minimally functional PTC (M-PTC) is composed of BoNT (~150 kDa)

and NTNHA (~140 kDa). In the M-PTC of BoNT/A, NTNHA-A protect BoNT/A from GI degradation by providing large and multivalent binding interfaces. Interestingly, NTNHA-A displays high similarity in structure with BoNT/A despite shares about 20% sequence identity with BoNT/A (**Figure 1.8C and D**). In addition, when compared with the M-PTCs of BoNT/A2, BoNT/E and BoNT/F, all of which formed HA-negative M-PTCs, the nLoop was missed, suggesting the nLoop may functioned in interacting with HAs to assemble larger PTCs (72-75). Other PTCs (500-900 kDa) are assembled by the addition of various combinations of HAs to the M-PTC, but the mechanisms are not clear now (65,76).

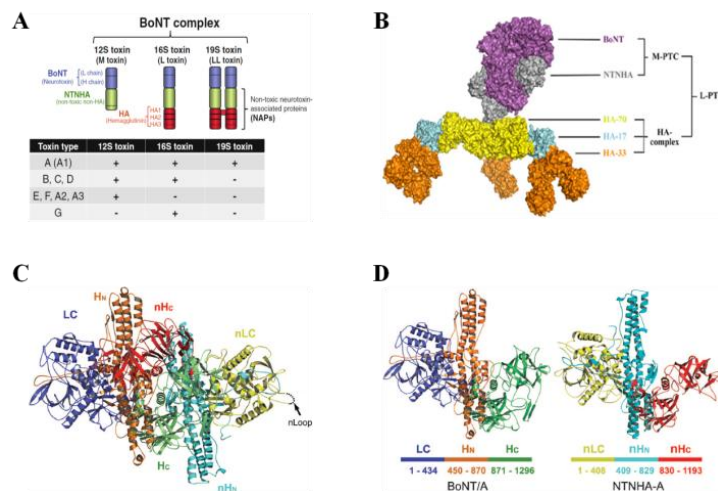


**Figure 1. 8 Molecular architecture of progenitor toxin complexes and structural comparison between BoNT/A and NTNHA-A.**

(A) The three major forms of PTCs, 12S toxin (M toxin), 16S toxin (L toxin), and 19S toxin (LL toxin) (Upper panel) (70,77,78). The different PTC forms of the six serotypes of BoNTs and some subtypes of BoNT/A are illustrated (79) (Lower panel). + presence of the complex forms; - not present. (B) In the surface representation of the large progenitor toxin complex (L-PTC) (16S complex) of BoNT/A, the M-PTC (12S complex) is composed of BoNT/A (magenta) and NTNHA (gray), and the incorporation of the three different HA proteins (HA70, three in yellow; HA 17, three in cyan, and HA33, six in orange) formed a complete L-PTC (80). (C) Cartoon presentation of the BoNT/A- NTNHA complex. The BoNT/A domains are colored as : LC in blue; H<sub>N</sub> in orange and H<sub>C</sub> in green. The NTNHA-A domains are yellow (nLC), cyan (nH<sub>N</sub>), and red (nH<sub>C</sub>). (D) The individual cartoon representation of the BoNT/A and NTNHA-A and both are labeled as that in (C).

### 1.5.2 Mode of action

As detailed above, BoNTs are produced in progenitor toxin complexes in order to survive harsh environment in human or animals and finally cause intoxication. Decades intense investigations began to unravel the action mode of BoNTs. The following sections describe the four major steps involving in the invasion of BoNTs.

### 1.5.2.1 Intestine uptake

The GI tract is weaponed with multiple barriers, such as layer of membrane anchored glycoproteins, exterior hydrated gel layer of mucins, continuous monolayer of epithelial cells and even many proteolytic enzymes (in the lumen of the small intestine) to protect host from the invasion of harmful external elements (81,82). However, in the most two common forms of human botulism, foodborne and intestinal botulism, BoNT holotoxin or its multi-subunit complexes must cross the well-protected GI tract barriers to enter the circulation and approach target neurons. Previous studies indicated that BoNT holotoxin alone showed slight toxicity in mice through oral administration, and the larger of the complex, the greater of the oral toxicity, suggesting the protective role played by both NTNHA and HA when BoNT traversed the digestive tract (70,83,84). The recently reported crystal structure of the 12S toxin of BoNT/A proved that NTNHA conferred resistance to low pH environment and proteolysis within the GI tract (72). In addition, T. I. Lam *et al.* observed that BoNT/A holotoxin alone translocated across the small intestines, but slower than that of the BoNT/A complex (85). In light of the findings in recent years from several laboratories that focused on the description of the internalization of BoNT and BoNT complex into the epithelial barrier by using in vitro model systems (86-90), a possible three-step transit mechanism of BoNT through the intestinal epithelial barrier was proposed (**Figure 1.9**). In the transcytosis step (Step 1), a small amount of luminally located BoNT complexes (Route ii) (91) or alone (Route i) (86,87,89,91-93) transits through the epithelial barrier without disrupting it; in the barrier disruption step (Step 2), when reach the basolateral surface, the HA moiety of the 16S toxin will disrupt the epithelial barrier translocated to the basolateral surface (91,94); in the absorption step (Step 3), the disrupted epithelial barrier allows the accumulated BoNT complexes or BoNT alone (Route iii) in the serosal to pass through the damaged barrier (91). However, more in vivo studies need to be carried out in order to confirm the in vivo relevance of these steps, in that the proposed model is based on the investigations of in vitro systems.

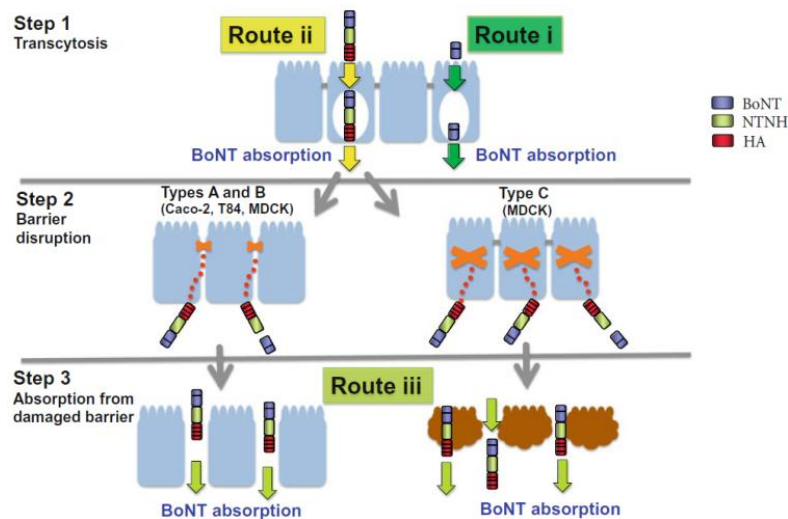


**Figure 1.9 A proposed transit mechanism of BoNT through the intestinal epithelial barrier.**

[Step 1] A small amount of luminally located BoNT complexes mediated by HA components (Route ii, yellow arrows) (91) or BoNT alone (Route i, green arrows) (86,87,89,91-93) transits through the epithelial barrier without disrupting it; [Step 2] After translocation to the basolateral surface, the HA moiety of the 16S toxin will disrupt the epithelial barrier translocated to the basolateral surface (91,94). HA proteins in the BoNT/A and /B complexes interact with E-cadherin and disrupt the intercellular barrier (95). HA in the BoNT/C complex may disrupt barrier function by exerting cytotoxic effects on the epithelial cells of susceptible animals (94). [Step 3] Accumulated BoNT complexes or BoNT alone (Route iii, light green arrows) in large amount pass through the damaged barrier (91). Image adapted from (96)with modifications.

### 1.5.2.2 Double receptor anchorage and endocytosis

The two members of the CNT (Clostridia Neurotoxin) family, TeNT and BoNT, share a same core structural characteristics and target the same class of intracellular substrates (SNARE complex) (97), but they traffick different pathways and lead to a different symptomatology of the pathologies after being endocytosed (**Figure 1.10**). BoNT mainly target the neuromuscular junction (NMJ) in vivo with a minor fraction back to the motor neuron (98), and cause botulism, in contrast, TeNT reaches the inhibitory interneurons in the spinal cord and lead to sustained spastic paralysis.

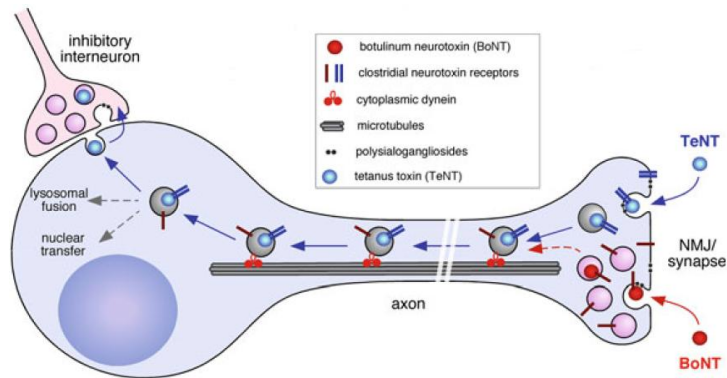


**Figure 1. 10 Schematic illustration of the trafficking pathways of BoNT and TeNT in neurons.**

TeNT (light blue) and BoNT (red) firstly bind to neuronal membranes via receptor complex(es) formed by polysialogangliosides (black dots) and synaptic proteins (blue and red bars) with specificity. After internalization, BoNT enters the synaptic vesicle recycling pathway, TeNT, under the help of microtubules (tracks, grey) and cytoplasmic dynein (molecular motor, red), is transcytosed into inhibitory interneurons at the soma. Image adapted from (99) with modifications.

The different and specific trafficking pathways utilized by CNT may due to their neurospecific receptor complexes. Polysialo-gangliosides (GD1a and GT1b, etc) were found abundantly present on the outer leaflet of the presynaptic membrane through the membrane incorporation of a ceramide part (Cer). Bullens *et al.* reported that the N-acetylgalactosamine-transferase (NAcGalT) which involving the the biosynthesis of ganglioside, knockout mice could not be affected by BoNT/A incubation (100). In addition, when incubated with the cultured hippocampal neurons of NAcGalT-deficient mice, the binding and entry of all the seven BoNT serotypes were reduced, but could be restored by the addition of exogenous bovine brain ganglioside mix (101-103). As mentioned previously, the HC domain of the CNT is responsible for the delivery of the LC into the cytosol of neuronal target cells to fulfill substrate cleavage, structural alignment of the H<sub>CC</sub> domain of all the seven BoNT serotypes and TeNT indicated that the 5-mer clusters in the  $\beta$ -trefoil architecture of the H<sub>CC</sub> domain were conserved though showed high sequence divergence at the whole H<sub>CC</sub> level (104). Combining the data derived from recent decades animal and biochemical analysis (**Table 1.2**), BoNT/A, E, F and G prefer the terminal NAcGal-Gal-NAcNeu moiety present in GD1a and GT1b, whereas BoNT/B, C, D and TeNT require the disialyl motif found in GD1b, GT1b and GQ1b (105). In contrast to the conserved CNT-ganglioside interaction mode, the reorganization between CNT and their protein receptors employ a serotype-specific strategy to avoid chaos occurred (**Table 1.2**).

**Table 1.2 The corresponding binding sites between CNT and dual receptors.**

Data were extracted from (105,106) with modifications.

Serotype	AA motif in the conserved ganglioside binding site	Key AA of the sialic acid binding site	SV protein receptor	Key AA of SV protein receptor binding site
BoNT/A	E...H...SXWY...G		SV2C>SV2A>SV2B, FGFR3 (?)	?
BoNT/B	E...H...SXWY...G		SytII>SytI	K1192, F1194, F1204
BoNT/C	W1258, Y1259; WY-loop <sup>§</sup>	Y1179	?	?
BoNT/DC	W1252, F1253; WF-loop <sup>§</sup>	Y1175	Syt	M1179, N1185, V1191, L1235, I1264
BoNT/D	DXY...VXN	R1239	SV2B>SV2C>SV2A	?
BoNT/E	E...K...SXWY...G		SV2A>SV2B	?
BoNT/F	E...H...SXWY...G		SV2	?
BoNT/G	Q...G...SXWY...G		SytI ~ SytII	Q1200, F1202, F1212
TeNT	D...H...SXWY...G	R1226	Nidogen, SV2	?

<sup>§</sup> no conserved ganglioside binding site present.

### 1.5.2.3 Neuron cytosol translocation of LC

After endocytosis mediated by the dual-receptor mechanism, CNT exposed to the acidic environment of endosomes, which triggered the conformation change of H<sub>N</sub> from a soluble protein to a protein that could be inserted into the bilayer membrane of endosomes, in order to facilitate the translocation of the LC through the protein-conducting channel into the cytosol of neuron (**Figure 1.11**) (97,107-109). Similar to other bacterial toxins, electrophysiological measurements indicated that the channel formed by the H<sub>N</sub> domain of BoNT is cation specific with a single channel conductance (109,110), and the belt region (residues 450-544) within the H<sub>N</sub> domain is believed function as pH trigger to promote channel formation only under acidic environment, the beltless H<sub>N</sub> (H<sub>N-bdt</sub>, residues 545-870) represented as a minimal channel forming unit (111,112). However, the formed channel remains primarily closed within the endosome, circular dichroism analysis revealed that the secondary structure of the H<sub>C</sub> domain did not undergo significant structure changes upon acidification (113,114), suggesting the acidic pH alone was not sufficient to induce an active channel state of the H<sub>C</sub>, the conformational changes depend on several factors, such as acidification, receptor binding and possible lipid association (115,116). In addition, studies suggested that the H<sub>C</sub> subdomain in the H<sub>C</sub> domain of BoNT determined the pH dependence of channel formation (112,113). Without the H<sub>C</sub>, the H<sub>N</sub> was readily inserted into the plasma

membrane of neuron and the LC was incapable of being translocating through the channel, indicating a chaperone role played by the H<sub>C</sub> subdomain to ensure the concurrence among the partial unfolding of LC and the H<sub>N-belt</sub>, thereby promoting a productive LC translocation (117). After the complete translocation of LC, the channel would be closed to preclude the passive dissipation of the ionic electrochemical gradients across endosomal membranes. Taken together, each domain in the BoNT functions in a synchronized cooperative manner to achieve the cellular intoxication with elegance, even though they can work independently.

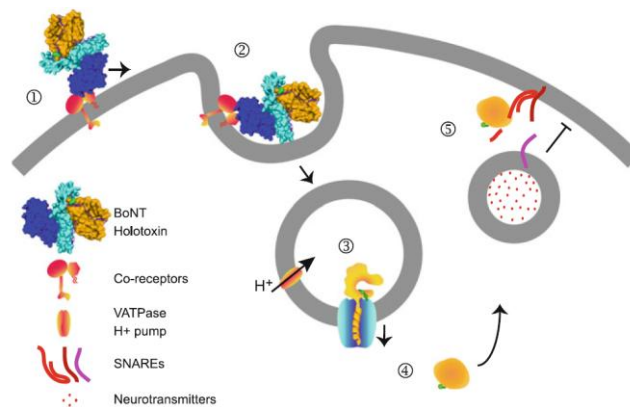


**Figure 1. 11 Schematic illustration of neuron cellular intoxication by BoNT.**

1. BoNT, via its H<sub>C</sub> domain (blue), specifically recognize and bind to its dual receptors located on the membrane surface of neuron; 2. Endocytosis occurs and BoNT is shuttled to vesicles destined for the endosome/lysosome pathway; 3, the H<sub>N</sub> domain (cyan) of BoNT undergoes conformation change to insert into the bilayer membrane of endosome/lysosome triggered by the acidic environment; 4, the LC (gold) of BoNT is delivered via the formed channel into the cytosol of neuron, and 5, the released LC traffics in the cytosol to approach its specific SNARE substrate to achieve substrate cleavage.

Image adapted from (117).

### 1.5.3 SNARE substrate recognition and cleavage

#### 1.5.3.1 Identification of CNT substrates

Based on sequence prediction, a conserved segment which contained the zinc-binding motif of zinc-endopeptidases (HEXXH) was identified in the LC of CNT (118). The activities of purified BoNT/A, B and E could be inhibited by chelating agents (such as EDTA), and the activities of them could be rescued by adding exogenous zinc ion. The finding further confirmed the zinc presence. In addition, previous study indicated that zinc atom coordinated with histidines in active site but not cysteines, suggesting the zinc atom contributes to the catalytic activity of BoNTs but rather keeps the conformation of the BoNTs structure, further indicating the irreplaceable role of zinc ion in the action of BoNTs

(119). The Ach release inhibition effect at synapses by TeNT provided the hint that the substrate of CNT may exist in synaptic vesicles (120). In order to directly prove the hypothesis, rat cerebral cortex small synaptic vesicles were purified, incubated with nicked CNTs. A 19kDa protein, which was proved later to be VAMP-2, was cleaved by both BoNT/B and TeNT at the same site (Q<sup>76</sup>-F<sup>77</sup>) (121). Similarly, the substrate of BoNT/F1 was proved as VAMP-2, with a scissile bond located between Q<sup>58</sup>-K<sup>59</sup> sequences. Recently, however, the BoNT/F5 subtype was found to recognize and cleave a different scissile bond in VAMP-2, namely L<sup>54</sup>-E<sup>55</sup> (122,123) (**Figure 1.12**). The identification of the stable SNARE protein complex (formed by VAMP-2, SNAP-25 and syntaxin) that functioned in vesicle exocytosis expanded the substrate test for other BoNTs (14,21). The substrate of BoNT/A and /E was found to be SNAP-25, but with distinct cleavage sites, Q<sup>197</sup>-R<sup>198</sup> and R<sup>180</sup>-I<sup>181</sup> respectively. Moreover, BoNT/D and BoNT/G cleaved substrate VAMP-2 at peptide bond between K<sup>59</sup>-L<sup>60</sup> and Ala<sup>81</sup>-Ala<sup>82</sup> respectively. Further researches suggested that BoNT/C could cleave both of SNAP-25 between R<sup>198</sup>-A<sup>199</sup> and a single K<sup>252</sup>-A<sup>253</sup> bond within the carboxyl-terminal region of syntaxins (124-126). The substrate and corresponding cleavage sites is summarized in **Table 1.3**.

**Table 1.3 Identified SNARE substrate and cleavage site of the CNTs.**

BoNT	Substrate	Scissile bond (P1-P1')
BoNT/A	SNAP-25	Q <sup>197</sup> -R <sup>198</sup>
BoNT/B	VAMP-2	Q <sup>76</sup> -F <sup>77</sup>
BoNT/C	SNAP-25	R <sup>198</sup> -A <sup>199</sup>
	Syntaxin-1a	K <sup>252</sup> -A <sup>253</sup>
BoNT/D	VAMP-2	K <sup>59</sup> -L <sup>60</sup>
BoNT/E	SNAP-25	R <sup>180</sup> -I <sup>181</sup>
BoNT/F1	VAMP-2	Q <sup>58</sup> -K <sup>59</sup>
BoNT/F5	VAMP-2	L <sup>54</sup> -E <sup>55</sup>
BoNT/G	VAMP-2	Ala <sup>81</sup> -Ala <sup>82</sup>
TeNT	VAMP-2	Q <sup>76</sup> -F <sup>77</sup>

### 1.5.3.2 CNT need extended substrate region for efficient cleavage

The LC of CNT is very particular zinc-dependent protease in that the substrate specificity of the CNT do require the help of other endogenous factors (127) and the LC of CNT need extended SNARE region in corresponding substrate for efficient substrate recognition and cleavage (128). The study on BoNT/D, /F and TeNT indicated that the VAMP-2 peptide substrate ranged from Arg<sup>47</sup> to Thr<sup>116</sup> could not be cleaved efficiently, while the peptide ranged from Thr<sup>27</sup>-Thr<sup>116</sup> could be efficiently cleaved by all three toxins (129). In addition,

the minimal VAMP-2 peptide substrate for BoNT/G is VAMP-2 (54-97), with its residue at P1' (Ala) plays an important role in substrate cleavage (130). Similarly, the minimal domains that have been determined for BoNT/A, E and C were 146-206, 156-206 and 93-206 of SNAP-25, respectively (128). It was also shown that the P1' site was essential for substrate cleavage by these three toxins.

Sequence analysis suggested that these three SNARE proteins shared common motifs composed of hydrophobic, negatively charged and other residues. There are two copies of motifs in VAMP-2 (V1 and V2) and syntaxin (X1 and X2) and 4 copies in SNAP-25 (S1, S2, S3 and S4). Peptides derived from SNARE motifs in particular, V2 and S3 could inhibit BoNTs and TeNT ability to inhibit Ach release. Antibody against SNARE motifs could also show cross-reaction to different SNARE proteins and influence substrate cleavage by neurotoxins (131). These results suggested that BoNTs and TeNT recognized their substrate through double interaction with one region for unique substrate cleavage by different neurotoxins and one common region, structural motif, to all three SNARE proteins. Mutation of the residues in the SNARE motif affected substrate recognition by BoNTs (132).

To better understand the mechanisms underline the extended substrate requirements for CNTs, saturation mutagenesis was performed on SNAP-25 and VAMP-2 to identify the essential residues in the substrate for CNT substrate hydrolysis. Alanine scanning of LC/A minimal substrate, SNAP-25 (156-202) identified that mutations of 18 of 48 residues did not affect LC/A or LC/E cleavage of SNAP-25, mutations of 11 of 48 residues inhibited the ability of LC/A and LC/E to cleave SNAP-25, whereas 18 of 48 residues had differential effects on SNAP-25 cleavage by LC/A or LC/E. Two regions were resolved that included mutated residues, which showed the greatest inhibitory action to LC/A, residues 193–202, termed the active site (**AS**) domain and residues 156–181, termed the binding (**B**) domain. With the AS domain, residues at P4', P1', P3, and P5 contributes to substrate hydrolysis. Relative to LC/A, mutation to fewer residues in SNAP25 inhibited LC/E cleavage. Mutations that influenced LC/E cleavage included residues 178–183 within the AS domain and residues 167–173 within the B domain. Within the AS domain, residues at P1' and P5 contributed to LC/E substrate hydrolysis. Kinetic constants were determined for significant mutations in both AS and B regions and results indicated that AS domain contributed to catalytic activity, whereas B domain contributes to high affinity binding of SNAP-25 by LC/A and LC/E. Furthermore, LC/A and LC/E were shown to cleave AS domain peptide, <sup>192</sup>DEANQRATK<sup>200</sup> and LC/E cleaved <sup>178</sup>IDRIME<sup>183</sup>, respectively, although at lower efficiency. These data suggested that AS domain determined the substrate specificity of LC/A and LC/E, while B domain contribute to high affinity substrate binding. Both domains were required for efficient substrate catalysis (133).

Saturation mutagenesis of VAMP-2 was performed by two independent groups to test the substrate requirements by LC/B, D, F and LC/T and consistent data were observed from these studies. Mapping experiments showed that residues 60-87 of VAMP-2 were sufficient for efficient cleavage by LC/B and that residues 40-87 of VAMP-2 were sufficient for efficient LC/T cleavage. Alanine-scanning mutagenesis and kinetic analysis identified three regions within VAMP-2 that were recognized by LC/B and LC/T: residues adjacent to the site of scissile bond cleavage (**AS**) and residues located within N-terminal and C-terminal regions relative to the cleavage region. Analysis of residues within the cleavage region showed that mutations at the P7, P4, P2, and P1' residues of VAMP-2 had the greatest inhibition of LC/B cleavage ( $\geq 32$ - fold), whereas mutations at P7, P4, P1', and P2' residues of VAMP-2 had the greatest inhibition of LC/T cleavage ( $\geq 64$ -fold). Residues within the **AS** influenced catalysis, whereas residues N-terminal and C-terminal to the cleavage region influenced binding affinity. Thus, LC/B and LC/T possess similar organization but have unique residues for VAMP-2 recognition and cleavage (134,135). Similar mapping and saturation mutagenesis characterization were also performed for LC/D and LC/F. minimal substrate for LC/F was VAMP-2 (27-63), while minimal substrate for LC/D was VAMP-2 (39-63). Mutagenesis characterization identified several residues in the minimal substrate that were significant for LC/D and LC/F substrate hydrolysis. Mutations of significant residues around the scissile bond affect substrate catalysis, while mutations of residues distal to the scissile bond affected substrate affinity(135). These results suggested that although unique to each of CNTs, these neurotoxins share the similar requirement for efficient substrate hydrolysis, a substrate recognition region and distal binding region/regions for efficient substrate affinity, which is exclusive for any other proteases (135). LC/C cleaved recombinant SNAP25 and syntaxin very inefficiently, therefore the detail characterization of substrate requirements was not investigated except for a preliminary characterization study (136).

### **1.5.3.3 Mode of SNAP-25 recognition by BoNTs**

The crystal structures of all LCs of CNTs have been resolved and showed very similar confirmation with Zn ion coordinated in the active sites of the LCs (136-142), while the mode of substrate specificity for each LC is unique. Decoding of complex structures of LC/A-SNAP-25 and LC/F-VAMP-2 has depicted the mode of LC recognition of their substrate, SNAP-25 or VAMP-2 (143,144). The recognition of SNAP-25 by LC/A is mediated by exosites: the  $\alpha$ -exosite, C-terminus of the active site, contributes to substrate binding, which is initiated by the helix formation and the extended anchoring points along SNAP-25; these sites binding reduces  $K_m$  and enhance binding at the  $\beta$ -exosite at the N-terminus of the active site, inducing conformational changes at the active site (AS), which

renders the endopeptidase competent to cleave its substrate. Further biochemical study resolve the step by step binding and recognition of SNAP-25 by LC/A(145). The mechanism of LC/A recognition and cleavage of SNAP-25 involves sequential steps representing SNAP-25 recognition and active site organization (**Figure 1.12**). Initial interactions involve discontinuous surfaces between residues within the belt region of LC/A and the B region residues of SNAP-25. The Velcro-like binding of SNAP-25 to LC/A aligns the P5 residue Asp<sup>193</sup> to form a salt bridge with Arg<sup>177</sup>, an S5 pocket residue at the periphery of one side of the active site. Although the exact order of each step of recognition of SNAP-25 by BoNT/A at the active site is not clear, the initial binding could subsequently orient SNAP-25 for the formation of a salt bridge between the P4'-residue SNAP-25(Lys<sup>201</sup>) and the S4'-residue LC/A(Asp<sup>257</sup>). These interactions broaden the LC/A active site cavity and dock Arg<sup>198</sup>, the P1'-residue, via electrostatic and hydrophobic interactions within the S1'-pocket. The fine tuning of the alignment of Arg<sup>198</sup> into the S1'-pocket resulting in the precise alignment of the scissile bond is facilitated by the binding of the P3 residue, SNAP-25-Ala<sup>195</sup>, into the hydrophobic S3 pocket of LC/A. The proper docking of the P1'-P1 sites into the AS initiates substrate cleavage. After cleavage, the P4'-residue dissociates from the S4'-residue of LC/A, which converts the AS to a smaller conformation, facilitating dissociation of the P1'-residue from the AS (**Figure 1.12**) (145).

The complex structure of LC/E-SNAP-25 was not available, while the identification of significant residues in AS and B region of SNAP-25 provided a starting point for the characterization of SNAP-25 recognition by LC/E. Structural modeling predicted that the active site region of LC/E had three interaction sites, termed S3, S2, and S1', with the AS of SNAP-25 and that LC/E made several contacts with the substrate binding region of SNAP-25 that were distanced from the active site of LC/E. Biochemical characterization of S pockets and binding site in LC/E depicted the multiple pocket recognition and cleavage of SNAP-25 by LC/E. LC/E initially interacts with the B site of SNAP-25 at the plasma membrane of neurons through the B region of LC/E. This interaction ends at the hydrophobic S3 pocket, which specifically recognizes P3, Ile178, through hydrophobic interactions. The binding of SNAP-25 to LC/E is facilitated through P1' and P2 site interactions with the S1' and S2 pockets of LC/E. Proper docking of P1' and P2 sites into S1' and S2 pockets initiates a final alignment that precisely aligns the substrate scissile bond for cleavage. After cleavage, the products of cleavage leave the AS and LC/E targets to another SNAP-25 molecule starting another cycle of substrate recognition and cleavage(146).

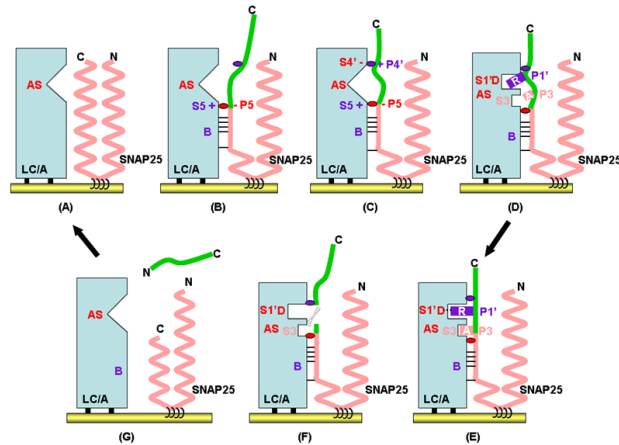


**Figure 1.12 Multistep recognition and cleavage of SNAP25 by LC/A.**

The step by step SNAP-25 recognition and binding at corresponding sites/pockets is illustrated in cartoon drawings. Detailed interaction mechanism refers to the text above. Image adapted from (145).

#### 1.5.3.4 Mode of VAMP-2 recognition by CNTs

The mode of VAMP-2 recognition by BoNT/B was first reported by a study that resolved the first co-crystal of LC/B and VAMP-2. However, the lack of electron density in the VAMP-2 sequence limited its contribution to understand the substrate recognition by LC/B(147). The recently resolved complex structure of LC/F bound to a VAMP-2-based peptide inhibitor provides information on the mode of LC/F binding to VAMP-2 distal to the active site and proposes a three-exosite-pocket substrate recognition model(144). However, these studies lack the detailed information with regard to how BoNTs recognize and hydrolyze their substrate VAMP-2 at the molecular level. Detailed characterization of the interactions between LC/F and VAMP-2 addressed the mechanisms of VAMP-2 cleavage by LC/F through a series of accumulative interactions (**Figure 1.13B**). The B1 pocket of LC/F recognizes the B1 region of VAMP-2 through hydrophobic, electrostatic and hydrogen-bond interactions. The B1 pocket substrate recognition facilitates the further recognition of the VAMP-2 B2 region by the B2 pocket of LC/F, which contributes to both the substrate binding and further substrate recognition. The B1 and B2 substrate recognition is further strengthened by the interactions between the hydrophobic B3 region of VAMP-2 and the hydrophobic S3 pocket of LC/F. At the B3 region, VAMP-2 maintains a helical confirmation as in the SNARE complex, which folds the hydrophobic residues into a surface. The primary role of the B3 pocket on substrate catalysis suggests that B3 substrate recognition may stabilize the active site substrate catalysis, where the P2, P1' and P2' sites are specifically recognized by the LC/F S2, S1' and S2' pockets. The S2-P2, P1'-S1' and S2'-P2' substrate recognition stabilizes the P1-P1' scissile bond alignment over the active site  $Zn^{2+}$ , which promotes the substrate hydrolysis. After substrate cleavage, the cleaved

substrate disassociates from LC/F, which then can recognize and cleave other VAMP-2 proteins (**Figure 1.13B**)(148).

Earlier studies showed that LC/B and LC/T recognized three regions in VAMP-2 that contribute to substrate recognition: a cleavage region (residues 70~78) that immediately surround the scissile bond and two regions that contribute to high affinity binding to VAMP-2 which are located N-terminal and C-terminal to the cleavage region (134,135). Together with the current study, the generation of a detailed model for how LC/B and LC/T recognize VAMP-2 and a molecular basis to explain the similarities and differences in substrate cleavage are now possible (**Figure 1.13A**). By analogy with LC/A-SNAP-25 interactions (133,145), upon N- terminal and C-terminal VAMP-2 binding, the S7 pocket residue (F<sup>26</sup> in LC/B and Y<sup>26</sup> in LC/T) associate with L<sup>70</sup> in the P7 site through hydrophobic interactions and the S2' pocket residue (R<sup>370</sup> for LC/B and R<sup>374</sup> for LC/T) associates through an ionic interaction with E<sup>78</sup> the P2' residue. These interactions facilitate P1 and P1' (Q<sup>76</sup>, F<sup>77</sup>) association to the LCs to align the scissile bond for substrate cleavage. In addition, interactions of the internal S pocket residues of LC/B and LC/T (S5, S4, S3 and S2) align VAMP-2 through physical interactions that allow physical orientations for the effective cleavage of a coiled substrate (**Figure 1.13A**)(149).

The similarity of LC/B and LC/T substrate recognition includes two binding sites that are unique in Clostridium neurotoxins and the specific recognition of several P sites by active site pockets of the LCs, where the P7-S7 and P1'-S1' interaction are the most important anchoring points, while other P-S interactions contribute to the tighter and more specific substrate recognition (**Figure 1.13A**). The different substrate recognition between these two neurotoxins includes their different binding sites that may contribute to their different  $K_m$  on substrate VAMP-2 and their different composition of the S pockets, which may contribute to their different  $k_{cat}$  on VAMP-2. The active site substrate recognition for LC/B includes the direct recognition of P7, P6, P1, P1', and P2' sites of VAMP-2 by the corresponding S pockets in LC/B and the fine alignment of P4 and P3 sites to the S4 and S3 pockets, while the substrate recognition for LC/T includes the direct recognition of P7, P6, P1, P1', and P2' sites of VAMP-2 by the corresponding S pockets in LC/T and the fine alignment of P4 and P2 sites to the S4 and S2 pockets. The less optimal composition of S1 pocket and the more complex interaction between P2'-S2' interactions in LC/T may contribute to the lower  $k_{cat}$  of LC/T on VAMP-2 (149).

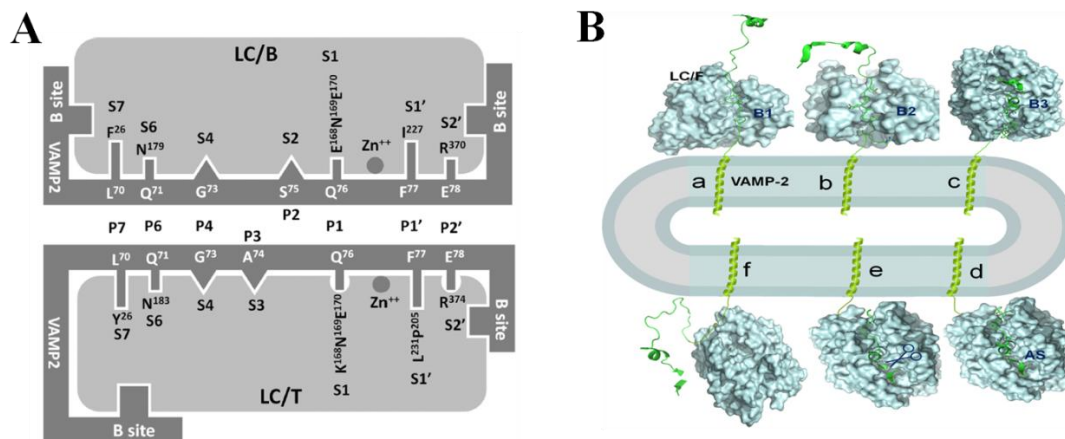


**Figure 1.13 Molecular mechanisms of substrate recognition by LC/B & LC/T and LC/F.**

(A) illustrates the similarities and differences in substrate recognition by LC/B and LC/T in multiple interaction sites/pockets. Image adapted from (150). The series of accumulative interactions between LC/F and VAMP-2 is illustrated as (B). Image adapted from (148). For detailed interaction mechanism, refer to the text above.

### 1.5.3.5 Substrate recognition by CNTs

Current knowledge on VAMP-2 and SNAP-25 recognition by CNTs suggested that different CNT substrate recognition is unique, while shares some common themes. The AS region of BoNT substrate normally includes at least three P sites, a P1' site that is significant to the substrate recognition, an upstream P site for the stabilization of P1' and a downstream P' site for the stabilizations of P1 site for efficient substrate cleavage (133-135,145,146,151) (**Figure 1.14**). The different rates of substrate hydrolysis by different serotypes of BoNTs might be attributed to their AS substrate recognition. Comparing the AS site substrate recognition of BoNTs, the P2' and P2 sites contribute to the LC/E and LC/F P1'-P1 scissile bond stabilization respectively, and the P4' and P5 sites, P2' and P7 sites contribute to the LC/A, LC/B and LC/TeNT P1'-P1 scissile bond stabilization, respectively (**Figure 1.14**). The different arrangements of P site for P1'-P1 scissile bond stabilization affect the substrate catalytic activity of BoNTs. The higher catalytic activity of LC/E and LC/F may be attributed to the tight stabilization of the P1'-P1 by the closest P sites, the P2' and P2 sites. The relatively low catalytic activity of LC/B and LC/TeNT might be due to the weak stabilization of the P1'-P1 by the further P sites, the P2' and P7 sites (133-135,145,146,151).

In addition to AS substrate recognition, substrate binding distal to the active site can also affect the catalytic activity of BoNTs. Within BoNTs, there are two types of substrate binding regions, a longer binding region in the case of LC/A and LC/F, and a relatively shorter binding region in the case of LC/B, LC/E and LC/TeNT, (**Figure 1.14**). The size of

binding region shows little correlation to the substrate binding affinity of the LCs (133-135,145,146,151). The mechanism of the contribution of substrate catalysis through substrate binding distal to the active site of LCs is not clear, but it may be due to the following reasons. One reason is that distal substrate binding may change the LC active site confirmation. The superimposition of LC/A structure over the LC/A-SNAP-25 complex structure and that of LC/F structure over the LC/F-peptide inhibitor complex structure indicated that only a minor confirmation change was seen at the active site after substrate binding. This mainly reflected at the side chain movement of the active site residues due to the substrate-LC interactions suggesting that distal substrate binding showed minor or no effect on the secondary confirmation of LC/A and LC/F active sites (143,144). In addition, although a cooperative exosite-dependent cleavage of VAMP-2 by LC/TeNT is reported, where distal substrate binding can enhance the active site substrate cleavage, this effect is only a minor effect and not enough to support the argument that distal substrate binding affects the active site confirmation change (152). Another reason is that substrate binding close to the active site contributes to the stabilization of AS substrate recognition and arrangement by affecting the substrate catalysis. The tightness of substrate binding close to the active site could stabilize the AS substrate interaction, recognition and further catalysis. LC/F and LC/E share similar organization of P-S interactions at the active sites, while LC/F shows higher hydrolytic activity than LC/E, which may be due to that the B3 interaction of LC/F-VAMP-2 is closer to the active site than the B region interaction in LC/E-SNAP-25, and the B1-B3 binding in LC/F-VAMP-2 is much stronger than the B region binding of LC/E-SNAP-25 (146) (**Figure 1.14**). In addition, compared to LC/TeNT, LC/B shares similar organization of P-S interactions at the active sites as LC/TeNT, while LC/B shows ~20-fold higher hydrolytic activity than LC/TeNT, which may be due to that the B region interaction of LC/B-VAMP-2 is closer to the active site than that of LC/TeNT (**Figure 1.14**).

LCs	$K_m(\mu\text{M})$	$K_{cat}(\text{S}^{-1})$	Binding	Active Site			Binding
LC/A	16.2	60.0	—————	S5	S3	S1'	S4'
LC/E	4.9	21.8	—————		S2	S1'	C-terminal
LC/F	7.1	220.8	————— ○	S5	S3	S1'	S4'
LC/B	1.7	1.1	————— S7		S6 4 3 1	S1'	S2'
LC/TeNT	4.1	1.6	—————	S7	S6 4 2 1	S1'	S2'

**Figure 1. 14 Substrate recognition and cleavage by the CNTs.**

Black boxes contributed to the direct substrate recognition, while the red boxes represent the pockets for active site substrate alignment. Different lengths and positions of the lines represent the number, length and their position relative to the active site of different substrate binding regions of the LCs. Image adapted from (153).

### 1.5.3.6 BoNT antitoxin development

The understanding of the specific substrate recognition and cleavage mechanisms of CNTs provide useful information to develop countermeasures for them. Vaccine and monoclonal antibodies (154-156), recombinant subunit vaccine produced from *E.coli* (157-159) and human-derived polyclonal- and neutralizing monoclonal- antibodies that block the entry of BoNTs into nerve cells have been intensively studied and developed. The major limit of vaccine and antibodies is they will be inefficient after the entry of BoNTs into nerve cells. Potent inhibitors that inactivate BoNTs activity in nerve cells urgently needed. Intensive efforts have been made to develop high-throughput assay for inhibitor screening, identification of target sites in the LCs for rational small inhibitor design and development of peptide and peptidomimetic inhibitors for CNTs. In addition, small molecular inhibitors targeting the active site of BoNTs using various approaches, including direct compound library screening, computer-aided small molecular design, screening of natural compounds, etc. However, the most potent small molecular inhibitors that have been identified so far showed inhibition effect at  $\mu\text{M}$  range. In addition, they have similar affinity ( $K_m$ ) as BoNTs substrates and has no potential to be a potent inhibitor (160-165). Attempts to develop natural product-based small inhibitors that target the binding domain of BoNTs did not lead to a potent inhibitor yet (165). The difficulties of developing small molecular inhibitors for BoNTs are probably due to the unique mechanism of extended substrate recognition of BoNTs, which requires a substrate binding and recognition regions for efficient substrate hydrolysis (133-135,145,146). Furthermore, structural and substrate-based small peptides targeting the active site of BoNTs have been studied and the most promising peptide inhibitors showed  $K_i$  as low as nM range. The mechanisms of inhibition of these peptide inhibitors are based on the interaction with BoNTs active site residues that are significant to substrate recognition (166-170). These studies showed the promising possibility of peptide-based inhibitor design for BoNTs. However, the limited contribution of affinity to BoNTs by a peptide that targets only to the active site of BoNTs limited further development of these peptide inhibitors with higher potency. Previous studies indicated that the LC/A-SNAP-25 interactions are not optimal and that the mutation at some residues can improve both of the substrate binding and catalysis (133,171), which strongly indicate that the peptide inhibitor containing both active site and binding regions could dramatically increase the affinity and potency. In Chapter Seven of the present thesis, some peptide inhibitor that specifically targeting BoNT/A were designed based on the above mentioned concept and their detailed in vitro and in vivo inhibition effects were tested as well.

### 1.5.3.7 Detection of CNT

For BoNT/A, the estimated lethal dose for humans is 1ug/kg for oral (172), but if diagnosed before the onset of symptoms, botulism can be effectively treated immunologically by using an equine trivalent antitoxin ([www.bt.cdc.gov/agent/agentlist-category.asp](http://www.bt.cdc.gov/agent/agentlist-category.asp)). Early BoNTs detection is critical to start medical treatment in due time. Currently, the “gold standard” in BoNT detection in culture, serum and food samples is mouse bioassay (MBA). It has a serotype and subtype depended sensitivity of between 10-100pg/ml (173,174), and can detect all serotypes and subtypes either in their free or complex forms, but it is time-consuming (175) and of serious ethical concern which encouraged the attempts to develop different alternative assays to replace the MBA. PCR-based techniques aiming at detecting *bont* genes by conventional or quantitative amplification reactions, leading to detection limit of  $10^3$ - $10^5$  genome equivalents (GE) per ml (176-179). Mass spectrometry (MS) is a powerful tool in detecting different BoNT serotypes unambiguously (180-184), an amino acid substitution database has been established by Barr and co-workers, allowing for the identification of multiple BoNT/B subtypes (185). By far, the most commonly employed methods for BoNT detection in vitro is ELISA (enzyme-linked immunosorbent assay)-based technologies, which have high sensitivity, simplicity in performing the assay and robust performance (174,186-189).

Since the identification of the substrates of CNTs and the understanding of their substrate recognition and specificity, detection assays focusing on the endopeptidase activity of the LCs of BoNTs have been developed and improved, displaying the serotype-specific proteolytic cleavage of SNAREs (190). The first peptide based FRET assay was the 17-mer peptide derived from SNAP25 around the cleavage site of BoNT/A. The 17-mer substrate is not the optimal substrate for BoNT/A, therefore the assay sensitivity is very low for effective inhibitor screening. A longer peptide may be needed to achieve the higher sensitivity of the assay for high throughput screening. In addition, there are several other substrate based fluorescence and FRET detection methods, which showed high efficiency and sensitivity and easy to be scaled up to high throughput assays. There are still some limitations of current high throughput assays due to the high false positive rate and narrow spectrum only targeting to some of the BoNTs. The understanding of substrate requirements of BoNTs would provide insights to the optimization of the assays. The combination of the endopeptidase assay with FRET (Förster resonance energy transfer), which utilizing the nature of fluorescence donor and fluorescence acceptor (or quencher) makes it more powerful and sensitive in detecting the activity of different BoNTs (191,192). A FRET based BoNT/B detection system was developed by our research group and will be detailed in Chapter Three (193).

## 1.6 Pharmaceutical applications of Botulinum Neurotoxins

Botulinum neurotoxins are the most potent protein neurotoxin identified. The extreme toxicity makes BoNTs a potential biological warfare agent, however, the reversible intoxication turns them from deadly agent to be effective for a range of common neuromuscular disorders (194-197). As early as 1989, BoNT/A was approved by the U.S. FDA to treat some common conditions (such as strabismus and blepharospasm), and its application was expanded for the treatment of cervical dystonia, glabellar facial lines, chronic migraine and cosmetic use. In addition, BoNT/A also has been proved to be effective and safe treatment in several less common conditions, vaginism wound healing, for example (198-200). Moreover, the efficacy of BoNT/A in treating disorders related to involuntary skeletal muscle activity prompted its empirical/off-label use in a variety of ophthalmological, gastrointestinal, urological, orthopedic, dermatological, secretory, and painful disorders (**Table 1.4**). Recently, There are three commercial available BoNT/A products approved by FDA. BOTOX (approved in 1989), Dysport (approved in 2009) and Xeomin (approved in 2010). In addition, MYOBLOC™ (a BoNT/B relative product) was approved by FDA as well on December 11, 2000, to as a alternative treatment for cervical dystonia. The corresponding trade names for the MYOBLOC are Solstice and Neurobloc in the US and EU markets respectively (201-203).

## 1.7 Summary and objectives of the thesis

Our knowledge of this unique species, *C. botulinum*, is increasing with the combined use of methods of microbiology and molecular and structural biology and intensive investigations from diverse aspects in the past century has furthered our knowledge on the powerful molecule of Botulinum Neurotoxins as well. But many questions remain to be addressed. The recently reported crystal structure of the minimal progenitor toxin complex of BoNT/A (72) shed light on the survive strategy of BoNT in the acidic environment and digestive proteases rich conditions in the GI tract. But how is the HA proteins recruited and assembled, and what is the interaction model of HA proteins with host receptors and facilitate translocation? Rigorous studies will be needed at structural and functional levels in the future to figure these questions out. The double receptor anchorage model employed by BoNTs has been elucidated recently, and our knowledge of their exquisite neurospecificity was enriched. But the studies of this aspect now only focused on the seven major serotypes. Therefore, in the future, all of the BoNT variants should be characterized in depth to avoid dangerous surprises and exploit more promising therapeutic applications. It well known that CNTs are a public health hazard and potential bioterrorism agent, but the only therapeutic available is antibody till now and it is useless for post-intoxication. Accordingly, effective

drugs for fighting against botulism is imperative. However, many different approaches have been utilized to discover new drugs with higher efficiency for CNTs related diseases, unfortunately, no relative drug is commercially available. In addition, viewing from the CNTs detection aspect, high toxicity, large complexes of different size and composition and increasingly identified variants are now challenging the detection of CNTs from environment samples. Taken together of all the issues, a better understanding of the mechanism of substrate recognition and cleavage by BoNTs is the prerequisite to develop inhibitors or antidotes for BoNTs intoxication, novel therapeutic applications and rapid detection system. This thesis focuses on the investigation of the substrate recognition mechanisms employed by BoNT/D, /F5 and /F7 to dissect their step by step substrate binding and cleavage. In addition, based on previous understanding and comparison of the substrate recognition mechanisms utilized by BoNT/B and Tetanus Neurotoxins (TeNT), a BoNT/B derivative was engineered with elevated substrate cleavage activity, with the hope to minimize the immunoresistance impact from patients during BoNT/B therapy. As an extension of this work, a FRET peptide (designated as FVP-B) was synthesized to develop a rapid and sensitive detection assay for BoNT/B detection. In the last part of the thesis, a set of potent peptide inhibitors were developed to inhibit BoNT/A activity both in vitro and in murine model.

**Table 1. 4 The current pharmaceutical applications of BoNT and relative products.**

Table adapted from (204).

<b>Status</b>	<b>Indications</b>	<b>BoNT product (Year of approval)</b>	<b>Remarks</b>	
<b>FDA approved indications</b>	Strabismus	Oculinum/BOTOX (1989)	Very effective but repetitive injections are required, therefore more suitable for temporary uses	
	Blepharospasm	Oculinum/BOTOX (1989)	Very effective and no more trials are required	
	Hemifacial spasm	Oculinum/BOTOX (1989)	Very effective and no more trials are required	
	Cervical dystonia	BOTOX (2001), Dysport (2009), Xeomin (2010), NeuroBloc (2000)	Very effective but larger doses may be needed, therefore immune-resistance might sometimes develop in some patients	
	Cosmetic use	BOTOX (2000, Canada) BOTOX (2012, US)	Very effective and safe for long-term use	
	Axillary hyperhidrosis	BOTOX (2001, UK and Canada), BOTOX(2004, US)	Effective and safe, but painful at the injection sites	
	Chronic migraine	BOTOX (2010)	Safe and effective for randomized studies but not placebo controlled trials	
	Neurogenic detrusor overactivity	BOTOX (2012)	Remarkable efficacy and minimal side effects	
	<b>Off-labeled use indications</b>	Lower urinary tract disorders	BOTOX	Remarkable efficacy and minimal side effects
		Gastrointestinal tract disorders	BOTOX	Commonly used for some indications, but effects are relatively short-lived
Spasticity		BOTOX	Can be considered as a first-line treatment, but should be used at the early stage	
Spasmodic dysphonia		BOTOX	Effective but more controlled studies are needed	
Sialorrhea		BOTOX	Effective on reducing excessive salivation but effective therapeutic dosages and the ideal form of application remain to be established	
Temporomandibular disorder		BOTOX	Correct injection technique and appropriate dosing guidelines are very important for successful results	
Chronic musculoskeletal pain		BOTOX	Effective for some patients who have not responded favorably to first-line treatments	
Vaginism		BOTOX	Effective but reports are limited	
Wound healing		BOTOX	Improvement of wound healing	
Diabetic neuropathy		BOTOX	Effective and safe treatment but reports are limited	

# Chapter Two: Engineering Clostridia Neurotoxins with elevated catalytic activity\*

## 2.1 Abstract

BoNT/B and TeNT cleave substrate VAMP-2 at the same scissile bond, yet these two toxins showed different efficiency on substrate hydrolysis and had different requirements for the recognition of P2' site of VAMP-2, E78. These differences may be due to their different composition of their substrate recognition pockets in the active site. Swapping of LC/T S1' pocket residue, L230, with the corresponding isoleucine in LC/B increased LC/T activity by ~25 fold, while swapping of LC/B S1' pocket residue, S201, with the corresponding proline in LC/T increased LC/B activity by ~10 fold. Optimization of both S1 and S1' pocket residues of LC/T, LC/T (K168E, L230I) elevated LC/T activity by more than 100-fold. The highly active LC/T derivative engineered in this study has the potential to be used as a more effective tool to study mechanisms of exocytosis in central neuron. The LC/B derivative with elevated activity has the potential to be developed into novel therapy to minimize the impact of immune resistance during BoNT/B therapy.

Key words: Botulinum Neurotoxin B, TeNT, light chain, VAMP-2, engineering, elevated activity

Abbreviations: CNTs, Clostridia Neurotoxins; BoNT/B, Botulinum Neurotoxin; TeNT, Tetanus neurotoxin; LC, light chain; VAMP-2, vesicle associated membrane protein-2; SNARE, soluble NSF attachment receptor

\*Most of the material of this chapter have been published as: Jiubiao Guo, Xuehua Pan, Yanxiang Zhao, Sheng Chen. Engineering Clostridia Neurotoxins with elevated catalytic activity. *Toxicon*. 2013 Nov; 74: 158-66.

## 2.2 Introduction

The clostridia neurotoxins (CNTs) are among the most potent protein toxins for humans. These include the botulinum neurotoxins (BoNT) that are responsible for botulism, and the tetanus neurotoxin (TeNT) that causes spastic paralysis. CNTs are 150 kDa dichain proteins with typical A-B structure-function properties, where the B (binding) domain binds to the surface components on mammalian cell and translocates the A (active) domain to an

intracellular location (205). CNTs are organized into three functional domains: an N-terminal catalytic domain (light chain, LC), an internal translocation domain (heavy chain, HCT), and a C-terminal receptor binding domain (heavy chain, HCR) (206). The CNTs are zinc metalloproteases that cleave SNARE (Soluble NSF Attachment REceptor) proteins, which are known to have the ability to interfere with synaptic vesicle fusion to the plasma membrane and ultimately block neurotransmitter release in nerve cells (205,207). Mammalian neuronal exocytosis is driven by the formation of protein complexes between the vesicle SNARE protein, VAMP-2, and the plasma membrane SNAREs, SNAP25 and syntaxin 1a (208). There are seven BoNT serotypes (termed A–G) that cleave specific residues on one of the three SNARE proteins: BoNT serotypes B, D, F, G, and TeNT cleave VAMP-2, BoNT serotypes A and E cleave SNAP25, and BoNT serotype C cleaves SNAP25 and syntaxin 1a (121,207,209,210).

BoNTs are the most widely used protein therapeutic agents. BoNT/A was approved by the US FDA to treat strabismus, blepharospasm, and hemifacial spasm and then for cervical dystonia, cosmetic use, glabellar facial lines and axillary hyperhidrosis as early as 1989. The efficacy of BoNT/A in treating dystonia and other disorders related to involuntary skeletal muscle activity, coupled with the satisfactory safety profile, has prompted empirical/off-label use in a variety of ophthalmological, gastrointestinal, urological, orthopedic, dermatological, secretory, and painful disorders(197,211-218). On December 11, 2000, a Botulinum Neurotoxin serotype B product (MYOBLOC™) was approved by the FDA in the United States as a treatment for patients with cervical dystonia to reduce the severity of abnormal head position and neck pain associated with cervical dystonia (201,203).

The therapeutic benefits of BoNT for treatment of conditions associated with involuntary muscle spasm and contractions, cosmetic use, and other applications are transient and repeated injections are necessary. In some patients, BoNT could elicits neutralizing antibodies against the corresponding toxin, thus reducing the beneficial effects or rendering the patient completely unresponsive to further treatment (219). The exact percentage of patients who may develop immunoresistance to BoNT treatment is unknown, but it is commonly believed that there are fewer patients who develop blocking antibodies when treated with BoNT/A than with BoNT/B(220,221). This is probably due to the use of lower dosages of BoNT/A complex than BoNT/B complex (222). The development of blocking antibodies is also more common in patients who receive treatment of cervical dystonia or spasticity, which requires larger dosages and periodic administration of toxin; on the other hand it is less common in patients who are treated for laryngeal dystonia, blepharospasm cosmetic use, all of which require smaller dosages for treatments (220,223,224). Thus reducing the treatment dosage may help to reduce the development of immune resistance.

In current study, comparative characterization of the substrate recognition pockets in the active sites of LC/B and LC/T was performed, producing results that lead to optimization of the substrate recognition of LC/B and LC/T and formation of LC derivatives with elevated catalytic activity. The highly active LC/T derivative engineered in this study has the potential to be used as a more effective tool to study mechanisms of exocytosis in central neuron. The LC/B derivative with elevated activity has the potential to be developed into novel therapy to minimize the immune resistance issue of BoNT/B therapy.

## 2.3 Experimental Section

### 2.3.1 Plasmid construction for protein expression

The genes that encoding BoNT LC/B (1-430) and LC/TeNT (1-436) were amplified from *Clostridium botulinum* serotype B Okra strain (225) and *Clostridium tetani*, respectively. The PCR products were then digested by *SacI* and *BamHI* restrictive enzymes (all reagents from NEB). The vector pET-15b which was modified by replacing original *XhoI* with *SacI*, was digested by the same restrictive enzymes used to digest the PCR products. Both restricted PCR products and vector were ligated using T4 DNA ligase (NEB) by following the manufacturer's instruction. Human VAMP-2 (1-97) fragment was amplified from a cDNA clone purchased from ATCC, digested by *SacI* and *BamHI* restrictive enzymes (all reagents from NEB). The modified vector pGEX-2T (with an extra *SacI* inserted into the original sequence) was digested by the same restrictive enzymes used to digest the DNA fragment and then ligated with restricted VAMP-2 (1-97) fragment as above mentioned. The success constructs were further confirmed by sequencing.

The confirmed constructs of pET-15b-LC/B (1-430) and pET-15b-LC/T (1-436) was transformed into *Escherichia coli* BL21(DE3)-RIL (Stratagene). The construct of pGEX-2T-VAMP-2 (1-97) was transformed into *E. coli* BL21 (DE3). Both of the 6xHis tagged LC proteins were expressed at 16 °C overnight induced by 0.75 mM IPTG (isopropyl 1-thio- $\beta$ -D-galactopyranoside). GST tagged VAMP-2 (1-97) protein was induced by 0.75 mM IPTG as well, but expressed at 30 °C for 3h. Cell pellets were collected by spin down at 4°C at 8000rpm for 6min, re-suspended in binding buffer (20 mM Tris-HCl, pH 7.9, 500 mM NaCl, and 1 mM DTT, for 6xHis-tagged protein), supplemented with 5 mM imidazole, or GST buffer (20 mM Tris-HCl, pH 7.6, 150 mM NaCl and 1% Triton X-100, for GST-tagged protein) supplemented with fresh DNase, RNase and PIC. Cells were then lysed by sonication or French press on ice; supernatant was collected by centrifugation at 18000 rpm for 1h at 4°C, and loaded onto either binding buffer pre-equilibrated Ni-NTA agarose (Invitrogen) or GST buffer pre-equilibrated glutathione-Sepharose 4B (Amersham

Biosciences). The tagged protein bound resins were washed as follows: 6xHis-tagged protein was successively washed by binding buffer, wash buffer 1 (binding buffer supplemented with 10 mM imidazole), wash buffer 2 (binding buffer supplemented with 20 mM imidazole), and finally eluted with elution buffer (binding buffer supplemented with 250 mM imidazole); the GST-tagged protein was washed with GST buffer for three times, then eluted with elution buffer (20 mM reduced Glutathione, 100 mM Tris-HCl, pH 8.0 and 1% Triton X-100). All collected samples were analyzed by SDS-PAGE and quantified by using BSA as standard. If further purification steps were necessary, the eluted target proteins were concentrated by using centrifugal filter with appropriate size (Millipore) at 3800 rpm at 4°C to desired volume and then further purified by gel filtration or ion exchange chromatography or both by linking the corresponding columns (S-200, 16/60 column, Pharmacia Biotech or HiTrap 5ml, Q HP, GE) with AKTA purifier (GE). All corresponding buffers or system operations were prepared or performed by following manufacturers' instructions.

Site directed mutagenesis of pLC/T and pVAMP-2 were performed using QuickChange (Stratagene) protocols from manufacturer. Plasmids were sequenced to confirm the mutation and that additional mutations were not present within the ORFs. Mutated proteins were produced and purified as described above .

### **2.3.2 Linear velocity and kinetic constant determinations for VAMP-2 cleavage by LC/B and LC/T**

Linear velocity reactions (10 $\mu$ l) were performed as previously described (134,145,146). VAMP-2 proteins (5  $\mu$ M) were incubated with varying concentrations of LC/T, LC/B or derivatives in 10 mM Tris-HCl (pH 7.6) with 20 mM NaCl at 37°C for 10 min. Reactions were stopped by adding SDS-PAGE buffer, and VAMP-2 and cleavage product were resolved by SDS-PAGE. The amount of VAMP-2 cleaved was determined by densitometry.  $K_m$  and  $k_{cat}$  determinations were performed with the same assay where VAMP-2 concentrations were adjusted to between 1 and 300  $\mu$ M to achieve ~ 10% cleavage by LC/T and derivatives. Reaction velocity versus substrate concentration was fit to the Michaelis-Menten equation and kinetic constants were derived using the GraphPad Program (San Diego, CA). At least five independent assays were performed to determine the kinetic constants for each protein.

### **2.3.3 Compensatory assay**

Effect of compensatory mutations within LC/T on the cleavage of VAMP-2 and mutated forms of VAMP-2 was performed as previously described with modification (145). Briefly,

5 $\mu$ M VAMP-2 or VAMP-2 derivatives were incubated with LC/T or derivatives, uncleaved and cleaved VAMP-2 were resolved by SDS-PAGE. The amount of wild type LC/T or derivatives in the reaction were plotted verses % cleavage and the amount of LC required to cleave 50% of VAMP-2 or VAMP-2 derivative were calculated.

#### **2.3.4 LC crystallization and structure determination**

LC/T derivative was crystallized by the hanging drop vapor diffusion method. The concentrated protein solution was in a buffer of 10mM Tris, 20mM NaCl PH7.9 and at a concentration of 7.5mg/ml. Each drop contained 1ul protein solution and 1ul well buffer, which was composed of 250mM Mg (NO<sub>3</sub>)<sub>2</sub> and 15% PEG 3350. Crystals were grown at 16°C for 4-5 days until maturation. For data collection, crystals were harvested and cryoprotected in mother buffer plus 20% glycerol. Data was collected at 100K on Rigaku MicroMax<sup>TM</sup>-007HF x-ray machine and processed using iMOSFLM (226). The crystals belonged to the monoclinic group C222 with a cell parameter of a = 105.38 Å, b = 176.83 Å, c = 57.36 Å and diffracted to 2.6 Å. There was one molecule per asymmetric unit. The structure of LC/T (E168E,L230I) was solved by molecular replacement using the PHASER module in the CCP4i suite of programs with LC/T (PDB ID: 1Z7H) as search model (227). The subsequent structural refinement was conducted using REFMAC module in CCP4 (228). Manual structure rebuilding was done using WINCOOT (229). The final structure was deposited to PDB data bank under the ID of 4J1L.

#### **2.3.5 Cleavage of endogenous VAMP of Neuro2A cell by recombinant LC/T, LC/B and their derivatives**

Neuro-2A cells were cultured in minimum essential medium supplemented with 10% newborn calf serum, 1.4% sodium bicarbonate, and 0.5% penicillin-streptomycin at 37 °C in 5% CO<sub>2</sub>. Confluent cells were harvested and lysed by passing through 25gauge needle 20~30 times on ice or in RIPA cell lysis buffer (SIGMA). Nuclei and unbroken cells were spun down by centrifuging for 5 min at 2500 rpm and the supernatant was used to assay for the cleavage of endogenous VAMP-2 by LCs. After incubating the cell lysate with different amount of LCs at 37°C for 10min in 10ul volume, the assay was stopped by adding equal amount of SDS-PAGE sample buffer and boiled at 100°C for 10min. The cleavage of VAMP-2 was detected by SDS-PAGE and probing with anti-VAMP-2 antibody.

### **2.4 Results**

BoNT/B and TeNT cleave substrate VAMP-2 at the same scissile bond but with different efficiencies. Our earlier characterization of VAMP-2 recognition by LC/B and LC/T showed

that the active site of both LCs displayed similar recognition of VAMP-2, while a major difference at the P2'-S2' substrate recognition was unexplainable (134,150). The mutation at P2' site E78A of

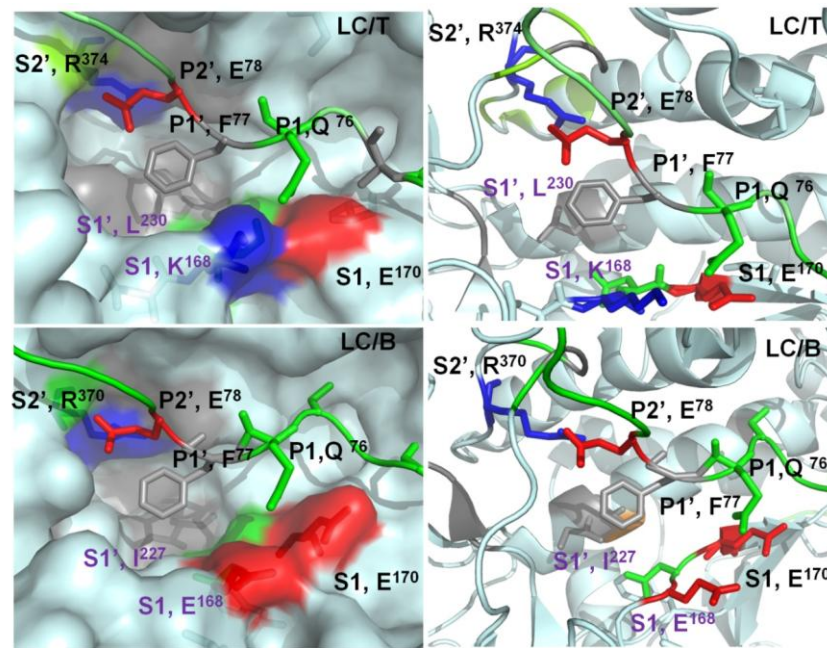


**Figure 2. 1 Schematic illustration of S2', S1' and S1 pockets, their constituent residues in LC/T and LC/B and their recognition of different VAMP-2 P sites.**

The nomenclature of P sites of VAMP-2 and S pockets of LCs is as follows. The two residues that formed the scissile bond of VAMP-2 were defined as P1-P1' from C- to N-terminus. Residues from P1 to the C-terminal direction were defined as P2, P3..., while residues from P1' to the N-terminal direction were defined as P2', P3'.... The pockets in LC/T that recognized specific P sites were defined as the corresponding S pockets. The S2' pocket of LC/T and LC/B, which recognize P2' site, E<sup>78</sup> of VAMP-2, was composed of R<sup>374</sup> and R<sup>370</sup> respectively. The S1' pocket of LC/T and LC/B that recognize P1' site, F<sup>77</sup> of VAMP-2 comprised L<sup>230</sup> and I<sup>227</sup> respectively. The S1 pocket of LC/T and LC/B that recognize P1 site, Q<sup>76</sup> of VAMP-2 contained K<sup>168</sup>NE<sup>170</sup> and E<sup>168</sup>NE<sup>170</sup>, respectively.

VAMP-2 reduced LC/B and LC/T cleavage by ~8-fold and ~240-fold respectively, suggesting the different role of VAMP-2, E78, on LC/B and LC/T substrate cleavage (134). Further biochemical characterization of S2' pocket of LC/B and LC/T showed that the S2' of LC/B and LC/T was formed by R370 and R374 respectively (**Figure 2.1**). Compensatory mutational assay showed that R370 of LC/B directly interacted with E78 of VAMP-2, whereas the interaction of R374 of LC/T with E78 of VAMP could not be proved (150). These data prompted the current study to investigate the mechanisms of different substrate recognition at P2' site by LC/B and LC/T.

### 2.4.1 Optimization of LC/T and LC/B S1' pockets enhanced their catalytic activities

Structure based sequence comparison of the active site of LC/B and LC/T showed that the S2' pocket of these two LCs were similar and comprised of an arginine residue, while their S1' pockets were different (**Figure 2.1**). The S1' pocket of LC/B was composed of F95, V200, S201, L226, and I227. Mutation of these residues to alanine showed no effect on LC/B substrate hydrolysis except for I227A that resulted in ~80-fold reduction of *k<sub>cat</sub>*, but not *K<sub>m</sub>* (150). The S1' pocket of LC/T contained the residues F199, V204, P205, L229, L230, and L231. Mutation of most of these residues showed no effect of LC/T substrate hydrolysis, while the mutation causing LC/T(L230A) or LC/T(P205A) changes did not affect *K<sub>m</sub>* but reduced the *k<sub>cat</sub>* by ~30-fold (150). Within these residues, P205 of LC/T structurally aligned well with S201 of LC/B and L230 of LC/T aligned well with I227 of LC/B (**Figure 2.1**). We questioned whether the different composition of S1' pocket contribute to not only the different recognition of P1', but also the P2' site of VAMP-2, which further affects the different catalytic activities of LC/B and LC/T.

Mutagenesis was then performed to swap the residues between the S1' pocket of LC/B and LC/T. Mutation of LC/T(P205S), which resulted in replacement of LC/T S1' residue P205 with LC/B S1' residue S201, showed ~80-fold reduction on *k<sub>cat</sub>*, yet the *K<sub>m</sub>* remained unchanged. The mutation LC/T(L230I) that resulted in the replacement of LC/T S1' residue L230 with LC/B S1' residue I227 showed ~20-fold elevated *k<sub>cat</sub>*, but similar *K<sub>m</sub>* (**Table 2.1, Figure 2.2a**). The data suggested that proline and isoleucine were the best residues to form the S1' pocket of LC/T and interact with P1', F77 of VAMP. To further confirm this hypothesis, swapping of residue was performed for the S1' pocket of LC/B. The mutation of LC/B (I227L) that resulted in replacement of LC/B S1' residue I227 with LC/T S1' residue L230, showed ~590-fold reduction of *k<sub>cat</sub>*, with no change of *K<sub>m</sub>*. The mutation of LC/B (S201P), which led to replacement of LC/B S1' residue S201 with LC/T S1' residue P205, showed ~10-fold increase of *k<sub>cat</sub>* and no change of *K<sub>m</sub>* (**Table 2.1, Figure 2.2b**). The data further confirmed that residues proline and isoleucine were the major components of optimal S1' pocket of LC/B and LC/T. The data also suggested that the substrate recognition pockets of LCB and LC/T were not optimal and the optimization of these pockets could improve their catalytic activity. To determine that the change of S1' pocket of LC/B and LC/T did not change their substrate specificities, all the four mutations were used to test their cleavage of VAMP-2 F77E. None of the above mutations could cleave F77E, suggesting that the scissile bond of VAMP-2 for LC/B and LC/T S1' pocket mutations remained the same (**Figure 2.2a, b**).

**Table 2.1 Kinetic constants of LC/B, LC/T and their derivatives.**

LCs	LC Pockets	LC derivative	$K_m$ ( $\mu\text{M}$ )	$k_{cat}$ ( $\text{S}^{-1}$ )	$k_{cat}/K_m$ ( $\text{S}^{-1} \cdot \mu\text{M}^{-1}$ )
		Wt-LC/B	$1.7 \pm 0.3$	1.1	$6.5 \times 10^{-1}$
LC/B	S1'	S <sup>201</sup> P	$1.6 \pm 0.2$	11.5	7.2
	swapping				
	S1' swapping	I <sup>227</sup> L	$1.6 \pm 0.4$	$1.8 \times 10^{-3}$	$1.1 \times 10^{-3}$
		Wt-LC/T	$4.1 \pm 0.2$	$1.6 \times 10^{-1}$	$3.9 \times 10^{-2}$
LC/T	S1' swapping	P <sup>205</sup> S	$4.4 \pm 0.4$	$2.1 \times 10^{-3}$	$4.7 \times 10^{-4}$
	S1' swapping	L <sup>230</sup> I	$4.2 \pm 0.2$	4.1	$9.7 \times 10^{-1}$
	S1, S1' swapping	K <sup>168</sup> E, L <sup>230</sup> I	$4.0 \pm 0.4$	15.9	4.0
	S3, S1, S1' swapping	K <sup>168</sup> E, L <sup>230</sup> I, R <sup>188</sup> M	ND	ND	ND

ND, Not Determined, the enzyme is too inactive to determine the kinetic constants.

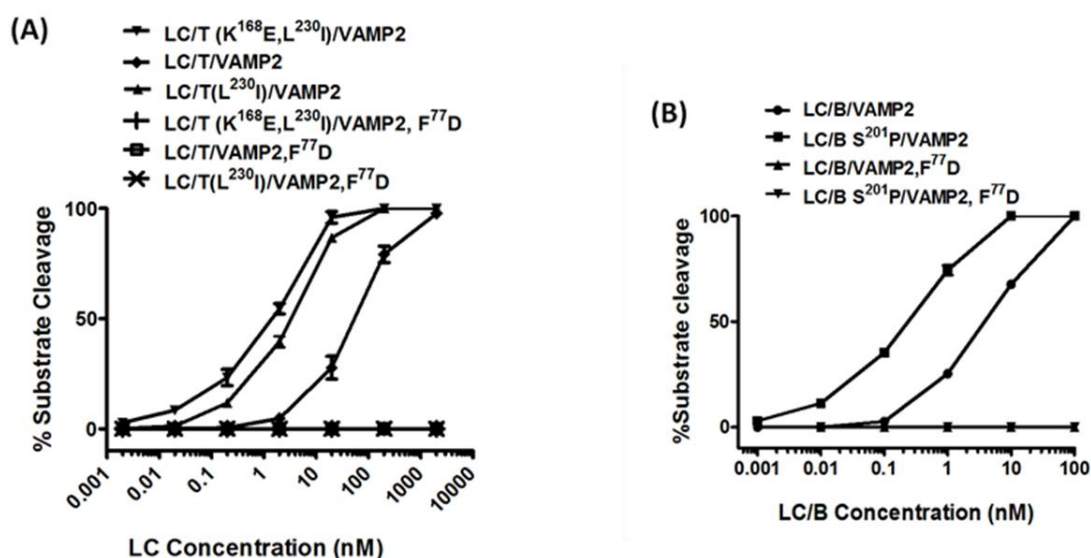


**Figure 2.2 Different catalytic activities of LC/T, LC/B and their derivatives to substrate VAMP-2.**

Recombinant VAMP-2 (5  $\mu\text{M}$ ) were incubated with varying concentrations of LC/T, LC/B or their derivatives in 10 mM Tris-HCl (pH 7.6) with 20 mM NaCl at 37°C for 10 min. Reactions were stopped by adding SDS-PAGE buffer and boiled for 5min. Cleaved and uncleaved VAMP-2 were resolved by SDS-PAGE. (A) Linear velocity of LC/T and derivatives on VAMP-2; (B) linear velocity of LC/B and derivatives on VAMP-2. Error bar represents the standard deviation of three independent repeats for each assay.

#### 2.4.2 Optimization of LC/T S1' pocket regained optimal recognition of P2' site

Since S1' and S2' pockets were side by side and closely resided in the active site of LC/B and LC/T, we then asked whether the different composition of S1' pocket of LC/B and LC/T were the causes of the difference between the S2' pocket of LC/B and LC/T. The S2'

pocket of both LC/B and LC/T contained an arginine residue. However, R370 of LC/B exhibited direct interaction with E78 of VAMP, while R374 of LC/T did not interact directly with E78 of VAMP-2. In addition, the mutation of P2' site of VAMP-2, E78A, showed less effect on LC/B cleavage but more for LC/T cleavage. Therefore, LC/T (L230I) with the optimal S1' pocket was used to test its activity on VAMP-2 mutation E78R. In our assay condition, the amount of LC/T to cleave 50% VAMP-2 was about 120nM, while at concentration of 36,000nM, LC/T still showed no cleavage on VAMP-2 (E78R). However, LC/T (L230I) cleaved VAMP-2 about~24 fold more efficiently than LC/T, while LC/T (L230I) cleaved VAMP (E78R) with the same efficiency of LC/T to cleave VAMP-2, with greater than 360-fold more efficient than LC/T to cleave VAMP E78R (**Table 2.2**). These data suggested that the optimization of S1' pocket of LC/T enhanced the tolerance of P2' site mutation. This also explained that the mutation of P2' site of E78resulting in much greater effect on LC/T substrate cleavage than that of LC/B substrate cleavage was due to less optimal composition of LC/T S1' pocket. Previous study also showed that LC/B S2' pocket residue, R370, interacted and formed salt bridge with P2 site E78, whereas theS2' pocket residue R374 did not (150). To test whether the different S2'-P2' interaction between LC/B and LC/T was due to the less optimal composition of S1' pocket, the efficiency of LC/T (L230I, R374E), a swap of LC/T residue R374 with E78 of VAMP-2, to cleave VAMP-2 (E78R), a swap of VAMP-2 residue E78 with R374of LC/T, was determined. LC/T (L230I, R374E) showed no cleavage on VAMP-2, while LC/T (L230I, R374E) was able to cleave VAMP-2 (E78R) more efficient than LC/T to cleave VAMP-2 (**Table 2.2**). The data suggested that the less optimal organization of LC/T S1' pocket affect the direct interaction between R374 of LC/T and E78 of VAMP-2.

**Table 2. 2 Results of a compensatory mutational assay for interactions of LC/T with VAMP-2 and derivatives.**

	50% cleavage of VAMP-2	ratio of activity (LC:LC derivative)	50% cleavage of VAMP-2 (R <sup>78</sup> E)	ratio of activity (LC:LC derivative)
LC/T	120nM		>36000nM	
LC/T(L <sup>230</sup> I)	5nM	24	100nM	>360
LC/T(K <sup>168</sup> E, L <sup>230</sup> I)	1.2nM	100	24nM	>1440
LC/T(L <sup>230</sup> I, R <sup>370</sup> E)	>36000nM	<1/300	50nM	>720

### 2.4.3 Optimization of S1' and S1 substrate recognition pockets further enhanced LC/T activity

Our previous study also identified two residues that contributed to the elevated activity of LC/T(150). Mutation of S1 pocket residue, LC/T (K168E), and S3 pocket residue, LC/T

(R188M), showed increased catalytic activity of LC/T. These mutations were incorporated into LC/T (L230I) mutation to test their effect on LC/T activity. Double mutations, LC/T (K168E, L230I) became ~100-fold more active than LC/T on substrate VAMP-2 through increasing its  $k_{cat}$ , but not  $K_m$  (**Table 2.1, Figure 2.2a**). A triple mutation, LC/T (K168E, L230I, R188M) showed no activity on VAMP-2 suggesting that combining these three mutations in the active site of LC/T may impair the correct conformation of the active site of LC/T (**Table 2.1**).

#### **2.4.4 Side chain positioning of L230 of LC/T affects its optimal recognition of both P1' and P2' sites**

Both isoleucine and leucine were hydrophobic residues and supposed to be able to interact with F77 of VAMP-2 through hydrophobic interaction. However, in the case of LC/B and LC/T, the isoleucine in S1' pocket of LC/B and LC/T worked much better than leucine in that position. It could be due to the different positioning of isoleucine residue in the pocket that interacted well with F77 of VAMP-2. Structural analysis of S1' pockets of LC/B and LC/T revealed that I227 in LC/B resided in a flatter position than L230 in LC/T. The bulky conformation of leucine in LC/T may push the interacting residue F77 outward, which restrained the interaction between R374 and E78 of VAMP-2. The flatter position of isoleucine in LC/B may provide an optimal position for fitting the F77 and E78 of VAMP-2 to the active site of LC/B, allowing the perfect interactions of both I227-F77 and R370-E78. To proof this hypothesis, the crystal structure of LC/T (K168E, L230I) was determined. **Figure 2.3a** illustrated the Fo-Fc electron density of L230I mutations in LC/T (K168E, L230I) structure. LC/T (K168E, L230I) structure showed perfect alignment to LC/T with RMSD=0.150(370 to 370 atoms with 421 atoms aligned) suggesting that the overall conformation of LC/T (K168E, L230I) remained intact compared to LC/T. LC/T (K168E, L230I) also aligned well with LC/B with RMSD=0.750 (341 to 341 atoms with 421 atoms aligned). The crystallographic statistics of LC/T(K168E, L230I) was summarized (**Table 2.3**). The structure showed that the mutation of leucine to isoleucine flatten the S1' pocket to similar level as LC/B (**Figure 2.3**). Most importantly, we observed that the distance between the side chain of L230 and R374 of LC/T was 7.2 Å and that of I227 and R370 was 7.9Å in LC/B. The mutation, L230I, increased the distance between the side chain of I230 and R374 of LC/T to 8.3Å (**Figure 2.4**). These data further supported that distance between S1' and S2' pockets in LC/B and LC/T determined their efficiency of recognition of P1' and P2' sites of VAMP-2. The wider space between the S1' and S2' pockets favored the proper fitting of both P1', F77 and P2', E78 of VAMP-2 into these two pockets.

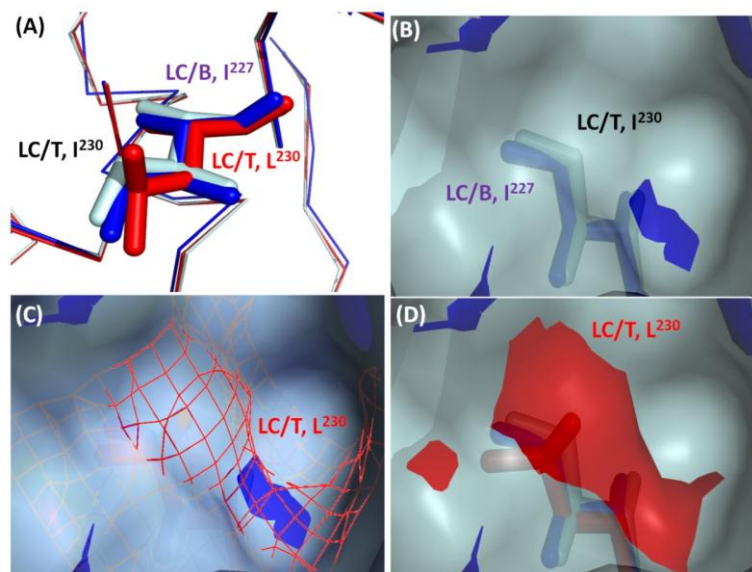


**Figure 2.3 Different positioning of S1' residue of LC/B, LC/T and LC/T(K<sup>168</sup>E, L<sup>230</sup>I).**

(A) Different positioning of S1' pocket residue, I<sup>227</sup> in LC/B (blue), L<sup>230</sup> in LC/T (red) and I<sup>230</sup> in LC/T(K<sup>168</sup>E, L<sup>230</sup>I) (gray); (B) surface demonstration of S1' pocket comprising I<sup>227</sup> in LC/B (blue), and I<sup>230</sup> in LC/T(K<sup>168</sup>E, L<sup>230</sup>I) (gray); (C) Bulking surface of S1' pocket of LC/T comprising L<sup>230</sup> (red) with mesh surface demonstration; (D) Bulking surface of S1' pocket of LC/T comprising L<sup>230</sup> (red) with solid surface demonstration.

**Table 2.3 The crystallographic statistics of LC/T (K<sup>168</sup>E, L<sup>230</sup>I).**

LC/T (K <sup>168</sup> E, L <sup>230</sup> I)	
<i>Data collection</i>	
Space group	C222
Unit cell parameters (Å)	
<i>a</i>	105.38
<i>b</i>	176.83
<i>c</i>	57.36
Resolution range (Å)	52.69-2.60 (2.74-2.60)
No. of total reflections	113923
No. of unique reflections	16451
<i>I</i> / $\sigma$	13.9 (3.9)
Completeness (%)	97.7 (97.4)
<i>R</i> <sub>merge</sub> (%)	9.5(18.1)
<i>Structure refinement</i>	
Resolution (Å)	48.12-2.60
<i>R</i> <sub>cryst</sub> / <i>R</i> <sub>free</sub> (%)	23.76/26.64
r.s.m.d. bonds (Å)/angles (°)	0.015/1.838
No. of reflections	15636
Working set	14815
Test set	821
No. of atoms	3317
Protein atoms	3179
Water molecules	138
Average <i>B</i> -factor (Å <sup>2</sup> )	
Main chain	34.52
Side chain	34.36
Water molecules	32.88

### 2.4.5 Activities of LC/B, LC/T and their derivatives on endogenous VAMP-2

To check the activities of LC/T derivatives on natural substrate VAMP-2 in neuronal cells, different constructs of LC/T derivatives were incubated with Neuro2A lysate. **Figure 2.5** showed that LC/T(K168E, L230I) was more active than LC/T in cleaving endogenous VAMP-2 from Neuro 2A cells. LC/B (S201P) was also more active than LC/B on endogenous VAMP-2. Surprisingly, LC/B and LC/B (S201P) were more active than LC/T and LC/T (K168E, L230I) on endogenous VAMP-2 even though the activity of LC/T(K168E, L230I) was slightly higher than Wt-LC/B on recombinant VAMP-2,

suggesting that LC/B is more active to cleave natural substrate VAMP-2, which imply that LC/B is more appropriate than LC/T to be used as human therapy.

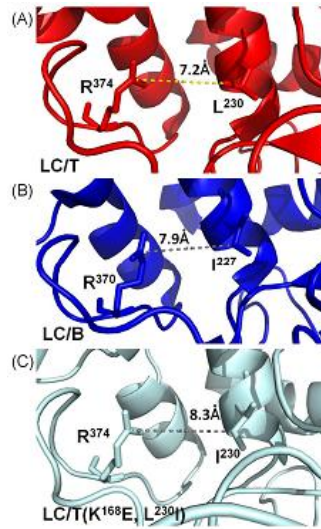


**Figure 2. 4 Different distances between the residues in S1' and S2' pockets.**

The distance between S1' residue and S2' residues of LC/T (A), LC/B (B) and LC/T(K<sup>168</sup>E, L<sup>230</sup>I) (C) were measured in PyMol program. The surface distance between these two residues were measured.

The distance between R<sup>370</sup> and L<sup>230</sup> in LC/T was about 7.2Å, distance between R370 and I227 in LC/B was 7.9Å, and distance between R<sup>374</sup> and I<sup>230</sup> in LC/T(K<sup>168</sup>E, L<sup>230</sup>I) was about 8.3Å.

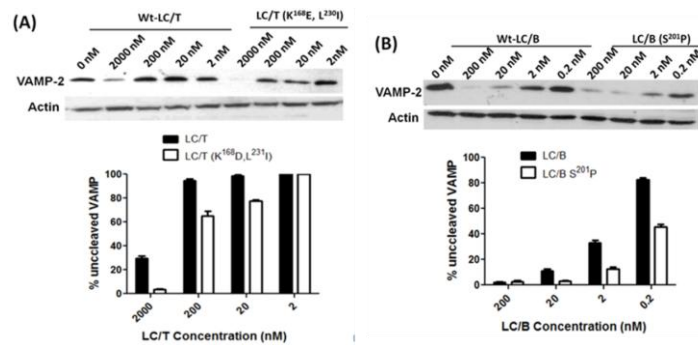


**Figure 2. 5 Cleavage of endogenous VAMP-2 by recombinant LC/B, LC/T and their derivatives.**

(a) Cleavage of endogenous VAMP-2 by LC/T and derivatives. Neuro 2A cell lysate was incubated with different amounts of LC/T and derivatives at 37°C for 10min in 10ul volume. The assays were stopped by adding equal amount of SDS-PAGE sample buffer and boiled for 10min. The cleavage of VAMP-2 was detected by SDS-PAGE and probing with anti-VAMP-2 antibody. Upper panel showed the Western blot of membrane by anti actin (as control for total protein level) and anti VAMP-2 antibodies. The decreasing VAMP-2 signal represents the proportion of cleaved endogenous VAMP-2. Lower panel was the quantification of the upper panel. (b) Cleavage of endogenous VAMP-2 by LC/B and derivatives. The assay condition and data interpretation were the same as that of LC/T assay.

## 2.5 Discussion

To date, there is no solution to immune resistance issue of BoNTs therapy. Attempt has been made to block the epitopes on the BoNTs that are involved in neutralizing antibody production. By probing the neutralizing antibodies from resistant patients to different domains of BoNT/A and B, a number of regions that may be involved in neutralizing antibody production have been identified (230-232). Based on researches that monomethoxypolyethylene glycol (mPEG) conjugated peptide could suppress the immune response, regions on the HC/B that showed strong immune response were conjugated to mmPEG and pre-immunized mice before the administration of BoNT/A. It was shown that some of the mPEG conjugated peptides could actually reduce the neutralizing antibody production (233). This finding suggests that the tolerization procedure might be potentially useful for clinical applications to immune resistant patients.

Since the BoNTs therapeutic doses have direct effect on the development of BoNTs immune resistance, the best way to overcome the immunoresistance problem in BoNTs is to engineer more active BoNTs, which will reduce the amounts of protein required for therapy and may decrease the development of immune response to the therapy. Rummel et al have modified a ganglioside binding motif of the HC domain of BoNT/B that enhances the binding and toxicity to up to three-fold relative to the wild type toxin (234). However, the engineering of BoNTs through modification(s) of its receptor binding sites may affect the selectivity of the binding event and protection by current vaccine derived from the HCs of BoNTs. In addition, the modification of binding site(s) may not successfully increase the potency enough to prevent the development of immunoresistance. Modification of LC to alter its activity may well be a better way to achieve this goal.

The understanding of the substrate recognition and specificity has opened up new opportunity to engineer novel BoNT LC with different activities and substrate specificities. In LC/A, mutation of an active site residue of LC/A, K165L, resulted in 4-fold increase in substrate hydrolysis (171). A comparative study was conducted for LC/B and LC/T to provide proof of principle to engineer LC of CNTs with elevated activities. Comparative study of LC/B and LC/T substrate recognition showed that the S1 pocket mutation LC/T (K168E) increased the rate of native VAMP-2 cleavage to a level approaching that of LC/B, depicting the molecular basis for the lower  $k_{cat}$  that LC/T possesses for VAMP-2 cleavage relative to LC/B. In addition, R188M, a S4 pocket mutation, increased LC/T substrate hydrolysis by ~5 fold (150). Further researches showed that the most important determinant of the activity of LC/B and LC/T resides in their S1' pocket. The side chain of L230 that formed a bulky shape in the active site of LC/T dramatically affected its recognition of P1'

and P2' site of VAMP-2, which also suggested that the recognition of different sites of VAMP-2 by different pockets of BoNT was closely related. Compromised optimization of one pocket could affect the substrate recognition efficiency of the other pocket. The mutation of L230I increased LC/T activity by ~25-fold and the double mutation LC/T (K168E, L230I) increased catalytic activity by ~100-fold. For LC/B, the original I227 conferred its high activity. However, compared to LC/T, the S201 in the S1 pocket seemed less optimal than proline in the corresponding site of LC/T. The mutation of LC/B S201P increased LC/B activity by more than 10-fold. The LC/T derivative also exhibited higher activity on native VAMP-2 in Neuro2A cell, with less amount of LC/T derivative being required to achieve the similar effect as LC/T. The highly active LC/T derivative can be used as a more effective tool to study mechanisms of exocytosis in central neuron. The LC/B derivative with elevated activity could be developed into novel therapy that may minimize the immune resistance issue of BoNT/B therapy.

Another interesting observation of this study is the different catalytic activities of LC/B and LC/T on recombinant VAMP-2 and native VAMP-2 from Neuro2A cells. LC/T showed much lower activity on native VAMP-2 substrate than LC/B. The LC/T(K168E, L230I) showed higher catalytic activity on recombinant VAMP-2 than Wt-LC/B, while it displayed lower activity on native VAMP-2 from Neuro2A cells than LC/B. These imply that the recognition of native VAMP-2 in neuron is a complicated process because inside the neuron, VAMP-2 is present as a SNARE complex formed by VAMP-2, SNAP25 and Syntaxin 1a. The accessibility of VAMP-2 for LC/B and LC/T may determine the efficiency of native VAMP-2 cleavage by BoNT LCs. Our previous study on LC/A also support the idea that in addition to the substrate recognition region, LC/A also interacts with SNAP25 at an additional site outside the SNARE complex to gain initial access to SNAP25(235). Further researches will be needed to figure out the different accessibility of LC/B and LC/T to VAMP-2 in a complex conformation.

# Chapter Three: A simple, rapid and sensitive FRET assay for Botulinum Neurotoxin Serotype B Detection\*

## 3.1 Abstract

BoNTs, the most potent naturally-occurring neurotoxins known to humans, comprise seven distinct serotypes (BoNT/A-G), each of which exhibits unique substrate specificity. Many methods have been developed for BoNT detection, in particular for BoNT/A, with various complexity and sensitivity, while substrate based FRET assay is considered as the most widely used approach due to its simplicity and sensitivity. In this study, we designed a VAMP-2 based FRET assay based on the understanding of the VAMP-2 and LC/B interactions in our previous studies. The current design constituted the shortest peptide, VAMP-2 (63-85), with FRET dyes (EDAN and Dabcyl) labeled at position 76 and 85, respectively, which showed minimal effect on VAMP-2 substrate catalysis by LC/B and therefore enhanced the sensitivity of the assay. The FRET peptide, designated as FVP-B, was specifically to LC/B, with a detection sensitivity as low as ~20 pM in 2 h. Importantly, FVP-B showed the potential to be scaled up and used in high throughput screening of LC/B inhibitor. The currently developed FRET assay is the most economic and sensitive FRET assay for LC/B detection so far.

Key words: Botulinum Neurotoxin B, FRET, rapid detection assay, sensitive

Abbreviations: BoNT/B, Botulinum Neurotoxin B; LC, light chain; VAMP-2, vesicle associated membrane protein-2; SNARE, soluble NSF attachment receptor

\*Most of the material of this chapter have been published as: Guo J, Xu C, Li X, Chen S. entitled "A simple, rapid and sensitive FRET assay for botulinum neurotoxin serotype B detection" published in *PLoS One*. 2014 Dec 1;9(12):e114124. doi: 10.1371/journal.pone.0114124. eCollection 2014.

## 3.2 Introduction

Botulinum neurotoxins (BoNTs), the most potent protein toxins identified so far, cause human botulism (172). There are seven different BoNT serotypes, designated as A to G, and more than 30 different subtypes being identified so far (185,236). BoNTs cause food-borne, wound and infant botulisms. Although large-scale outbreak of botulism rarely occurred

nowadays, sporadic cases of natural botulisms and medical emergencies due to the clinical uses of BoNTs are still a huge threat to human. Most importantly, due to its potency and ease of distribution, the Centres for Disease Control and Prevention (CDC) in the US have listed botulism as one of the six most dangerous bioterrorist threats ([www.bt.cdc.gov/agent/agentlist-category.asp](http://www.bt.cdc.gov/agent/agentlist-category.asp)).

BoNTs are zinc-dependent protease; they are activated by proteolysis to generate 150-kDa dichain molecules, which mediate their exquisite specificity and neurotoxicity. BoNTs are typical A-B toxins that comprised of three independent domains. A 50 kDa *N*-terminal light chain (LC) is responsible for its enzymatic activity and a zinc-dependent protease. A 100 kDa *C*-terminal heavy chain (HC) involved in receptor binding and cellular uptake is composed of a translocation domain (HCT) and a receptor binding domain (HCR) (195,237,238). BoNTs apply a four-stage mechanism when penetrating cells: binding, internalization, membrane translocation and target modification. However, two mechanisms by which the BoNT complex crosses the epithelial barrier have been suggested: receptor-mediated endocytosis and ternary HA complex mediated destruction of the intercellular junctions, followed by paracellular influx (239-241). The driving force in mammalian neuronal exocytosis process is the formation of complexes between the family of soluble *N*-ethylmaleimide-sensitive factor attachment protein receptors (SNAREs): the vesicle VAMP-2, the plasma membrane SNARs, SNAP25 and syntaxin 1a (242), which are the targets of the seven BoNTs: serotypes B, D, F and G cleave VAMP-2, serotypes A and E cleave SNAP25, and serotype C cleaves both SNAP25 and syntaxin 1a (237). The neurotransmitter release will be blocked upon the cleavage of any of the aforementioned SNARE proteins, leading to the classical paralytic symptoms of botulism.

For BoNT/A, the estimated lethal dose for humans is 1 $\mu$ g/kg for oral administration (172). If diagnosed before the onset of symptoms, botulism can be effectively treated immunologically by using an equine trivalent antitoxin ([www.bt.cdc.gov/agent/agentlist-category.asp](http://www.bt.cdc.gov/agent/agentlist-category.asp)). Early BoNTs detection is critical to apply medical treatment on time. Currently, the “golden standard” in BoNT detection in culture, serum and food samples is mouse bioassay (MBA). It has a serotype and subtype dependent sensitivity of between 10-100pg/ml (173,174), and can detect all serotypes and subtypes both in their free and complex forms. However, it is time-consuming (175) and causes serious ethical concern, which encouraged the attempts to develop different alternative assays to replace the MBA. PCR-based techniques aiming at detecting *bont* genes by conventional or quantitative amplification reactions, leading to detection limit of 10<sup>3</sup>-10<sup>5</sup> genome equivalents (GE) per ml (176-179). Mass spectrometry (MS) is a powerful tool in detecting different BoNT serotypes unambiguously (180-184), an amino acid substitution database has been

established by Barr and co-workers, allowing for the identification of multiple BoNT/B subtypes (185). By far, the most commonly employed methods for BoNT detection in vitro is ELISA (enzyme-linked immunosorbent assay)-based technologies, which have high sensitivity, simplicity in performing the assay and robust performance (174,186-189). Since the identification of the substrates of BoNTs, substrate based activity assays of BoNTs have been developed and improved, displaying the serotype-specific proteolytic cleavage of SNAREs (190). The combination of the endopeptidase assay with FRET (Förster resonance energy transfer) that utilizes the nature of fluorescence donor and fluorescence acceptor (or quencher) makes it very powerful and sensitive BoNTs detection (191,192). Substrate based FRET assay has the advantages of simple, fast, cost effective and easy for scale up, while the detection sensitivity was shown to be very low due to the reduced activity of FRET peptide.

In the current work, we developed a VAMP-2 based FRET assay for BoNT/B detection based on our research on the characterization of VAMP-2 and LC/B interactions. We found that VAMP-2(60~87) is the optimal substrate for LC/B (243). In addition, the contribution of each residue in this fragment of VAMP-2 has also been well understood for LC/B substrate hydrolysis. Based on our understanding of LC/B recognition of VAMP-2, we developed a VAMP-2 based FRET assay for simple, rapid and sensitive detection of LC/B.

### **3.3 Experimental Section**

#### **3.3.1 BoNT LCs Recombinant Proteins**

Recombinant LC/B protein was purified as detailed in Chapter Two and previously described(243). Other BoNT LCs including LC/A (1-425), LC/E (1-408), LC/F (1-446), LC/D (1-442) and LC/TeNT-(1-436) were expressed and purified as that of LC/B and as described previously (243-246).

#### **3.3.2 Fluorogenic Peptide design**

Previous study showed that the optimal substrate for LC/B is VAMP-2 (63~85). Mutational analysis data also showed that Q76 of VAMP-2 contributed limited effect on the activity of LC/B(243). Therefore, the FRET peptide includes the 63~85 of VAMP-2 with EDANS labeled L-Glu at replaced Q76 and Dabcyl labeled Lys at the C-terminus. The peptide sequence is as follow, Leu-Asp-Asp-Arg-Ala-Asp-Ala-Leu-Gln-Ala-Gly-Ala-Ser-L-Glu(EDANS)-Phe-Glu-Thr-Ser-Ala-Ala-Lys-Leu-L-Lys (Dabcyl) (**Figure 3.1**). EDANS (L-glutamic acid g-[b-(5-naphthyl sulfonic acid)-ethylenediamine] ester) and Dabcyl (*N*<sup>ε</sup>-dimethylaminophenyldiazobenzoyl) is a FRET pair (**Figure 3.1**). EDANS works as

fluorescent donor and Dabcyl acts as fluorescent dye. In this design, the FRET peptide showed limited fluorescent signal. After cleavage by LC/B, EDANS was separated from Dabcyl and fluorescent signal increased. The FRET peptide was named as FVP-B.

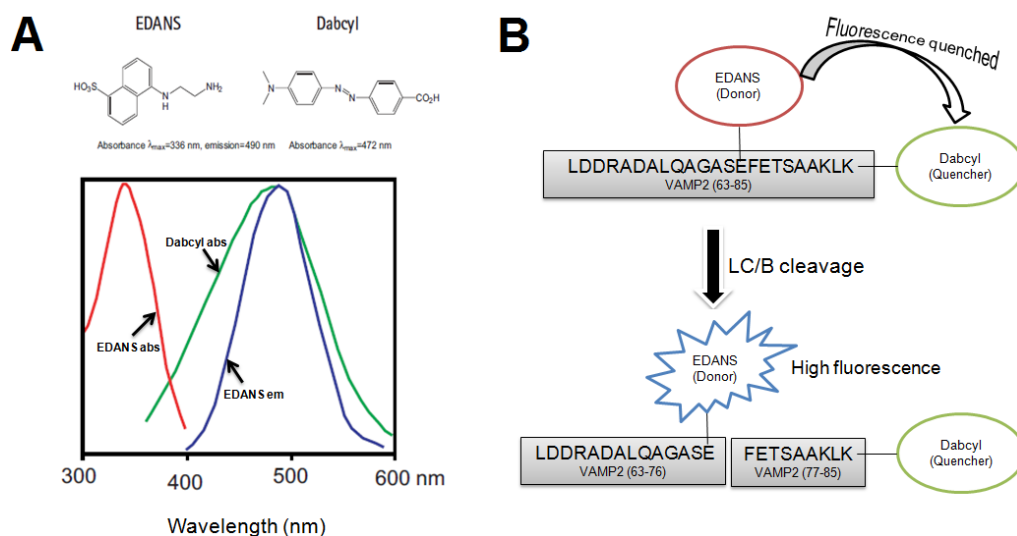


**Figure 3.1 Spectral properties of EDANS-Dabcyl pair (247) and the flowchart of the experimental design.**

(A) EDANS-Dabcyl is a widely used donor-quencher pair. The optimal absorbance and emission wavelength of EDANS are  $\lambda_{\text{abs}}=336$  nm and  $\lambda_{\text{em}}=490$  nm respectively, and for Dabcyl, the maximum absorbance wavelength is  $\lambda_{\text{abs}}=472$  nm, which, to a large extent, overlap with the emission spectra of EDANS. When they are in a close proximity (10-100 Å), the energy emitted from EDANS will be quenched by Dabcyl, resulting in low or no fluorescence; and when they are separated upon substrate cleavage, for example in this design, the fluorescence will increase. So from the fluorescence intensity change, the enzyme could be detected continuously and directly. (B) Based on the principle of FRET and our previous study, we chose the optical LC/B cleavage length of VAMP-2 (63-85) as the linker between EDANS-Dabcyl.

### 3.3.3 Fluorogenic Peptide synthesis

All commercial materials (Sigma-Aldrich, Fluka of USA and GL Biochem of China) were used without further purification. All solvents were reagent grade or HPLC grade (DUKSAN). Dry dichloromethane (DCM) was distilled from calcium hydride ( $\text{CaH}_2$ ). All separations involved a mobile phase of 0.05% TFA (*v/v*) in acetonitrile (solvent A)/0.05% TFA (*v/v*) in water (Solvent B). HPLC separations were performed with a Waters HPLC system equipped with a photodiode array detector (Waters 2996) using a Vydac C18 column (5  $\mu\text{m}$ , 300 Å, 4.6 x 150 mm) at a flow rate of 0.6 mL/min for analytical HPLC and Vydac Prep C18 column (10  $\mu\text{m}$ , 300 Å, 22 x 250 mm) at a flow rate of 10 mL/min for preparative HPLC. Low-resolution mass spectral analyses were performed with a Waters 3100 mass spectrometer.

The solid phase peptide synthesis was carried out manually using 2-Chlorotrityl chloride resin (loading 0.5mmol/g). Peptides were synthesized under standard Fmoc/*t*-Bu protocols. The following Fmoc amino acids from GL Biochem were employed: Fmoc-Ala-OH, Fmoc-Arg(Pbf)-OH, Fmoc-Asn(Trt)-OH, Fmoc-Asp(O*t*Bu)-OH, Fmoc-Gln(Trt)-OH, Fmoc-Glu(EDANS)-OH, Fmoc-Glu(O*t*Bu)-OH, Fmoc-Gly-OH, Fmoc-Ile-OH, Fmoc-Leu-OH, Fmoc-Lys(Boc)-OH, Fmoc-Lys(DABCYL)-OH, Fmoc-Met-OH, Fmoc-Phe-OH, Fmoc-Ser(*t*Bu)-OH, Fmoc-Thr(*t*Bu)-OH. Fmoc removal was executed using a solution of 20% piperidine in dimethylformamide (DMF) at room temperature for 30 min. Coupling of Fmoc protected amino acid units was carried out by activation with (*O*-(7-azabenzotriazol-1-yl)-*N,N,N',N'*-tetramethyluronium hexafluorophosphate (HATU) using *N,N*-diisopropylethylamine (DIPEA) in DMF at room temperature for 40 min. The Fmoc amino acids (2.0 equiv), HATU (2.0 equiv) and DIPEA (5.0 equiv) were dissolved in DMF and subsequently mixed with the resin manually. This procedure was repeated twice for each coupling. Upon completion of synthesis, the peptide resin was subjected to a cleavage of cocktail (TFA/*i*Pr<sub>3</sub>SiH/H<sub>2</sub>O, 95/2.5/2.5, *v/v/v*) for 2 h. The resin was filtered and the combined filtrates were blown off under a stream of condensed air. The crude product was triturated with cold diethyl ether to give a white suspension, which was centrifuged and the ether subsequently decanted. The remaining solid was purified by HPLC.

### 3.3.4 Proteolytic activity of LC/B and other LCs

All LCs used in this study was quantified using by SDS-PAGE using BSA standards. The FVP-B was prepared in 21mM stock in DMSO, aliquoted and stored at -20°C. It was diluted in reaction buffer (10mM Tris-HCl, 20mM NaCl, pH7.9) for assay.

For LC/B activity assay using FVP-B, certain amounts of FVP-B were mixed with different concentrations of LC/B and incubated in 500ul of reaction buffer in eppendorf tubes at 37°C for different time courses. The reaction mixture was transferred to a quartz Hellma® fluorescence cuvette (Sigma-Aldrich Co. LLC. USA). Fluorescent intensity was scanned using the LS-55 Fluorescence Spectrometer (PerkinElmer Inc. Massachusetts, USA), with the following parameters set: excitation: 336nm (slit: 10nm), emission: 380-650nm (slit: 10nm), speed: 100nm/min. For EDTA inhibition assays, different concentrations of EDTA were incubated with LC/B and FVP-B in the similar assay as described above, but detected both in fluorescence cuvette and black 96 well plate (OptiPlate™-96F, PerkinElmer, USA). All the data were repeated at least three times.

### 3.3.5 LC/MS analysis of the FVP-B cleavage by LC/B

200 nM LC/B, plus 8.4 μM FVP-B were mixed in reaction buffer to final volume of 500 μl, incubated at 37°C for 1 h. LC/MS analysis then was carried out on a Agilent 6540 Ultra

High Definition Accurate-Mass Q-TOF (Agilent-Technologies Inc., Wilmington, United States of America) equipped with an Agilent 1290 Infinity binary LC system. A 2  $\mu$ l portion of sample was injected into a C18 reverse column (Agilent Zorbax SB-C18, 2.1 x 100 mm, 1.8  $\mu$ m). The mobile phase solvent system included solvent A, Milli-Q<sup>®</sup> water with 0.1% formic acid, and solvent B, acetonitrile with 0.1% formic acid. The sample was firstly desalted with 5% solvent B at a flow rate of 0.3 ml/min for 3 min, eluted with a 17 min linear gradient of 5% to 90% solvent B at a flow rate of 0.3 ml/min. The mass spectrometer was operated in positive electrospray ionization mode. Other instrumental parameters were set as follow: Capillary voltage: 3500 V, Nozzle voltage: 1000 V, Fragmentor voltage: 175 V, Skimmer: 65 V, Octopole RF: 750 V.

### **3.4 Result**

#### **3.4.1 LC/B specificity of FVP-B**

The FRET assay is based on the detection of continuous signal increase resulting from the hydrolysis of FVP-B to separate quencher Dabcyl from the fluorescent donor EDANS. To verify the specificity of FVP-B to LC/B, FVP-B was used to test the cleavage by different LCs of BoNTs. In this assay condition where 200 nM each of the LCs were mixed with 8.4  $\mu$ M FVP-B in reaction buffer in 500  $\mu$ l reaction volume for 1 h incubation at 37°C, the fluorescence intensity of each reaction was quantified. The negative control was performed exactly the same as other reactions, but without adding the LCs in the reaction. **Figure 3.2** showed the fluorescent intensity of each reaction and the negative control. The result showed that dramatic increase of fluorescence intensity could be seen after incubating LC/B with FVP-B, whereas incubation of other LCs with FVP-B did not produce dramatic increase of fluorescence intensity, suggesting that FVP-B was specific for LC/B cleavage (**Figure 3.2**).

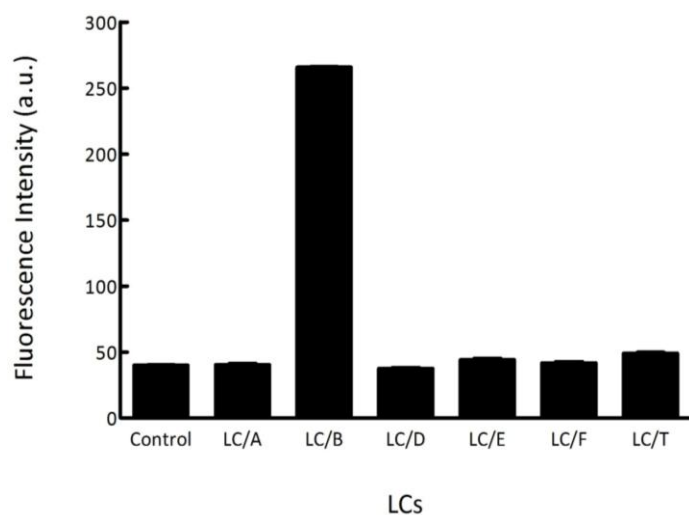


**Figure 3. 2 The specificity of the synthesized FVP-B.**

LCs (200 nM each) were mixed with 8.4  $\mu$ M FVP-B in reaction buffer to a final volume of 500  $\mu$ l, incubated at 37°C for 1 h, fluorescent intensity was measured by a Fluorescence Spectrometer in quartz cuvette. The data obtained were processed with GraphPad Prism.

The mixture sample of LC/B and FVP-B was then analyzed by LC/MS to prove the specific cleavage of FVP-B by LC/B. As shown in **Figure 3.3**, the uncleaved FVP-B could be detected (**Figure 3.3A**), and the C-terminal product (CT-product, **Figure 3.3B**) and the N-terminal product (NT-product, **Figure 3.3C**). The LC/MS results also prove that the sum of the molecular weights ( $M_r$ ) of CT-product ( $M_r = 1214.6$ ) and NT-product ( $M_r = 1708.8$ ) is about 2905.4 (with a  $H_2O$  molecular deducted), which is consistent with the uncleaved FVP-B ( $M_r = 2906.4$ ), indicating that LC/B can specifically cleave FVP-B at the desired site.

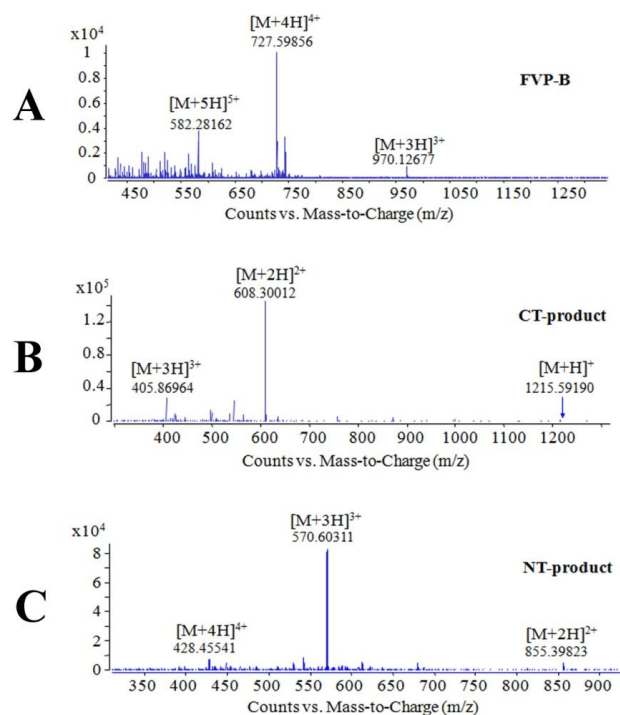


**Figure 3.3 LC/MS analysis of specific cleavage of FVP-B by LC/B.**

Mixture sample of FVP-B (8.4  $\mu\text{M}$ ) and LC/B (200 nM) from Figure 2 was analyzed by LC/MS to detect the full length FVP-B (A), CT-product (B) and NT-product (C).

### 3.4.2 FVP-B assay for LC/B activity detection

The effect of cleavage of FVP-B by LC/B over a specific time period was determined. Firstly, 228 nM LC/B was mixed with 8.4  $\mu\text{M}$  FVP-B in reaction buffer in 500  $\mu\text{l}$  reaction system and incubated at 37°C. The fluorescent intensity between 400 and 650 nm was measured every 30 min (except the last 1 h) over 480 min assay time. After 30 min incubation, dramatic increase of fluorescence intensity could be observed. The signal increased steadily until reaching a steady stage at 480 min. Sharp increase of fluorescent intensity continued for at least 120 min and the rate of fluorescence increase slowed down after about 180 min and finally reached to a steady state at 480 min (**Figure 3.4A**). LC/B velocity curve was generated by recording the rate of increase in fluorescence intensity at 502 nm. The curve clearly indicated that fluorescence intensity increased over time (**Figure 3.4B**). To optimize the assay and test the sensitivity of FVP-B for LC/B detection, the LC/B concentration was titrated. First, FVP-B concentration was fixed at 8.4  $\mu\text{M}$  and 10-fold dilution of LC/B concentration was performed. A dramatic fluorescent intensity increase was shown at LC/B concentration of 228 nM. Obvious fluorescent intensity increase can be seen at LC/B concentration of 22.8 nM, yet no fluorescent intensity change can be observed at lower concentration of LC/B (**Figure 3.5A**). Secondly, LC/B concentration was fixed at 22.8 nM and 5-fold FVP-B titration was performed. Significant fluorescent intensity

increase can be seen when FVP-B concentration was at 8.4  $\mu\text{M}$ , and relatively obvious fluorescent change can be seen at 1.68  $\mu\text{M}$  of FVP-B, but not at lower concentration (**Figure 3.5B**). However, when the concentration of FVP-B was fixed at 1.68  $\mu\text{M}$ , we further diluted the LC/B to 22.8 pM with extended incubation time. After 2 h incubation at 37°C, obvious fluorescent intensity change can be detected, and 4 h incubation showed even dramatic fluorescent intensity change, but longer incubation time up to 8 h cannot produce any further increase in fluorescent intensity. The fluorescent intensity was stable (**Figure 3.5C and 3.5D**). Taken together, the assay optimization results showed that the detection sensitivity of the developed assay is about 20 nM of LC/B within 30 min, but the sensitivity can be improved to  $\sim$ 20 pM of LC/B with 2 h incubation. Additionally, we have tested the effect of different concentrations of zinc on LC/B activity and did not observe any association between zinc ion and LC/B activity (data not shown).

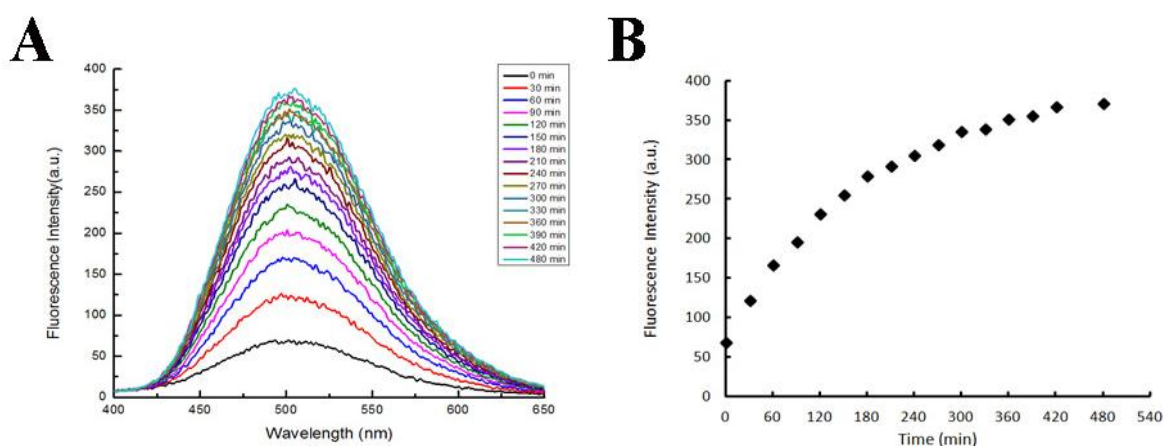


**Figure 3. 4 The feasibility of the synthesized FVP-B and our developed assay.**

(A) 228 nM purified LC/B was mixed with 8.4  $\mu\text{M}$  FVP-B in reaction buffer to a final volume of 500  $\mu\text{l}$ . Reaction was incubated at 37°C and the fluorescent intensity was measured in quartz cuvette every 30 min. The total duration of measurement was 8 h. The data were processed by Origin85. (B) The fluorescent intensity peak at 502 nm was selected to represent the trend of the whole data. The data were processed with Excel.

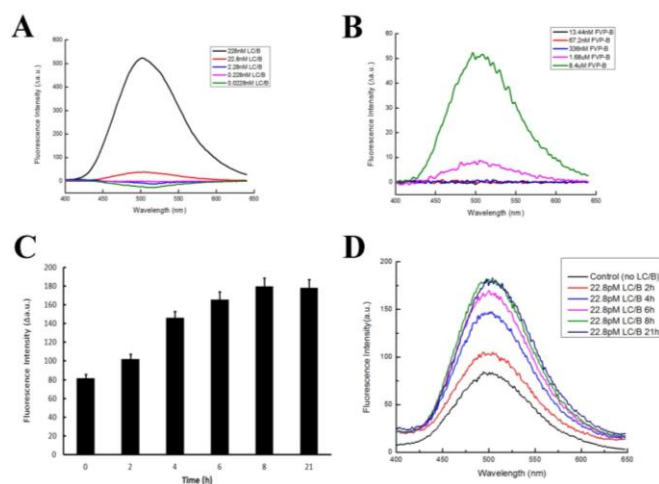


**Figure 3.5 Optimization of the developed assay system.**

To optimize the assay and test the sensitivity of our detection assay, ten-fold dilution of LC/B was performed with the concentration of FVP-B fixed at 8.4  $\mu\text{M}$  (A); five-fold dilution of FVP-B, with the LC/B concentration fixed at 22.8 nM (B); the fluorescent intensity change at 502 nm of further diluted LC/B to 22.8 pM with 1.68  $\mu\text{M}$  FVP-B and extended incubation time (C); and a spectrum representative of 22.8 pM LC/B incubated with 1.68  $\mu\text{M}$  FVP-B for extended time span (D). Viewing from the data, the detection sensitivity of the developed assay is about 22.8 nM of LC/B within 30 min, but the sensitivity can be improved to 22.8 pM of LC/B with 2 h incubation. The data were processed by Origin85 and Excel.

To further illustrate the sensitivity of the developed system, various amounts of LC/B were incubated with 8.4  $\mu\text{M}$  FVP-B in 500  $\mu\text{l}$  reaction volume for 1 h incubation at 37°C. The fluorescence intensities are potted as a function of LC/B concentrations (**Figure 3.6**). The limit of detection (LOD) is about 4.1ng/mL.

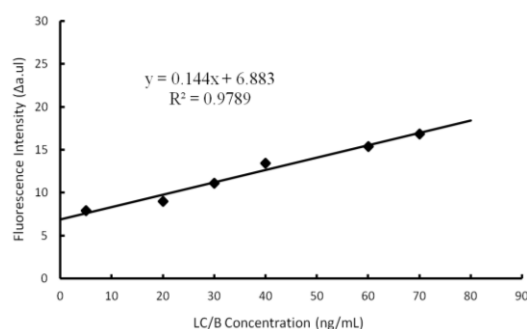


**Figure 3.6 Limit of detection of the developed LC/B detection system.**

Serial LC/B concentrations were incubated with 8.4  $\mu\text{M}$  FVP-B in 500  $\mu\text{l}$  reaction volume for 1 h incubation at 37°C. The fluorescence intensities are potted as a function of LC/B concentrations. At least five replicates were carried out.  $\text{LOD}=3\ast\text{S}/\text{k}$  (S means standard deviation of negative control, k means slope).

### 3.4.3 FVP-B as LC/B inhibitor screening assay

To prove that this assay can be scaled up for BoNT/B inhibitor screening, EDTA was used as an inhibitor of LC/B to test the validity of the assay. Different concentrations of EDTA were tested in the assay, where 228 nM of LC/B and 8.4  $\mu$ M FVP-B were mixed and incubated for 1 h at 37°C. The fluorescent intensity was recorded at 502 nm, measured both in fluorescent cuvette (500  $\mu$ l reaction volume, **Figure 3.7A**) and 96 well plate (100  $\mu$ l reaction volume, **Figure 3.7B**). At 0.1, 0.3, 0.5 and 1 mM EDTA, fluorescent intensity remained at the same level as control (no LC/B added), while at 0 mM of EDTA, the fluorescent intensity showed dramatic increase (**Figure 3.7A and 3.7B**). The data indicated that FVP-B based assay is a useful tool for LC/B inhibitor high throughput screening.

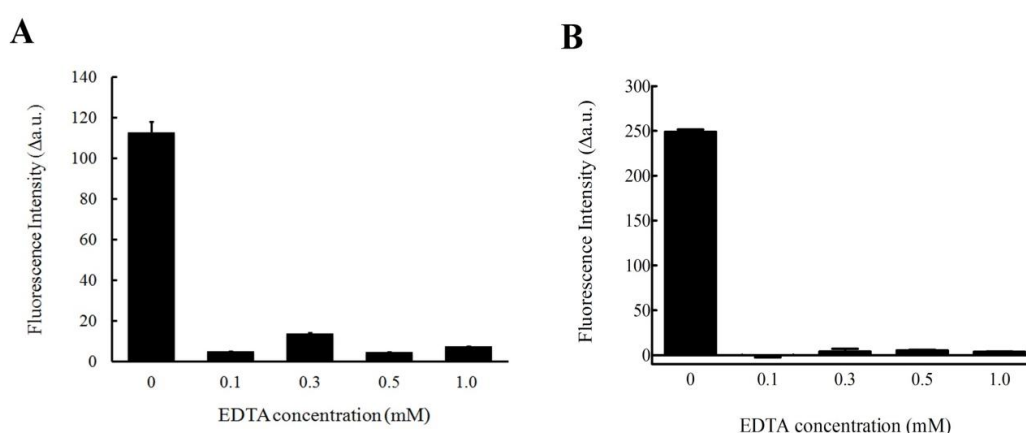


**Figure 3. 7 The inhibitory effect of EDTA on LC/B.**

228 nM of LC/B was mixed with 8.4  $\mu$ M FVP-B with reaction buffer to a final volume of 500  $\mu$ l, incubated at 37°C for 1 h, and then the fluorescent intensity was measured by a Fluorescence Spectrometer in quartz cuvette (A); 100  $\mu$ l reaction volume, which contained 228 nM LC/B with 8.4  $\mu$ M FVP-B, were carried out in 96 well plate after 1 h incubation at 37°C (B) For simplicity, the fluorescent intensity peak at 502 nm was selected. The data obtained were generated from at least three repeats, processed with Excel and GraphPad Prism, with the negative control data subtracted.

## 3.5 Discussion

BoNTs are the most potent naturally-occurring toxins known. Although BoNT/B is not as clinically important as BoNT/A in term of its ability to cause human botulism and its usefulness in various therapeutic processes, BoNT/B is still frequently linked to human botulism, in particular infant botulism. Data from CDC showed that 58.4% cases of infant botulism (387 out of 663) were attributed to BoNT/B during a 2001 to 2007 surveillance (248). In addition, BoNT/B is also used as human therapy to treat dystonia in addition to BoNT/A. Moreover, because of the many ethical and legal concerns over the standard

mouse bioassay, an alternative, simple and sensitive detection method is urgently needed to either detect trace of BoNT/B in food or for designing new potent inhibitor to neutralize the toxin. Recently, several new methods have been reported to detect BoNT/B with higher sensitivity in the picomolar to femtomol ranges (249); these include common methods like ELISA with comparable sensitivity as mouse bioassay (248,250), and fast detection methods such as micromachined BoNT/B detection sensor for BoNT/B detection within minutes, but with lower sensitivity (251). However, all these methods need complicated procedures, expensive apparatus and are difficult to be scaled up. FRET coupled LC/B detection methods have been reported before (191,252). However, the synthesized peptides were much longer (either contained VAMP-2 (residues 55-94) or VAMP-2 (residues 60-94)) than the peptide reported here. Most importantly, some have mutated or replaced the residue F<sup>77</sup> of VAMP-2, which will dramatically reduce the efficiency of LC/B to cleave this substrate according to our previous data that the P1' site played a very important role in enzyme catalysis: the mutant VAMP-2 (F<sup>77</sup>A) reduced the LC/B cleavage efficiency to more than 320-fold (243). In addition, there are several versions of FRET based peptides, for example, VAMPtide® (o-Abz/Dnp), VAMPtide® (FITC/DABCYL) and VAMPtide® (PL 150, Pya/Nop) available in market (List Biological Laboratories, INC. USA), and the latter one, VAMPtide® (PL 150, Pya/Nop), has been claimed with a LOD as low as 140 pg/mL after 5 h digest or 8 pg/mL after 24 h digest. Christine Anne *et al* reported a fluorogenic assay system for BoNT/B activity determination by using the VAMPtide® (PL 150, Pya/Nop), they claimed a 3.5 pg/mL detection sensitivity after 4 h incubation time (191). However, it is questionable that there is no effect of BoNT/B cleavage of peptide, as claimed by the authors, by replacing the native phenylalanine in position 77 by a *p*-nitrophenylalanine. Moreover, the cost of the claimed high sensitivity is longer incubation time, 4 h or even longer, for example, when compared with the present results which need as short as 1 h incubation to reach a 4.1 ng/mL LOD. The different applied reaction conditions, buffer, spectrometer sensitivity, for example, are another major factors affect the different sensitivities and LOD reported.

In this study, we developed a simple, fast and sensitive VAMP-2 based FRET peptide for LC/B detection. The detection sensitivity is about 20 pM of BoNT/B with 2h incubation. FRET based BoNTs detection method has been proven to be very useful in both clinical application and research. SNAPtide, a commercial 13mer FRET peptide developed for BoNT/A detected has been widely used in BoNT/detection and inhibitor screening in many researches (253-255). However, due to the lower cleavage efficiency by BoNT/A, the role of SNAPtide as high throughput assay was limited. Since FVP-B is designed based on the optimal substrate for BoNT/B, the FRET peptide we developed has similar cleavage

efficiency by BoNT/B as natural substrate VAMP-2. Actually, we have designed another version of FRET based peptide, the positions modified were A74 and T79, the single-letter sequences are 63-L D D R A D A L Q A G E-(Edans) S Q F E K-(Dabcyl) S S A K L K-85. Based on the previous investigation, the mutation or modification on 74 or 79 has less effect on LC/B cleavage than that of 76 or 85 (the two sites modified in the present FVP-B peptide) (243), but it showed much lower sensitivity and lower LC/B cleavage activity than FVP-B (data not shown). Therefore, FVP-B based assay represents a good FRET assay for BoNT/B detection and also proved to be useful for BoNT/B inhibitor screening when scaled up.

# Chapter Four: Unique substrate recognition mechanism of Botulinum Neurotoxin D light chain\*

## 4.1 Abstract

Botulinum neurotoxins (BoNTs) are the most potent protein toxins in nature. Despite the potential to block the release of neurotransmitter at the neuromuscular junction and cause human botulism, they are widely used in protein therapies. Among the seven BoNT serotypes, mechanisms of substrate recognition and specificity are known to a certain extent in LC/A, B, E and F, but not LC/D. In this study, we addressed the unique substrate recognition mechanism of LC/D and showed that this serotype underwent hydrophobic interactions with VAMP-2 at its V1 motif. The LC/D B3, B4 and B5 binding sites specifically recognize the hydrophobic residues in the V1 motif of VAMP-2. Interestingly, we identified a novel dual recognition mechanism employed by LC/D in recognition of VAMP-2 sites both at the active site and distal binding sites, where one site of VAMP-2 was recognized by two independent, but functionally similar LC/D sites that were complementary to each other. The dual recognition strategy increased LC/D tolerance to mutations and rendered it a good candidate for LC/D engineering to improve its therapeutic properties. In conclusion, the current study identified a unique, multistep substrate recognition mechanism by LC/D and provided insights for LC/D engineering and antitoxin development.

Key words: Botulinum Neurotoxin D, light chain, VAMP-2, substrate recognition and specificity, dual recognition

Abbreviations: BoNT/D, Botulinum Neurotoxin D; LC, light chain; VAMP-2, vesicle associated membrane protein-2; SNARE, soluble NSF attachment receptor

\*Most of the material of this chapter have been published as: Jiubiao Guo and Sheng Chen. Unique Substrate Recognition Mechanism of the Botulinum Neurotoxin D Light Chain. *J. Biol. Chem.* 2013 288: 27881-27887.

## 4.2 Introduction

The existing seven different botulinum neurotoxins (BoNTs) serotypes, A-G, are the most potent protein toxins. BoNT causes human and animal botulism, a flaccid paralysis caused by the blocking of neurotransmitter (usually acetylcholine) release at the neuromuscular

junction. Among the seven different serotypes: BoNT/A, B, E and F are involved in human botulism, whereas BoNT/D is mainly responsible for animal botulism (205,207,256).

BoNTs are zinc-dependent proteases, containing a His-Glu-X-X-His zinc-binding motif of metallo-endopeptidases in the central region of their light chains (210). BoNTs are 150kDa di-chain proteins with typical A (Active)-B (Binding) structure-function. BoNTs are activated by proteolysis to generate di-chain organization (205). There are three domains found for BoNTs including a N-terminal catalytic domain (light chain, LC), an internal translocation domain (heavy chain, HCT), and a C-terminal receptor binding domain (heavy chain, HCR) (206). SNARE complex formed by the vesicle SNARE, VAMP-2, and the plasma membrane SNAREs, SNAP25 and syntaxin 1a, is the driving force of vesicle fusion during the mammalian neuronal exocytosis process (208). These SNARE proteins are the targets of the seven BoNTs: serotypes B, D, F and G cleave VAMP-2, serotypes A and E cleave SNAP25, and serotype C cleaves both SNAP25 and syntaxin 1a (205).

Due to their extreme toxicity, ease of production, handling and delivery through aerosol or liquid route, BoNTs represent a potential biological warfare agent and have been classified as a category A agent by the CDC (Centre for Disease Control and Prevention) in the US (257,258). However, another key feature of BoNTs is that their intoxication can be reversed by the replacement of affected nerves by new ones (194,206,259), thus making BoNTs effective agents for the therapies of a range of neuromuscular disorders, such as strabismus (197,213). A better understanding of the mechanism of action and substrate recognition of BoNTs will enable us to develop antidote for BoNT intoxication and novel therapies to extend its clinical applications. Recently, the mechanism of BoNT/A, B, E and F have been thoroughly studied, with results indicating that an extended region (exosite) is necessary for substrate binding and cleavage (133,143,145,146). In 2006, Arndt et al. reported the structure of light chain of BoNT/D and proposed the recognition of hydrophobic V1 SNARE motif through structural comparison with LC/F (138). Stefan Sikorra et al. reported the contribution of VAMP-2 residues on LC/D substrate recognition and found that LC/D required a relatively short sequence for optimal substrate cleavage when compared to other serotypes such as LC/F and LC/TeNT(135). However, the mechanism underlying the effective recognition and cleavage of VAMP-2 by LC/D is still unclear, which prompts the current study to depict the mechanism of substrate recognition and specificity by LC/D.

Our data showed that, similar to other serotypes, LC/D recognition of VAMP-2 occurs through multistep binding and, in particular, recognition of VAMP-2 sites by LC/D substrate recognition pockets. Interestingly, different from all other BoNT LCs and metalloprotease, LC/D employed a novel dual recognition mechanism, where one VAMP-2 site was

recognized by two independent LC/D sites that were complementary to each other. The dual recognition strategy increased LC/D tolerance to mutations and makes it a good candidate for LC/D engineering to improve its pharmacological properties.

## **4.3 Materials and Methods**

### **4.3.1 Molecular Modelling**

The complex structure of LC/D-VAMP-2 was modeled and analyzed using SWISS-MODEL and refined by PyMol (<http://www.pymol.org/>) as described previously (146). Briefly, the crystal structure of LC/D (PDB 2FPQ) and the LC/A-SNAP-25 complex structure (PDB 1XTG) were opened in PyMoL software. The LC/D structure was aligned to the LC/A-SNAP-25 complex structure. The structure of VAMP-2 was extracted from the SNARE complex crystal structure (chain A, PDB 1SFC) and aligned to the LC/A-SNAP-25 complex structure as well. The modification and refinement were carried out by PyMoL.

### **4.3.2 Plasmids Construction and Protein Expression**

Codon-optimized DNA encoding the LC domain of BoNT/D (residues 1-430) was synthesized by EZBiolab (Westfield, IN). The PCR product was then subcloned into the pET-15b vector and transformed into *E. coli* BL21 (DE3)-RIL (StratageneBiochemicals). Protein expression and purification were achieved as that of LC/B detailed in Chapter Two and as described previously (134,145,146). VAMP-2-(1-97) was constructed by PCR amplifying the cDNA clone purchased from ATCC (accession code NM014232) and subcloning into pGEX-2T. The plasmid containing VAMP-2 (1-97) fragment was transformed into *E. coli* BL21 (DE3) and expression and purification of VAMP-2 were achieved as detailed in Chapter Two and as described previously (134,145,146).

### **4.3.3 VAMP-2 and LC/D mutagenesis**

The introduction of point mutations into LC/D and VAMP-2 genes were also performed using the QuikChange® protocols as described previously (133,146). Plasmids were sequenced to confirm the mutations and that additional mutations were not present within the open reading frame of VAMP-2 and LC/D. Mutated proteins were produced and purified as described previously (133,146).

### **4.3.4 Linear velocity and kinetic constants**

The linear velocity and kinetic constant determination of LC/D and its derivatives were performed as previously described (134,145,146). Briefly, 10  $\mu$ M VAMP-2 or the indicated VAMP-2 derivatives were incubated with various concentrations of LC/D or its derivatives,

in 10ul reaction buffer (10 mMTris/HCl,pH 7.6 with 20 mMNaCl) at 37°C for 20 min. The reactions were stopped by adding equal volume of SDS-PAGE sample buffer, boiled at 100°C for 5 min, then analysed for the relative abundance of the substrate and cleaved product by SDS/PAGE (12% gels). The amount of cleavedVAMP-2 was determined by densitometry.  $K_m$  and  $k_{cat}$  determinations were performed using the same assay where VAMP-2 concentrations were adjusted to between 1 and 20  $\mu$ M to achieve ~10% cleavage by LC/D or its derivatives. The amount of cleaved substrate VAMP-2 was determined by densitometry and the velocity was determined by dividing the amount of substrate cleavage to the reaction time. Reaction velocity against substrate concentration was fitted to the Michaelis–Menten equation and kinetic constants were derived using the GraphPad program (La Jolla, CA). At least five independent assays were performed to determine the kinetic constants for each protein.

#### **4.3.5 Trypsin digestion of LC/D and its derivatives**

10uM LC/D and its derivatives were incubated with 2mM trypsin in 20ul reaction volume at 37°C for 30min. The reactions were stopped by adding SDS-PAGE sampling buffer and subjected to SDS-PAGE and stained to visualize the partial trypsin digestion profiles.

#### **4.3.6 Far UV-Circular dichroism analysis**

LC/D and its derivatives were subjected to far UV-CD analysis. Circular dichroism (CD) spectroscopy was collected in the wavelength range from 200 to 250nm at room temperature with a JASCO (J-810) spectrometer. Far UV-CD data were obtained with a 10mm path length quartz cuvette containing 500ul of the protein solutions (0.1-0.4mg/ml protein in 10mM Tris/HCl, pH 7.9, 20mM NaCl), with a scanning speed of 50nm/min, 2s response time. Each sample was measured in triplicate, and the CD data were converted to molar ellipticity, and the spectrum was generated using GraphPad.

### **4.4 Results**

A previous study has shown that several residues of VAMP-2 contributed to substrate cleavage by LC/D, including V<sup>39</sup>, V<sup>42</sup>, M<sup>46</sup>, V<sup>49</sup>, D<sup>53</sup>, K<sup>59</sup>, L<sup>60</sup>, and S<sup>61</sup>(135). To better quantify the degree of contribution of these residues to LC/D substrate cleavage, linear velocity assays were performed to depict the impact of alanine mutagenesis of these residues. The results showed that amino acid changes in VAMP-2, including V<sup>39</sup>A, V<sup>42</sup>A, M<sup>46</sup>A, V<sup>49</sup>A, D<sup>53</sup>A, D<sup>57</sup>A, K<sup>59</sup>A, L<sup>60</sup>A and S<sup>61</sup>A, caused ~25-, 10-, 125-, 20-, 25-, 10-, 20-, 25-, and 20-fold reduction in LC/D cleavage respectively. These data confirmed that the residues in VAMP-2 contributed significantly to LC/D substrate recognition and cleavage. Analysis of the modeled complex structure of LC/D-VAMP-2 identified three putative

substrate recognition pockets in the active site of LC/D, S2', S1', and S3, which may specifically recognize the VAMP-2P sites, P2'(S<sup>61</sup>), P1'(L<sup>60</sup>), and P3(D<sup>57</sup>) respectively (**Figure 4.1**). In addition, we have also predicted several other substrate binding pockets distal to the active site of LC/D including the B1~B5 binding sites (**Figure 4.1**). To characterize the substrate recognition pockets and confirm the specific recognition of VAMP-2 sites, the LC/D residues comprising the substrate recognition pockets were converted to different amino acid residues to test the effects of these changes on substrate recognition. To exclude the possibility that the effect was due to the overall conformational changes as a result of the mutations, we performed partial trypsin digestion on different mutant proteins and the result indicated that all the LC/D mutants have identical digestion profile as Wt-LC/D, suggesting that the mutations did not cause any conformational change of LC/D (Data Not Shown). In addition, far UV-CD analysis of LC/D and its derivatives indicated that LC/D (I<sup>151</sup>D) showed slightly different spectrum from Wt-LC/D, while all other LC/D derivatives had the same far UV-CD spectrum as Wt-LC/D (**Figure 4.2**). The curve vertexes of LC/D and its derivatives at around 240nm looked different, which is probably due to high degree of flexibility of LC/D owing to its relatively high amount of turn and random coils. Therefore, the different curves at around 240nm did not reflect the conformational changes of LC/D derivatives (**Figure 4.2**). The CD spectra of the other LC/D derivatives were similar to the Wt-LC/D and the data were not shown.

#### **4.4.1 Recognition of P2' site of VAMP-2, S<sup>61</sup> by the S2' pocket of LC/D**

The P2' site, S<sup>61</sup>, of VAMP-2 played a certain role on LC/D substrate recognition as the mutation, S61A, of VAMP-2 reduced LC/D substrate hydrolysis by ~20-fold. A S2' pocket in LC/D that recognized the P2' site of VAMP-2 at S<sup>61</sup> was identified through the analysis of the modeled complex structure of LC/D and VAMP-2. The S2' pocket was composed of a residue, R<sup>372</sup>, and the mutation of R372A showed ~40-fold reduction of LC/D activity with almost the same Km and ~40-fold lower kcat compared to Wt-LC/D (**Figure 4.3a, Table 4.1**). The data suggested that S2' pocket residue, R<sup>372</sup>, of LC/D may recognize the P2' site of VAMP-2 by forming a hydrogen bond between these two residues.

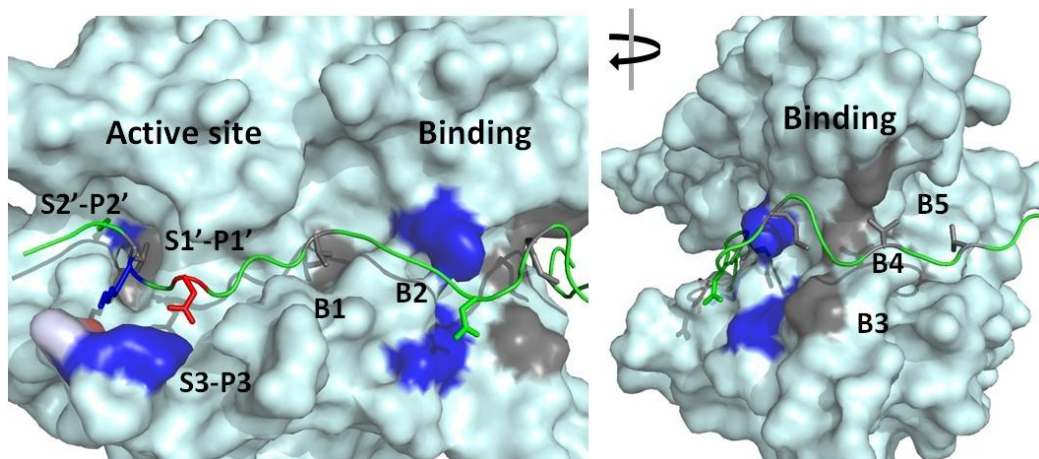


**Figure 4. 1 The overall view of the modeled LC/D-VAMP-2 complex structure.**

Left panel represents the view on the active site side and right panel represents a view after 90 degree clockwise turn. LC/D was shown as surface structure and VAMP-2 was shown as ribbon structure.

The active site recognition and binding site interactions were highlighted. Red color represents negatively charged residues, blue color represents positively charged residues, grey color represents hydrophobic residues and green color represents polar residues.

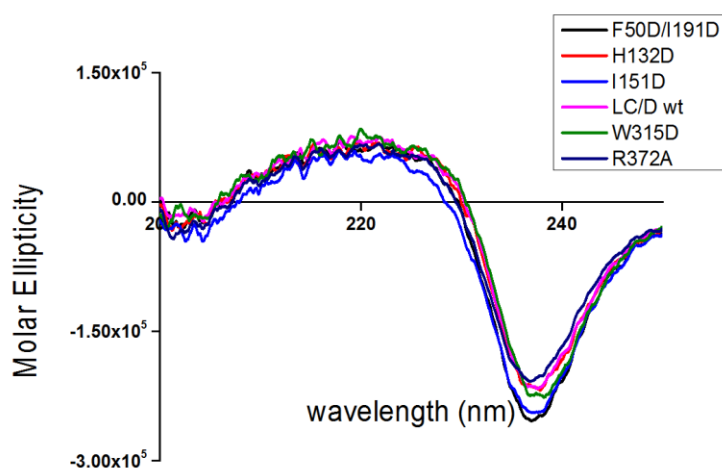


**Figure 4. 2 CD spectroscopy analysis of LC/D and its derivatives.**

Far UV-CD (200-250nm) data were obtained for LC/D and its derivatives with a JASCO (J-810) spectrometer room temperature. The data for the most representative LC/D derivatives were shown with different colors.

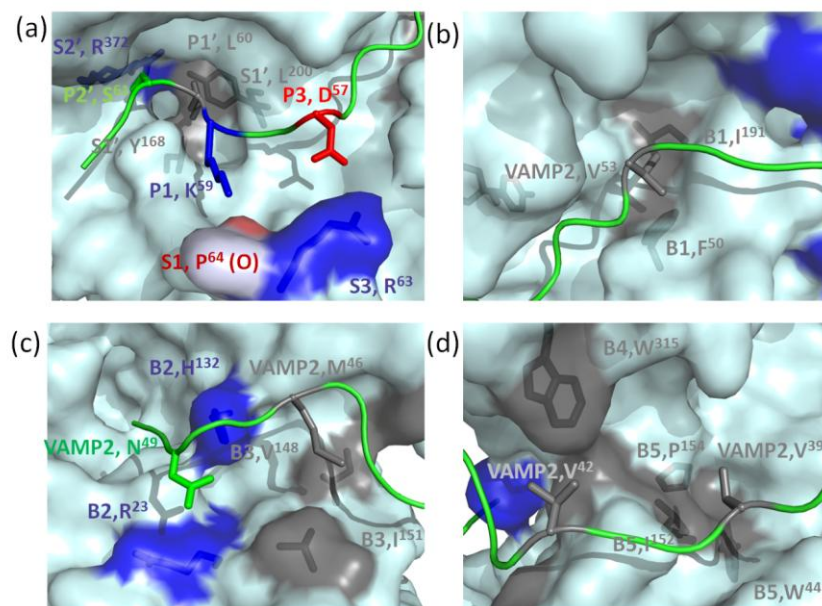


**Figure 4. 3 The specific recognition of VAMP-2 by LC/D pockets.**

Representations of the recognition of different P sites of VAMP-2 by the S pockets and recognition of VAMP-2 binding sites by B1-B5 binding sites of LC/D. Red color represents negatively charged residues, blue color represents positively charged residues, grey color represents hydrophobic residues and green color represents polar residues. (a) recognition of P sites of VAMP-2 by active site pockets of LC/D, where P2' site of VAMP-2, S<sup>61</sup>, was recognized by S2' pocket, R<sup>372</sup>; P1' site of VAMP-2, L<sup>60</sup>, was recognized by S1' pocket of LC/D, Y<sup>168</sup> and L<sup>200</sup>; P1 site of VAMP-2, K<sup>59</sup>, interacted with O atom of P<sup>64</sup> of LC/D; and P3 site of VAMP-2, D<sup>57</sup>, was recognized by S3 pocket, R<sup>63</sup>, of LC/D. (b) recognition of V<sup>53</sup> by B1, F<sup>50</sup> and I<sup>191</sup>, of LC/D. (c) recognition of N<sup>49</sup> of VAMP-2 by B2, R<sup>23</sup> and H<sup>132</sup> of LC/D; and recognition of M<sup>46</sup> of VAMP-2 by B3, V<sup>148</sup> and I<sup>151</sup> of LC/D. (d) recognition of V<sup>42</sup> by B4, W<sup>315</sup> of LC/D; and recognition of V<sup>39</sup> by B5, W<sup>44</sup>, I<sup>152</sup> and P<sup>154</sup> of LC/D.

**Table 4.1 Efficiency of VAMP-2 hydrolysis and kinetic constants of LC/D and its derivatives.**

LC/D pockets	VAMP-2 site recognition	LC/D derivatives	Activity reduction (fold) <sup>d</sup>	$K_m$ (uM)	$k_{cat}$ (s <sup>-1</sup> )	$k_{cat}/K_m$ (s <sup>-1</sup> uM <sup>-1</sup> )
AS-S2'	P2', S <sup>61</sup>	Wt- LC/D	1	2.91 (0.74 <sup>a</sup> )	6.88	2.36
		R <sup>372</sup> A	40	2.09 (0.23)	0.17	8.1×10 <sup>-2</sup>
		Y <sup>168</sup> A	1	- <sup>b</sup>	-	-
		Y <sup>168</sup> D	2	-	-	-
AS-S1'	P1', L <sup>60</sup>	L <sup>200</sup> A	2	-	-	-
		L <sup>200</sup> D	8	2.40(0.36)	0.81	3.4×10 <sup>-1</sup>
		Y <sup>168</sup> A,L <sup>200</sup> A	2	-	-	-
		Y <sup>168</sup> D,L <sup>200</sup> D	60	3.33 (0.66)	0.12	3.6×10 <sup>-2</sup>
AS-S3	P3, D <sup>57</sup>	R <sup>63</sup> A	10	2.19 (0.24)	0.40	1.8×10 <sup>-1</sup>
		R <sup>63</sup> E	50	2.26 (0.35)	0.15	6.6×10 <sup>-2</sup>
		F <sup>50</sup> A	1	-	-	-
		I <sup>191</sup> A	1	-	-	-
Binding-B1	V <sup>53</sup>	F <sup>50</sup> D	4	3.24 (0.12)	1.60	4.9×10 <sup>-1</sup>
		I <sup>191</sup> D	4	3.56 (0.21)	1.40	3.9×10 <sup>-1</sup>
		F <sup>50</sup> A,I <sup>191</sup> A	60	4.81(0.64)	0.28	5.8×10 <sup>-2</sup>
		F <sup>50</sup> D,I <sup>191</sup> D	400	4.46 (0.57)	0.04	8.9×10 <sup>-3</sup>
Binding-B2	N <sup>49</sup>	R <sup>23</sup> A	1	-	-	-
		H <sup>132</sup> A	1	-	-	-
		H <sup>132</sup> D	ND	ND <sup>c</sup>	ND	ND
		H <sup>132</sup> Q	100	35.56 (3.48)	0.86	2.4×10 <sup>-2</sup>
Binding-B3	M <sup>46</sup>	R <sup>23</sup> D,H <sup>132</sup> A	25	32.87(5.25)	2.38	7.2×10 <sup>-2</sup>
		V <sup>148</sup> A	1	-	-	-
		V <sup>148</sup> D	1	-	-	-
		I <sup>151</sup> A	2	-	-	-
Binding-B4	V <sup>42</sup>	I <sup>151</sup> D	1000	7.96 (1.284)	0.02	2.5×10 <sup>-3</sup>
		V <sup>148</sup> , I <sup>151</sup> A	15	-	-	-
		W <sup>315</sup> A	20	9.90 (1.51)	1.52	1.5×10 <sup>-1</sup>
Binding-B5	V <sup>39</sup>	W <sup>315</sup> D	40	47.63 (15.12)	3.92	8.2×10 <sup>-2</sup>
		W <sup>44</sup> D	2	-	-	-
		I <sup>152</sup> D	2	-	-	-
		P <sup>154</sup> D	4	11.86(3.46)	6.35	5.4×10 <sup>-1</sup>
		W <sup>44</sup> A, I <sup>152</sup> A, P <sup>154</sup> A	20	32.45(8.87)	5.86	1.8×10 <sup>-1</sup>

<sup>a</sup>The number in the parentheses is the standard error of at least five independent experiments; <sup>b</sup>Kinetic constants were not determined; <sup>c</sup>ND: Not Detectable, the mutant is too inactive to determine its kinetic constants in our experiments; <sup>d</sup>The wt-VAMP-2 hydrolysis was measured as the ratio of the amount of LC/D derivatives needed to cleave 50% of the Wt - VAMP-2 against the amount of Wt-LC/D needed to cleave 50% of the Wt-VAMP-2.

#### 4.4.2 Dual recognition of VAMP-2, P1' site by S1' pocket of LC/D

The P1' site of VAMP-2 was shown to be important for LC/D substrate recognition as seen in the other serotypes of BoNT (145,146,148,150). Mutation of the VAMP-2 P1' residue,

L60A, reduced LC/D substrate hydrolysis by ~25-fold. A corresponding S1' pocket composed of two hydrophobic residues, Y<sup>168</sup> and L<sup>200</sup>, was identified in LC/D (**Figure 1.3a**). The mutation of LC/D(Y168A) showed no effect on LC/D substrate hydrolysis, and LC/D(Y168D) only affected substrate hydrolysis by ~2-fold. The mutation, LC/D (L200A) showed ~2-fold reduction of LC/D substrate hydrolysis, whereas LC/D (L200D) affected substrate hydrolysis by ~8-fold (**Table 4.1**). The complementary effect of Y<sup>168</sup> and L<sup>200</sup> was also examined and we found that although LC/D (Y168A, L200A) only showed ~2-fold reduction of substrate hydrolysis, LC/D (Y168D, L200D) showed 60-fold reduction of substrate hydrolysis with no effect on Km and ~60-fold reduction of kcat. These data suggested that a hydrophobic S1' pocket was necessary to maintain the full recognition of VAMP-2, L<sup>60</sup> and both hydrophobic residues in S1' pocket, Y<sup>168</sup> and L<sup>200</sup>, played complementary role on L<sup>60</sup> recognition.

#### **4.4.3 S3 pocket residue of LC/D interacts with the VAMP-2 P3 (D<sup>57</sup>)**

D<sup>57</sup> at the P3 site of VAMP-2 played a certain role in LC/D substrate recognition as the mutation, D57A, reduced LC/D substrate hydrolysis by ~20-fold. The S3 pocket of LC/D that specifically recognized the P3 of VAMP-2, D<sup>57</sup>, contained residue R<sup>63</sup>. The mutation of R63A showed almost no effect on Km but ~13-fold reduction of substrate catalysis (**Figure 4.3a, Table 4.1**). A charge reversal mutation, LC/D (R63E), caused ~50-fold reduction of LC/D substrate hydrolysis with no effect on Km and ~50-fold reduction of kcat. The data suggested that a salt bridge or a side-chain hydrogen bond was important for recognition of D<sup>57</sup> of VAMP-2 by R<sup>63</sup> of LC/D.

#### **4.4.4 Main chain of P<sup>64</sup> of LC/D interacts with P1 site, K<sup>59</sup> of VAMP-2**

There is no obvious residue or pocket that showed interaction with P1 site of VAMP-2, K<sup>59</sup>. The mutation leading to a VAMP-2 (K59A) change caused ~20-fold reduction of LC/D substrate hydrolysis, suggesting a role of K<sup>59</sup> in LC/D substrate recognition. Structural analysis indicated that K<sup>59</sup> could potentially interact with the O atom of LC/D residue P<sup>64</sup> through the formation of hydrogen bond. This interaction cannot be tested through mutational analysis (**Figure 4.3a**).

#### **4.4.5 Substrate binding and recognition distal to the active site of LC/D**

##### **4.4.5.1 Recognition of VAMP-2, V<sup>53</sup> by LC/D B1 binding site**

The VAMP-2 V<sup>53</sup>A mutation caused about 25-fold reduction of LC/D hydrolysis. A B1 binding site of LC/D formed by two residues, F<sup>50</sup> and I<sup>191</sup>, may show interaction with V<sup>53</sup> (**Figure 4.3b**). The mutations underlying LC/D (F<sup>50</sup>A) or LC/D (I<sup>191</sup>A) changes had no effect on LC/D substrate hydrolysis, while LC/D (F<sup>50</sup>D) or LC/D(I<sup>191</sup>D) caused ~4-fold

reduction of VAMP-2 hydrolysis. To test for the complementary effect of these two residues on V<sup>53</sup> recognition, the effects of double mutations of these two residues were tested. This double mutations, LC/D (F<sup>50</sup>A, I<sup>191</sup>A), showed ~60-fold reduction of substrate hydrolysis with ~2-fold increase of  $K_m$  and ~25-fold decrease on  $k_{cat}$ , whereas LC/D (F<sup>50</sup>D, I<sup>191</sup>D) exhibited ~400-fold reduction of substrate hydrolysis with ~2-fold increase of  $K_m$  and ~200-fold decrease on  $k_{cat}$ , (**Table 4.1**). The data suggested that F<sup>50</sup> and I<sup>191</sup> showed independent, but complementary effect on V<sup>53</sup> substrate recognition. The recognition of V<sup>53</sup> might mainly contribute to the fine orientation of VAMP-2 for optimal substrate recognition in the active site of LC/D since this recognition site mainly contributed to the substrate catalysis ( $k_{cat}$ ), but not substrate binding ( $K_m$ ).

#### 4.4.5.2 Recognition of VAMP-2, N<sup>49</sup> by LC/D B2 binding site

The VAMP-2 mutation, N49A, was associated with ~20-fold reduction in cleavage efficiency of LC/D.A B2 binding site that was composed of R<sup>23</sup> and H<sup>132</sup> of LC/D and may be interacting with N49 was revealed though analysis of the complex structure of LC/D-VAMP-2 (**Figure 4.3c**). The mutations of LC/D (R23A) and LC/D(H132A) showed no effect on LC/D substrate hydrolysis (**Table 1.1**). Surprisingly, a charge reversal mutation LC/D (R23D) still maintained the full activity on VAMP-2 as Wt-LC/D; a charge reversal mutation LC/D (H132D) became inactive in cleaving VAMP-2, while LC/D (H132Q) showed ~100-fold reduction of substrate hydrolysis, suggesting that the formation of hydrogen bond between LC/D (H<sup>132</sup>) and VAMP-2 (N<sup>49</sup>) may contribute to this recognition and a negatively charged residue at the 132 position may impair this interaction (**Table 4.1**). However, the minimal effect of the LC/D (H132A) change on LC/D substrate hydrolysis may be due to the complementary effect of R<sup>23</sup>. To test this hypothesis, the effect of R23D and H132A double mutations on LC/D substrate hydrolysis was tested. LC/D (R23D, H132A) reduced  $K_m$  by ~11-fold and  $k_{cat}$  by ~3-fold, suggesting that both R<sup>23</sup> and H<sup>132</sup> played a role in LC/D substrate catalysis, and that H<sup>132</sup> played a dominant role in N<sup>49</sup> recognition (**Table 4.1**). This substrate recognition contributed significant to substrate binding.

#### 4.4.5.3 Recognition of VAMP-2, M<sup>46</sup> by LC/D B3 binding site

Compared to N<sup>49</sup>, M<sup>46</sup> of VAMP-2 played a more important role in VAMP-2 recognition by LC/D. Consistent with previous data (135), in our assay condition, the VAMP-2 mutation, M46A, reduced LC/D substrate hydrolysis by ~125-fold. Structural analysis also identified a B3 binding site comprising two residues, I<sup>151</sup> and V<sup>148</sup>, which may interact with M<sup>46</sup> (**Figure 4.3c**). The point mutations associated with the LC/D (V148A) and LC/D (I151A) alterations did not show any effect on VAMP-2 hydrolysis. LC/D (V148D) also did not have any

impact on VAMP-2 hydrolysis, but the LC/D (I151D) change reduced LC/D substrate hydrolysis by ~1000-fold (**Table 4.1**). The dramatic effect on LC/D (I151D) mutation may be partially due to its conformational change based on our far UV-CD analysis. Similar to N<sup>49</sup> recognition, the minimal effect of LC/D (I151A) mutation may be related to the complementary effect of V<sup>148</sup>. To test this hypothesis, the effect of I151 and V148 double mutations on LC/D substrate hydrolysis was tested. LC/D (I151A, V148D) reduced  $K_m$  by ~10-fold and  $k_{cat}$  by ~2-fold, suggesting that both I<sup>151</sup> and V<sup>148</sup> played a role in LC/D substrate catalysis, with I<sup>151</sup> playing a dominant role in substrate recognition (**Table 4.1**). This substrate recognition contributed significantly to substrate binding.

#### 4.4.5.4 Recognition of VAMP-2, V<sup>42</sup> by LC/D B4 binding site

V<sup>42</sup> of VAMP-2 was also important for LC/D substrate hydrolysis and the VAMP-2 (V42A) mutation affected LC/D cleavage of VAMP-2 by ~10-fold. Based on the modeled complex structure of LC/D-VAMP-2, W<sup>315</sup> of LC/D comprising the B4 binding site was predicted to have direct interaction with V<sup>42</sup> (**Figure 4.3d**). The LC/D (W315A) mutation showed ~20-fold reduction of VAMP-2 hydrolysis with ~4-fold increase in  $K_m$  and ~5-fold decrease in  $k_{cat}$ , while LC/D (W315D) showed ~40-fold reduction of VAMP-2 hydrolysis with ~20-fold increase in  $K_m$  and ~2-fold decrease in  $k_{cat}$ . These data suggested that LC/D, W<sup>315</sup> and VAMP-2, V<sup>42</sup> substrate recognition contributed significantly to substrate binding.

#### 4.4.5.5 Recognition of VAMP-2, V<sup>39</sup> by LC/D B5 binding site

Another hydrophobic residue in VAMP-2 that contributed to LC/D substrate hydrolysis was V<sup>39</sup>. The mutation VAMP-2(V39A) showed ~25-fold reduction of LC/D hydrolysis. A hydrophobic pocket in LC/D, B5 binding site, which was formed by W<sup>44</sup>, I<sup>152</sup> and P<sup>154</sup>, was identified through analysis of the complex structure of LC/D-VAMP-2 (**Figure 4.3d**). The W44D, P152D and P154D mutations were associated with ~2, 2, and 4-fold reduction of substrate hydrolysis respectively (**Table 4.1**). All these mutations had no effect on  $k_{cat}$  but caused a 4-fold increase in  $K_m$ , suggesting the role of this pocket on substrate binding. Interestingly, triple mutations LC/D(W44A, I152A, P154A) showed ~20-fold increase of  $K_m$  and no effect on  $k_{cat}$ , suggesting the complementary effect of three residues on V<sup>39</sup> recognition and VAMP-2 binding (**Table 4.1**).

## 4.5 Discussion

It was proposed that botulinum neurotoxins recognize their substrates through two separate regions, one that contains the scissile bond and the other distal to the scissile bond and containing the SNARE motif (131). A two-region substrate recognition model has been demonstrated in LC/A, B, E, F and LC/TeNT (145,146,148,150). The significance of the

SNARE motif was not consistently proven in these toxins. However, for LC/D, SNARE motif V1, <sup>38</sup>QVDEVVDIMR<sup>47</sup> was shown to be important for substrate recognition and hydrolysis. Three conservative hydrophobic residues in the V1 motif of VAMP-2, V<sup>39</sup>, V<sup>42</sup> and M<sup>47</sup>, were critical for efficient LC/D substrate hydrolysis. In addition, LC/D also utilizes other hydrophobic interactions to recognize substrate VAMP-2, such as the recognition of P1' site of VAMP-2, L<sup>60</sup>, by the hydrophobic S1' pocket of LC/D, and the recognition of V<sup>53</sup> of VAMP-2 by hydrophobic B1 binding site of LC/D. In contrast to the substrate binding contributed by SNARE motif V1 (B3, B4 and B5), binding sites B1 and B2 contributed more to LC/D substrate catalysis than substrate binding. The data suggested that the V1 motif played a significant role on LC/D substrate binding, while B1 and B2 binding site may help more on fine tuning the orientation of the substrate for specific recognition by the active site of LC/D, rather than direct substrate binding.

The current study revealed the mechanism of LC/D substrate recognition and specificity. After internalization to the cytoplasm of neuronal cells, LC/D attacks the free form of VAMP-2 through interaction and recognition of hydrophobic residues in the V1 motif of VAMP-2 including residues V<sup>39</sup>, V<sup>42</sup> and M<sup>46</sup>, by the substrate binding region B5, B4 and B3 of LC/D on the substrate binding cleft respectively. In particular, binding of M<sup>46</sup> of VAMP-2 to LC/D B3 was suggested to be very important for LC/D substrate recognition. This binding facilitates further binding of VAMP-2 residues, N<sup>49</sup> and V<sup>53</sup>, to the B2 and B1 sites located at the active site surface of LC/D. The recognition of VAMP-2, V<sup>53</sup>, by LC/D F<sup>50</sup>, I<sup>191</sup> pocket further orientates and stabilizes VAMP-2 for subsequent recognition of different P sites of VAMP-2 by the corresponding S pockets in the active site of LC/D. The active P sites recognition includes the formation of salt-bridge between P3, D<sup>57</sup> of VAMP-2 and S3, R<sup>63</sup> of LC/D, hydrogen bond interaction between P1, K<sup>58</sup> of VAMP-2 and main chain O atom of P<sup>64</sup>, recognition of P1', L<sup>60</sup> of VAMP-2 by S1' pocket, Y<sup>168</sup> and L<sup>200</sup> of LC/D, and finally the hydrogen bond interaction between P2', S<sup>61</sup> of VAMP-2 and S2' pocket residue R<sup>372</sup> of LC/D. The anchoring of VAMP-2 P sites to different S pockets in the active site of LC/D aligns VAMP-2 scissile bond close enough to the active site Zinc ion to facilitate the peptide bond cleavage (**Figure 4.4**).

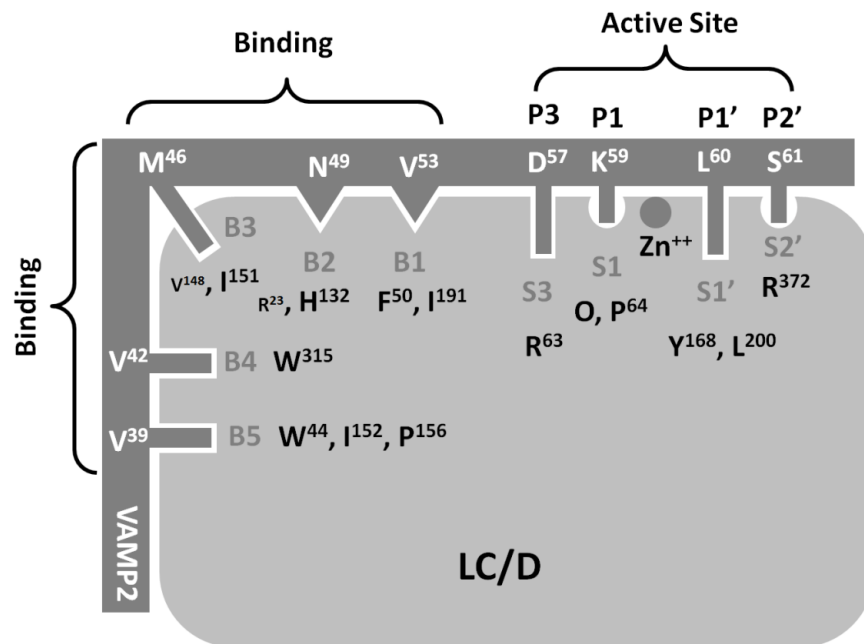


**Figure 4. 4 Mechanism of substrate recognition by LC/D.**

After internalization to the cytoplasm of neuronal cells, LC/D attacks the free form of VAMP-2 through interaction and recognition of hydrophobic residues in the V1 motif of VAMP-2 including residues V<sup>39</sup>, V<sup>42</sup> and M<sup>46</sup>, by the substrate binding region B5, B4 and B3 of LC/D on the substrate binding cleft respectively. In particular, binding of M<sup>46</sup> of VAMP-2 to LC/D B3 was suggested to be very important for LC/D substrate recognition. This binding facilitates further binding of VAMP-2 residues, N<sup>49</sup> and V<sup>53</sup>, to the B2 and B1 sites located at the active site surface of LC/D. The recognition of VAMP-2, V<sup>53</sup>, by LC/D F<sup>50</sup>, I<sup>191</sup> pocket further orientates and stabilizes VAMP-2 for subsequent recognition of different P sites of VAMP-2 by the corresponding S pockets in the active site of LC/D. The active P sites recognition includes the formation of salt-bridge between P3, D<sup>57</sup> of VAMP-2 and S3, R<sup>63</sup> of LC/D, hydrogen bond interaction between P1, K<sup>58</sup> of VAMP-2 and main chain O atom of P<sup>64</sup>, recognition of P1', L<sup>60</sup> of VAMP-2 by S1' pocket, Y<sup>168</sup> and L<sup>200</sup> of LC/D, and finally the hydrogen bond interaction between P2', S<sup>61</sup> of VAMP-2 and S2' pocket residue R<sup>372</sup> of LC/D. The anchoring of VAMP-2 P sites to different S pockets in the active site of LC/D aligns VAMP-2 scissile bond close enough to the active site Zinc ion to facilitate the peptide bond cleavage.

Compared to substrate recognition by other serotypes of BoNT, LC/D possesses unique features of substrate recognition (145,146,148,150). First, hydrophobic interaction between LC/D and VAMP-2 played an important role in substrate recognition. The interaction between VAMP-2, M<sup>46</sup> and LC/D, I151 seems critical for LC/D substrate recognition. This may be the first step of substrate recognition, which may facilitate the conformational

change of VAMP-2 from double helix to a free loop conformation favoring the subsequent substrate binding and catalysis by different regions of LC/D. Further research may be needed to test this hypothesis. However, far UV-CD analysis showed that I151D displayed slightly different conformation from wt-LC/D, suggesting that the significant effect of I<sup>151</sup>D substrate recognition may be partially due to the conformational change of the whole protein but not the loss of I<sup>151</sup> site recognition. Second, different from the recognition of one site of substrate by one pocket of LC for other serotypes of BoNT, LC/D utilizes two functionally similar residues to recognize one site of VAMP-2, such as S1' pocket, Y<sup>168</sup>-L<sup>200</sup> of LC/D for recognition of P1' site, L<sup>60</sup> of VAMP-2 in the active site of LC/D. In addition, dual recognition was also commonly employed at the substrate binding regions. VAMP-2, V<sup>53</sup>, was recognized by the LC/D pocket formed by F<sup>50</sup> and I<sup>191</sup>. Mutation to each residue did not show much effect (maximum 4 fold) on substrate hydrolysis, while mutation to both residues showed dramatic reduction (400 fold) on substrate hydrolysis. VAMP-2 residues N<sup>49</sup> and M<sup>46</sup> were also recognized by pockets with dual recognition mechanism. The pocket that recognized N<sup>49</sup> of VAMP-2 was formed by R<sup>23</sup> and H<sup>132</sup> of LC/D. Although H<sup>132</sup> played a dominant role in N<sup>49</sup> recognition, the H<sup>132</sup>A mutation can be complemented by R<sup>23</sup>. Similar to N<sup>49</sup>, the pocket that recognized M<sup>46</sup> of VAMP-2 was formed by V<sup>148</sup> and I<sup>151</sup> of LC/D. I<sup>151</sup> played a dominant role in M<sup>46</sup> recognition, whereas V<sup>148</sup> of VAMP-2 can play a complementary role when I<sup>151</sup> was mutated to alanine. Lastly, the pocket that recognized V<sup>39</sup> of VAMP-2 was formed by three hydrophobic residues, W<sup>44</sup>, I<sup>152</sup> and P<sup>154</sup> of LC/D. Mutation of each residue to alanine or asparagine showed no or minor effect on substrate hydrolysis, whereas triple mutations to alanine showed much stronger reduction of substrate hydrolysis, highlighting the complementary effects of three residues forming this pocket. The presence of two or more functionally similar residues in the same substrate recognition pocket enables LC/D to tolerate mutations. This property of LC/D makes it a good candidate for further protein engineering.

Unlike BoNT/A that is the most toxic botulinum neurotoxin and implicates in human botulism, BoNT/D is mainly responsible for animal botulism such as cattle botulism. However, our data indicated that LC/D exhibited similar potency as LC/A in hydrolysing their substrates in vitro condition (133). Its role as a human therapy or bioterrorism weapon remains to be investigated. Our data provided insights into the development of novel BoNT based therapies and BoNT/D antitoxins.

# **Chapter Five: Distinct evolutionary routes of Botulinum Neurotoxin subtypes F1 and F7 featuring differential substrate recognition and cleavage mechanisms\***

## **5.1 Abstract**

BoNT/F7, one of the seven subtypes of BoNT/F (F1 to F7) identified based on phylogenetic analysis, is the second-most divergent subtype, which shares >60% identity with BoNT/F1 at both holotoxin and enzymatic domain levels but needs an N-terminal extended peptide substrate for efficient substrate cleavage as previously reported. The present study identified the multistep substrate recognition mechanism employed by LC/F7 for efficient substrate hydrolysis. Our findings further indicated that both LC/F and LC/F7 shared similarity in substrate recognition, but LC/F7 utilized a unique substrate recognition in some binding pockets and active sites, such as the B1, B2 and S2 pockets. The broadened understandings of substrate recognition and cleavage at molecular level by LC/F7 may be helpful in antitoxins and novel detection systems development and in addition, may throw light on the evolution trace among different serotypes and subtypes of BoNTs.

Key words: Botulinum Neurotoxin F serotype, light chain, VAMP2, subtype, substrate recognition mechanism

Abbreviations: BoNT/F1 and /F7, Botulinum Neurotoxin subtype F1 and F7; LC, light chain; VAMP2, vesicle associated membrane protein-2; SNARE, soluble NSF attachment receptor

\* The work of this chapter has been done, and manuscript will be submitted soon.

## **5.2 Introduction**

BoNTs are the most potent toxins identified till now, which have attracted much interest in divers fields. Originally they are treated as a cause of deadly disease botulism, military and terrorist intended to misuse them as biological weapon, thus they are classified by the Centers for Disease Control and Prevention as category A agent, and listed in the Biological and Toxin Weapons Convention (257,258). In the past about 80 years, seven serologically distinct botulinum neurotoxins (BoNTs, designated as A-G) have been identified, grouped into different groups based on *16S rRNA* sequence diversity (64,236) and more than 30 subtypes have been identified and reported as well (260). Moreover, an eighth serotype, BoNT/H, was reported recently (55), however, some scientists question of the new

identification and more experiments need to be performed to further prove it as a new serotype.

Botulinum Neurotoxin serotype F (BoNT/F), one of the seven serotypes, was firstly described in 1960 following an outbreak in Denmark (123). Like other serotypes, BoNT/F belongs to AB toxin family, its 150 kDa dichain, linked via a disulfide bond, toxin protein can be separated into two functional domains: an N-terminal 50 kDa light chain (LC, catalytic domain) and a C-terminal 100 kDa heavy chain (HC) which can be further separated into two sub-domains: translocation domain (HCT) and receptor binding domain (HCR) (195,237). The LC of BoNT is zinc-dependent protease, containing a His-Glu-X-X-His motif for zinc binding in the active cleft (238); the HC specifically recognize and bind receptors on the presynaptic motor nerve cells and then translocate the LC across the endosomal membrane into nerve cell cytosol, thus abort the neurotransmitter release process by specific cleavage of the SNARE complex - the synaptic vesicle docking/fusion complex (21,113,121,261).

Besides as deadly agent, the reversible intoxication (259) of BoNT makes them to be efficient treatment for a wide range of disorders (196,197). BoNTs employed a very complex and multiple steps in substrate recognition and cleavage (243,244,262), a thorough investigation of the underling mechanism will give a better understanding of BoNTs, and on the other hand, will help in the development of antidote or inhibitor to fight against them, and develop or extend novel therapeutic application. Seven subtypes of BoNT/F (F1 to F7) have been identified based on phylogenetic analysis and BoNT/F7 is the second-most divergent subtype, which shares 73.7% and 63.3% identity with BoNT/F1 at holotoxin and enzymatic domain level respectively (122,123). Although BoNT/F7 cleave substrate VAMP-2 at the same location as BoNT/F1, it has a different peptide substrate recognition requirement and needs an N-terminal extended peptide substrate to cleave (263). The different substrate cleavage mechanism and limited substrate recognition information make BoNT/F7 as a good candidate to perform a comprehensive study of its substrate recognition mechanism, with the hope of better understanding of BoNT substrates recognition and cleavage mechanism and furthermore provide more useful information for the development of relative antidote or inhibitor. The present study uncovered that LC/F7 utilized a unique substrate recognition and cleavage mechanism even though it shared some similarities with LC/F in certain interaction pockets. The detailed molecular level investigation of substrate recognition mechanism may be helpful in antitoxins, novel detection systems and inhibitor development and in addition, may throw light on the evolution trace among different serotypes and subtypes of BoNTs.

## 5.3 MATERIALS AND METHODS

### 5.3.1 Plasmid Construction and Protein Purification

The *E. coli* codons optimized full length LC/F7 residues 1-450 (GenBank: ADA79579.1) were obtained through total gene synthesis by Tech Dragon (Hong Kong, China), which was then firstly sub-cloned into pGEX-2T vector through *SacI/BamHI* restrictive sites. Our previous study indicates that GST-LC/F7(1-405) has the highest solubility and activity compared with other derivatives of LC/F7 (data not shown), so in the present study, all the following assays were carried out by using purified GST-LC/F7(1-405) protein. The purification of GST-LC/F7(1-405) and VAMP-2 (1-97) was achieved as previously described (246).

### 5.3.2 Molecular Modeling

The complex structure of LC/F7-VAMP-2 was modeled by using SWISS-MODEL and refined with PyMoL software as detailed previously (245). Briefly, the structure of LC/F7 was modeled by SWISS-MODEL by using the crystal structure of LC/F (PDB 2A8A) as searching template and the structure of VAMP-2 was extracted from the SNARE complex crystal structure (chain A, PDB 1SFC) and both structures were modified by PyMoL. The LC/F7-VAMP-2 complex structure was modeled then by aligning to the LC/A-SNAP-25 complex structure (PDB 1XTG) and refined in the PyMoL software.

### 5.3.3 LC/F7 and VAMP-2 Derivatives Generation and purification

Based on the complex model and predictions, the mutated derivatives of LC/F7 and VAMP-2 were performed by using QuickChange (Stratagene) commercial kit following the manufacturer's instruction. Success mutations were confirmed by sequencing and mutant proteins were expressed and purified as described above.

### 5.3.4 Standard Linear Velocity Reaction

Linear velocity assays were performed as previously described (246). Briefly, 5-10  $\mu$ M VAMP-2 or derivatives was mixed with indicated amount of LC/F7 in reaction buffer (10 mM Tris-HCl, pH 7.6, 20 mM NaCl, designated as 10:20 buffer), with a total reaction volume of 10  $\mu$ l. After 20min incubation at 37°C, the reactions were stopped by adding SDS-PAGE sample buffer, heated at 100°C for 5min, analyzed by SDS-PAGE. The amount of VAMP-2 cleaved was determined by densitometry.

### 5.3.5 Kinetic Parameters Determination

The detailed  $K_m$  and  $k_{cat}$  determination procedure was reported previously (262). The amount of LC/F7 or its derivatives was adjusted to achieve <10% cleavage of VAMP-2 with

the concentrations ranged from 1 to 72  $\mu\text{M}$ . Reaction velocity against substrate concentration was fitted to the Michaelis–Menten equation and kinetic constants were derived using the GraphPad program. For each protein, at least three independent assays were performed to determine the kinetic constants.

### **5.3.6 Far-UV Circular Dichroism Analysis**

As detailed previously (262), LC/F7 and its derivatives were analyzed by far-UV CD for the check of secondary structure change in a 10-mm path length quartz cuvette with 400  $\mu\text{l}$  volume (containing 0.1–0.4 mg/ml protein in 10:20 buffer). A JASCO J-810 spectropolarimeter was used with parameters set as: scanning speed 50 nm/min, 1s response time, 1nm data pitch, 1 nm band width and accumulation times was set as 3. The wavelength range of 200-250nm was scanned, and raw CD data were converted to molar ellipticity using Yang as reference (264), and the spectrum was generated using GraphPad Prism.

## **5.4 Results**

### **5.4.1 VAMP-2 regions mapping analysis for efficient cleavage by LC/F7**

BoNT/F7 shares >60% identity with BoNT/F1 both at holotoxin and enzymatic domain levels, but it was reported that BoNT/F7 could not recognize or cleave the optimal peptide substrate (VAMP-2 32-65) for BoNT/F1. An N-terminal extended peptide substrate is required for cleavage by BoNT/F7 (263). The detailed substrate recognition mechanism employed by LC/F1 has been investigated previously (246), in order to dissect the molecular recognition mechanism of VAMP-2 by BoNT/F7, regions mapping of VAMP-2 that would give efficient cleavage by LC/F7 was performed firstly (data not shown). The N-terminal 20 residues deletion, VAMP-2 (20-97), did not exhibit reduced VAMP-2 cleavage efficiency by LC/F7, however, both the VAMP-2 (30-97) and VAMP-2 (40-97) truncated mutants showed >4000-fold reduction in VAMP-2 cleavage efficiency by LC/F7, suggesting a significant role played by the N-terminal region from residues 20 to 30 in recognition by LC/F7. In addition, no dramatic substrate cleavage efficiency reduction was detected for the C-terminal truncated VAMP-2 (1-65). Taken together, the finding indicated that a likely minimal efficient substrate for LC/F7 was VAMP-2 (20-65), with the SNARE motif V2 (62-71) exert minor contribution to LC/F7 cleavage of VAMP-2.

### **5.4.2 Contribution of individual residues of VAMP-2 on LC/F7 cleavage**

Based on the results mentioned above, alanine-scanning mutagenesis within VAMP-2 (22-66) was performed to investigate the individual point mutation effect on substrate cleavage by LC/F7. Surprisingly, no individual residue within the N-terminal 20-30 region were

found exerted significant effect on the hydrolysis efficiency of LC/F7 on VAMP-2 (**Figure 5.1**), indicating the VAMP-2 N-terminal 20-30 region works as a whole to contribute to substrate recognition and cleavage by LC/F7. In addition, dramatic differences were detected at certain individual residues of VAMP-2 which contributed differently to the hydrolysis by LC/F and LC/F7. For example, the R31A, L32A, Q34A, Q38A, V39A, D40A, I45A, M46A, V53A, L54A, D57A, and K59A mutants of VAMP-2 displayed ~500-, 100-, 7-, 6-, 12-, 25-, 5-, 8-, 16-, 16-, 25-, and 2000-fold reductive effect on LC/F7 substrate hydrolysis respectively, however, these VAMP-2 mutants showed ~10-, 1-, 1-, 30-, 100-, 1-, 20-, 1-, 10-, 30-, 500-, and 1000-fold reductions in LC/F substrate cleavage efficiency respectively. Unexpectedly, the VAMP-2 P2' site mutant, L60A, showed almost no effect on LC/F7 substrate cleavage capacity, but displayed 30-fold reduction in LC/F substrate cleavage efficiency (**Figure 5.1**) (246). To conclude, LC/F7 employed a different and unique mechanism in substrate recognition and cleavage when compared with LC/F.

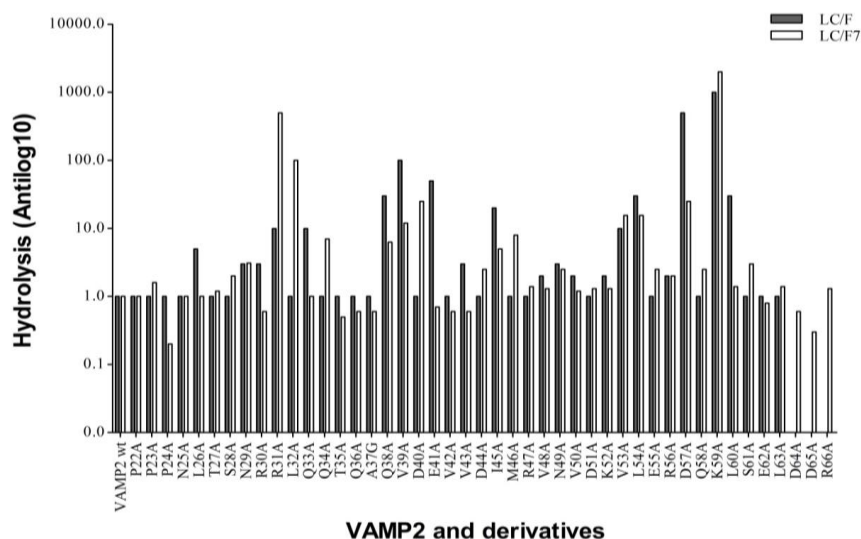


**Figure 5. 1 Hydrolysis comparison of LC/F and LC/F7 on the cleavage of VAMP-2 and its derivatives.**

Hydrolysis was measured as the ratio of the amount of LC/F7 to cleave 50% of VAMP-2 and derivatives against the amount of LC/F to cleave 50% of VAMP-2 wt. The data of VAMP-2 and its derivatives cleavage by LC/F were from reference (246).

### 5.4.3 CD analysis of LC/F7 and derivatives

The LC/F7 structure was modeled by using SWISS MODEL based on the structure of LC/F (chain A, PDB accession number 2A8A), and then LC/F7-VAMP-2 complex structure was modeled by aligning with the complex structure of LC/F with a peptide inhibitor (PDB 3FIE) and modified with PyMOL software (**Figure 5.2**). Based on the alanine mutagenesis scanning and modeled complex structure, the residues/pockets in LC/F7 that specifically recognized the corresponding residues in VAMP-2 were predicted and further proved by

biochemical characterization. To make sure the substrate cleavage efficiency changes were not caused by the mutations of LC/F7, far-UV CD analysis of LC/F7 and derivatives were performed. All of the mutants showed identical CD spectra, and only F168A displayed a slightly different pattern (**Figure 5.3**). In addition, partial trypsin digestion analysis for LC/F7 and derivatives was performed as well, and the result indicated that all of the LC/F7 mutants had an identical digestion profile, when compared with LC/F7 wt, suggesting the mutations of LC/F7 analyzed did not cause significant conformational change in the overall structure of LC/F7 (data not shown).

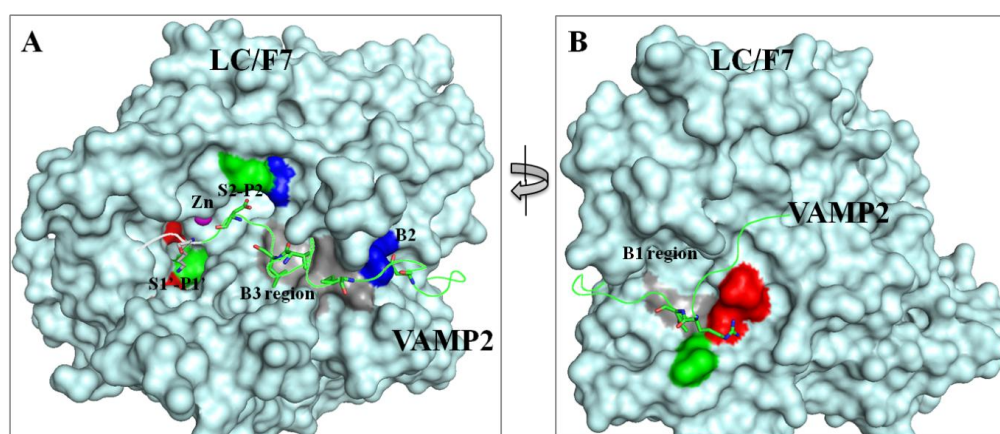


**Figure 5.2 Overall view of the modeled LC/F7-VAMP-2 complex structure and aligned interactions between LC/F7 and VAMP-2.**

A, view of the active site and B2 and B3 region alignment; B, view after a 90° clockwise turn, displaying the B1 region interactions. LC/F7 is shown as a surface structure, and VAMP-2 in ribbon structure. The active site recognition and binding site interactions are highlighted. The residues were colored based on side chain: negatively charged (red), positively charged (blue), hydrophobic (gray) polar (green) and zinc (magenta sphere).

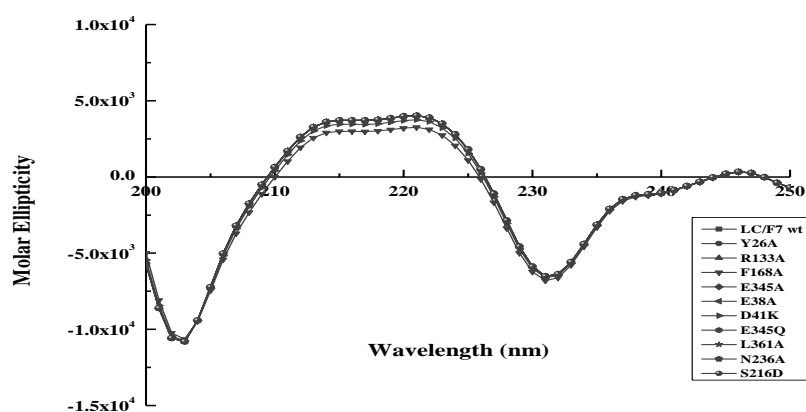


**Figure 5.3 CD spectroscopy analysis of LC/F7 and its derivatives.**

Far-UV CD data were obtained for LC/F7 and its derivatives with a spectropolarimeter at room temperature. The data for the representative LC/F7 derivatives are shown in different symbols.

#### 5.4.4 LC/F7 active site substrate recognition

Through alanine scanning analysis of VAMP-2, the alanine mutations of P1' (K<sup>59</sup>) and P2 (D<sup>57</sup>) could reduced the LC/F7 substrate cleavage efficiency by about 2000- and 25-fold respectively (**Figure 5.1**). Both sites also found exerted significant effect on the LC/F substrate cleavage efficiency, with ~1000- and ~500-fold effect respectively (**Figure 5.1**) (246). Based on the modeled complex structure of LC/F7-VAMP-2, the potentially corresponding interaction pockets (designated as S1' and S2) were identified and characterized.

##### 5.4.4.1 Triple recognition between the P1' (K<sup>59</sup>) of VAMP-2 and the S1' pocket of LC/F7

The S1' pocket in LC/F7 that specifically recognized the positively charged K<sup>59</sup> of VAMP-2 comprised two negatively charged residues (E<sup>199</sup> and E<sup>345</sup>) which located on the either side of K<sup>59</sup> of VAMP-2, and one polar residue (S<sup>216</sup>) located in the middle of the S1' pocket (**Figure 5.4A**). LC/F7 cleaved VAMP-2 (K59A) mutant with an about 2000-fold lower efficiency, indicating the important role played by the VAMP-2 P1' site on the interaction with LC/F7 (**Figure 5.1**). The activity of LC/F7 could be abolished by either E199A or E345A mutation. In addition, the activity of LC/F7 (E199Q) mutant was also too low to detect, and LC/F7 (E345Q) derivative showed about 3000-fold deduction in VAMP-2 cleavage efficiency by affecting both *K<sub>m</sub>* and *k<sub>cat</sub>*, suggesting the significant role of the salt bridge formed between K59 of VAMP-2 and E199/E345 of LC/F7 (**Table 5.1**). Moreover, S<sup>216</sup> in the S1' pocket of LC/F7 also displayed significant role in the interaction with K<sup>59</sup> site of VAMP-2. The LC/F7 (S216A) mutant showed about 63-fold lower substrate cleavage efficiency through mainly affecting *k<sub>cat</sub>*, suggesting a possible side-chain hydrogen bond interaction with the K59 residue of VAMP-2. The activity of LC/F7 was totally abolished by LC/F7 (S216D) mutant which likely exerted the significant effect via repelling with the other two adjacent negatively charged residue in the pocket (**Table 5.1**). For LC/F, its S1' pocket was formed by two residues, E200 and S224 (246), with a missing negatively charged residue when compared with LC/F7 which may determined the unique substrate recognition mechanism of LC/F7.

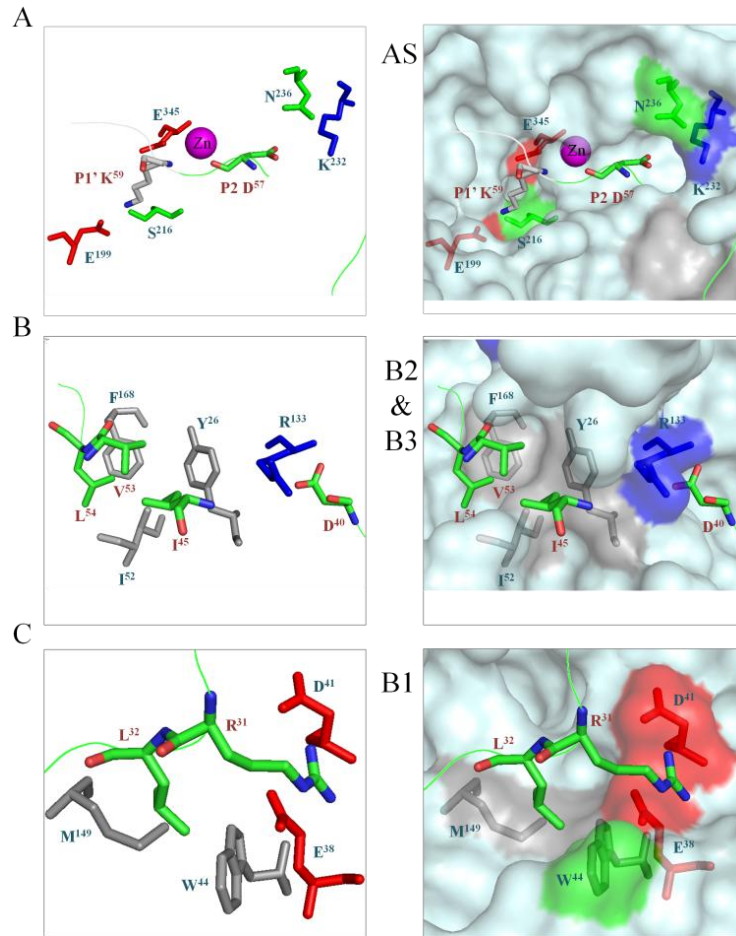


**Figure 5.4 Recognition specificity of VAMP-2 by LC/F7 pockets.**

The structure of LC/F7 in the right panel is shown as surface, the residues of VAMP-2 that identified interacting with the corresponding residues of LC/F7 were shown in stick. The active site recognition and binding site interactions of LC/F7 were shown in stick and highlighted based on side chain: negatively charged (red), positively charged (blue), hydrophobic (gray) polar (green) and zinc (magenta sphere). (A) At the active site (AS) of LC/F7, the S1' pocket in LC/F7 comprised two negatively charged residues (E<sup>199</sup> and E<sup>345</sup>) and one polar residue (S<sup>216</sup>), which may interacted the P1' (K<sup>59</sup>) of VAMP-2 through salt bridge and side-chain hydrogen bond interaction. In the S2 pocket of LC/F7, two residues (K<sup>232</sup> and N<sup>236</sup>) were indentified to interact with P2 (D<sup>57</sup>) of VAMP-2, likely via salt bridge and hydrogen bond in stabilizing the P1 site for an efficient scissile bond hydrolysis. (B) In the B3 pocket of LC/F7, three major hydrophobic residues (F<sup>168</sup>, Y<sup>26</sup> and I<sup>52</sup>) were identified to interact with the three hydrophobic residues, L<sup>54</sup>, V<sup>53</sup> and I<sup>45</sup> in the VAMP-2 B3 region. In the B2 pocket of LC/F7, the positively charged residue, R<sup>133</sup>, interacted with the D<sup>40</sup> residue in the B2 region of VAMP-2 via salt bridge interaction. (C) The B1 pocket in LC/F7, located on the opposite surface of the active site, was composed of D<sup>41</sup>, E<sup>38</sup>, W<sup>44</sup> and M<sup>149</sup> which were found have a very clear division of roles and synergetic effect in interacting with the corresponding residues in the B1 region of VAMP-2: the D<sup>41</sup> and E<sup>38</sup> synergistically interacted with the R<sup>31</sup> residue of VAMP-2, and the W<sup>44</sup> and M<sup>149</sup> residues displayed synergetic effect in interacting with the L<sup>32</sup> of VAMP-2.

**Table 5.1 Efficiency of VAMP-2 hydrolysis and kinetic constants of LC/F7 and derivatives.**

VAMP-2 site/region (residue)	LC/F7 pockets	LC/F7 derivatives	Activity reduction (-fold) <sup>a</sup>	<i>K<sub>m</sub></i> ( $\mu$ M)	<i>K<sub>cat</sub></i> ( $s^{-1}$ )	<i>k<sub>cat</sub>/K<sub>m</sub></i> ( $s^{-1} \mu$ M <sup>-1</sup> )
<b>P1' (K<sup>59</sup>)</b>	AS <sup>b</sup> -S1'	GST-LCF7 (1-405)	1	13.10±6.60	291.00	22.21
		E199A	ND <sup>c</sup>	ND	ND	ND
		E199Q	ND	ND	ND	ND
		E345A	ND	ND	ND	ND
		E345Q	<b>3000</b>	2.22±0.45	0.20	0.09
		S216D	ND	ND	ND	ND
<b>P2 (D<sup>57</sup>)</b>	AS-S2	S216A	<b>62.5</b>	6.66±2.33	2.24	0.34
		K232A	<b>2000</b>	3.25±0.80	0.18	0.06
<b>B3 region (L<sup>54</sup>, I<sup>45</sup>, V<sup>53</sup>)</b>	B3	N236A	7.5	- <sup>d</sup>	-	-
		F168A	<b>10</b>	2.74±0.67	6.82	2.49
		Y26A	ND	ND	ND	ND
<b>B2 site (D<sup>40</sup>)</b>	B2	I52A	<b>500</b>	4.22±1.24	0.31	0.07
		R133A	ND	ND	ND	ND
<b>B1 region (R<sup>31</sup>, L<sup>32</sup>)</b>	B1	D41A	<b>20</b>	2.02±1.22	4.07	2.01
		D41K	<b>600</b>	4.91±2.10	0.29	0.06
		T17A	0.7	-	-	-
		E38A	<b>80</b>	2.53±0.68	1.46	0.58
		E38K	ND	ND	ND	ND
		E38A/D41A	<b>&gt;3000</b>	-	-	-
		W44A	6.3	-	-	-
		M149A	6.3	-	-	-
W44A/M149A	<b>50</b>	2.34±0.49	3.30	1.41		

<sup>a</sup> The ratio of the amount of LC/F7 derivatives needed to cleave 50% of VAMP-2 wt to the amount of LC/F7 wt needed to cleave 50% of VAMP-2 wt.

<sup>b</sup> Active site.

<sup>c</sup> ND, not detectable. The mutant was too inactive to determine its kinetic constants in the present study.

<sup>d</sup> -, kinetic constants were not determined.

#### 5.4.4.2 Salt bridge mediates the interaction between the P2 (D<sup>57</sup>) of VAMP-2 and the S2 pocket of LC/F7

The VAMP-2 P2 site residue alanine mutant, VAMP-2 (D57A), could reduce the substrate cleavage efficiency of LC/F and LC/F7 by about 500- and 25-fold respectively (**Figure 5.1**) (246), suggesting its important role in LC/F and LC/F7 substrate recognition. The corresponding S2 pocket that specifically recognized the P2 site of VAMP-2 in LC/F was composed of two positively charged residues (R<sup>240</sup> and R<sup>263</sup>), both of which played significant contribution in substrate hydrolysis by LC/F (246). In the S2 pocket of LC/F7, two residues were identified playing roles in interacting with D<sup>57</sup> as well, one positively charge residue (K<sup>232</sup>) and one polar residue (N<sup>236</sup>) (**Figure 5.4A**). The mutations K232A and

N236A in LC/F7 exerted about 2000- and 7.5-fold reduction in substrate hydrolysis respectively, and the LC/F7 (K232A) showed significant effect on *k<sub>cat</sub>* (**Table 5.1**), indicating the very important role of the salt bridge formed between K232 and D57 in stabilizing the P1 site for an efficient scissile bond hydrolysis. In addition, the N<sup>236</sup> in the S2 pocket of LC/F7 may play role in the stabilization of the P1 site via hydrogen bond interaction with the D<sup>57</sup> of VAMP-2. In the interactions between P2-S2, LC/F employed two positively charged residues to interact with D<sup>57</sup> of VAMP-2, and both of the two Arginines played significant contributions (246). However, in LC/F7, one Arginine and one Asparagine were identified in the S2 pocket, and the Arginine displayed a dominant role in interacting with D<sup>57</sup> of VAMP-2. The difference may contribute to the unique substrate recognition mechanism employed by LC/F7 when compared with LC/F as well.

#### **5.4.5 LC/F7 binding pockets interactions with VAMP-2**

Alanine scanning and LC/F7-VAMP-2 complex structure analysis identified three binding pockets in LC/F7 that interacted with the corresponding sites in VAMP-2 (**Figure 5.2**).

##### **5.4.5.1 LC/F7 B2&B3 pockets**

The pockets specifically recognize the B sites of VAMP-2 were designated to be B pockets. The VAMP-2 B3 region located on a helix immediately downstream of the active site was composed of three major hydrophobic residues, L<sup>54</sup>, V<sup>53</sup> and I<sup>45</sup>. The VAMP-2 alanine mutations L54A, V53A and I45A showed ~16-, ~16- and ~5-fold reduced effect on hydrolysis of LC/F7 on VAMP-2 respectively (**Figure 5.1**). Predicted from the modeled LC/F7-VAMP-2 complex structure, three major hydrophobic residues (F<sup>168</sup>, Y<sup>26</sup> and I<sup>52</sup>) in the corresponding B3 pocket in LC/F7 were identified (**Figure 5.4B**). The F168A mutant displayed ~16-fold reductive effect on the hydrolysis activity of LC/F7 mainly by decreasing *k<sub>cat</sub>* (~42-fold); the I52A derivative showed ~500-fold effect on LC/F7 activity in cleaving VAMP-2, with ~3-fold increase in *K<sub>m</sub>* and more than 900-fold reduction effect on *k<sub>cat</sub>*; in addition, the Y26A mutant tested totally abolished the activity of LC/F7 to cleave substrate VAMP-2 (**Table 5.1**). The findings suggested that Y<sup>26</sup> and I<sup>52</sup> in the B3 pocket of LC/F7 may played dominant role in interacting with the corresponding residue in VAMP-2. Previous study showed that in the B3 pocket of LC/F, three hydrophobic residues (Y<sup>168</sup>, Y<sup>26</sup> and I<sup>52</sup>) were identified, but with two Tyrosines employed (246). It seemed at the B3 pocket, both LC/F and LC/F7 employ a slightly different but similar strategy to interact with the B3 region of VAMP-2.

The VAMP-2 B2 site was located a little far away from but still adjacent to the active region (**Figure 5.2**). One negatively charge residue (D<sup>40</sup>) in VAMP-2 was identified to

interact with the corresponding residue, R<sup>133</sup>, in the B2 pocket of LC/F7 (**Figure 5.4B**). The VAMP-2 mutant, D40A exerted about 25-fold in decreasing the hydrolysis efficiency of LC/7 (**Figure 5.1**). The activity of LC/F7 could be abolished by the R133A mutant in the B2 pocket (**Table 5.1**), indicating the significant role of the salt bridge formed between the D<sup>40</sup> of VAMP-2 and the R<sup>133</sup> of LC/F7. In LC/F, a more complicate interaction strategy was applied in the B2 region via the residues E<sup>41</sup>, V<sup>39</sup> and Q<sup>38</sup> of VAMP-2 and R<sup>133</sup>, K<sup>172</sup>, P<sup>25</sup>, V<sup>137</sup> and S<sup>147</sup> residues of LC/F (246), however, the same effect was achieved by LC/F7 in the B2 region through simply utilizing a salt bridge between D<sup>40</sup> of VAMP-2 and R<sup>133</sup> of LC/F7, uncovering the trace of evolution among the different subtypes of BoNT/F.

#### 5.4.5.2 LC/F7 B1 pocket

Like LC/F, the B1 pocket in LC/F7 was located on the opposite surface of the active site and was composed of D<sup>41</sup>, E<sup>38</sup>, W<sup>44</sup> and M<sup>149</sup> (**Figure 5.4C**). The residues, R<sup>31</sup> and L<sup>32</sup>, in the B1 region of VAMP-2 interacted with the corresponding residues in the B1 pocket of LC/F7. The mutants of R31A and L32A showed about 500-fold and 100-fold reductive effect respectively on the hydrolysis efficiency of LC/F7 on VAMP-2 (**Figure 5.1**). The D<sup>41</sup> and E<sup>38</sup> in the B1 pocket of LC/F7 may interacted with the residue R<sup>31</sup> of VAMP-2 via salt bridge. The LC/F7 derivatives, D41A and E38A reduced the substrate cleavage efficiency by about 20-fold and 80-fold respectively. In addition, the double mutant, D41A/E38A of LC/F7 showed more than 3000-fold reductive effect on the hydrolysis efficiency, indicating the synergetic effect of residues D<sup>41</sup> and E<sup>38</sup> in interacting with the R<sup>31</sup> in VAMP-2. Moreover, the charge reversed mutant of D41K decreased the LC/F7 activity to about 600-fold, and E38K mutant totally abolished the substrate cleavage activity of LC/F7, further suggesting the significant role played by negatively charged residues in the B1 pocket in interacting with the R31 residue in the B1 region of VAMP-2 (**Table 5.1**). Similar as the residues of D<sup>41</sup> and E<sup>38</sup>, the W<sup>44</sup> and M<sup>149</sup> residues employed a synergetic effect to interact with L<sup>32</sup> of VAMP-2 as well, the double mutant W44A/M149A displayed about 50-fold reductive effect on the LC/F7 substrate cleavage efficiency by affecting both *K<sub>m</sub>* and *k<sub>cat</sub>*, but mainly on *k<sub>cat</sub>* (**Table 5.1**). In addition, T<sup>17</sup> was within the B1 pocket of LC/F7, and the T17A mutant could slightly increased the activity of LC/F7 (**Table 5.1**), suggesting the potency to optimize the interaction between LC/F7 and VAMP-2 at this site and some other sites that need to be identified. Take together, in the B1 pocket of LC/F7, a very clear division of roles and synergetic effect were discovered among residues, with the D<sup>41</sup> and E<sup>38</sup> synergistically interacted with the R<sup>31</sup> residue of VAMP-2, and the W<sup>44</sup> and M<sup>149</sup> residues displayed synergetic effect in interacting with the L<sup>32</sup> of VAMP-2. Moreover, our finding proved that the interactions between LC/F7 and VAMP-2 have space, at least in the B1

pocket, to improve and optimize to give a more optimal interactions, and thus elevated substrate hydrolysis efficiency.

## 5.5 Discussion

Unlike other metalloendopeptidases, BoNTs need an extended region (exosite) for efficient substrate binding and cleavage. Recently, the mechanisms of BoNT/A, /B, /E, /D and /F and the tetanus neurotoxin have been demonstrated. Each of them employed different strategies in interacting with substrates in order to efficiently cleave corresponding substrates (133,150,243-246,262). In addition, the different subtypes within a serotype also displayed distinctive substrate hydrolysis efficiency. BoNT/A5 was previously reported has a different substrate recognition mechanism when compared with BoNT/A1, even though the former shared 97.1% identity and 97.9% similarity with the later at the amino acid level (265). For the BoNT/F, seven subtypes (F1 through F7) have been identified, and the substrate recognition and cleavage mechanism of subtype BoNT/F1 has been dissected previously. Three binding pockets in the light chain of BoNT/F1 were identified which directed the scissile bond in substrate VAMP-2 to the active site and then get be cleaved (246). BoNT/F7 shares > 60% identity with BoNT/F1 both at holotoxin and enzymatic domain levels, but it is the second-most divergent subtype. And it was discovered that BoNT/F7 required a longer peptide substrate for cleavage than other BoNT/F subtypes, suggesting a different substrate recognition mechanism employed by BoNT/F7(263).

In the present study, VAMP-2 region mapping analysis revealed that the N-terminal 30 residues deletion of VAMP-2 (30-97) showed >4000 fold reduction in VAMP-2 cleavage efficiency by LC/F7, and the N-terminal 20 residues deletion mapping did not exhibit reduced effect (data not shown). No single residue, however, within the N-terminal 20-30 region displayed significant effect on the hydrolysis efficiency of LC/F7 on VAMP-2 (**Figure 5.1**), indicating the VAMP-2 N-terminal 20-30 region, as a whole, exerted important role in the substrate recognition and cleavage process by LC/F7. Taken together, our findings suggested a likely minimal efficient substrate for LC/F7 was VAMP-2 (20-65), with the SNARE motif V1 (38-47) played significant contribution to substrate hydrolysis of LC/F7. Further alanine scanning of VAMP-2 and protein complex modeling and characterization analysis enabled the possible substrate recognition and cleavage mechanism employed by LC/F7 to be uncovered.

Like the mechanism employed by LC/F, three substrate binding pockets distal to the active site in LC/F7 were identified, which facilitate the LC/F7 active site to recognize and catalyze substrate VAMP-2. Firstly, D<sup>41</sup> and E<sup>38</sup> in the B1 pocket of LC/F7 specifically

recognize and interact with the R<sup>31</sup> residue in VAMP-2 with synergetic effect through salt bridge interaction, meanwhile, another two residues in the B1 pocket, W<sup>44</sup> and M<sup>149</sup> synergistically interact with the L<sup>32</sup> of VAMP-2 via hydrophobic interactions (**Figure 5.5**). The results suggested that all the four residues in the B1 pocket of LC/F7 were grouped into two groups with distinctive and clear roles in recognizing and interacting with corresponding residues in the B1 region of VAMP-2. As comparison, such distinctive division of synergetic work of different residues has not been witnessed in the B1 pocket of LC/F. In addition, the slightly increased substrate hydrolysis efficiency of LC/F7 (T17A) indicating the potency of optimization for LC/F7 with elevated activity. After anchored into the LC/F7 B1 pocket, VAMP-2 was further oriented and aligned along the LC/F7 through salt bridge interaction between the R<sup>133</sup>, in the B2 pocket of LC/F7, and the D<sup>40</sup> in the B2 region of VAMP-2. A dramatic difference and more complicated interaction strategy was employed by LC/F in B2 pocket to recognize the residues in the B2 region of VAMP-2 (**Figure 5.5**). The difference in the B2 pocket recognition mechanism employed by LC/F and LC/F7 may throw light onto the evolution of BoNTs. Adjacent to the B2 pocket, the B3 pocket in LC/F7 further oriented and stabilized VAMP-2 to active site via interactions with the corresponding residues in the B3 region of VAMP-2. Both LC/F and LC/F7 utilized a similar VAMP-2 interaction strategy at the B3 pocket, suggesting its significant role in stabilizing substrate for hydrolysis (**Figure 5.5**). Then the scissile bond in VAMP-2 was further stabilized and oriented through interactions between S2-P2, and finally substrate VAMP-2 was cleaved at the process during the interactions between S1'-P1'. Interestingly, in the S2' pocket of LC/F, several hydrophobic residues were identified to interact with the P2' (L<sup>60</sup>) of VAMP-2, and the S2'-P2' hydrophobic interactions between LC/F and VAMP-2 could stabilized the scissile bond arrangement for efficient substrate cleavage. However, it seemed that the role of the P2' site of VAMP-2 was diminished in the interaction with the S2' pocket of LC/F7. Together with the differences in the B1 and B2 pockets, the dramatic differences in the active site also contributed to the unique substrate recognition and cleavage mechanism employed by LC/F7, when compared with LC/F (**Figure 5.5**).

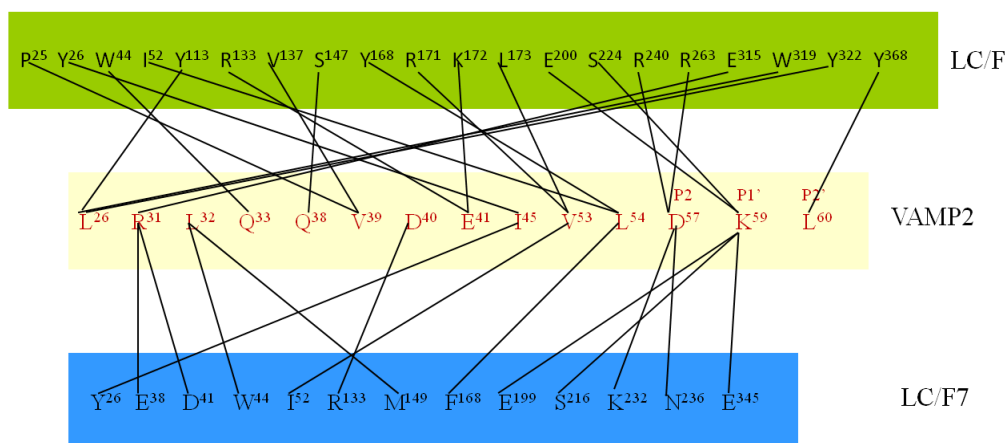


**Figure 5.5 Schematic representation of interactions between LC/F-VAMP-2 and LC/F7-VAMP-2.**

The interaction data of LC/F-VAMP-2 were from reference (246).

In conclusion, the present detailed investigation of the unique substrate recognition and cleavage mechanism of LC/F7 dissected the step by step substrate recognition and hydrolysis though further studies are needed to uncover the exact substrate recognition steps. The present studying broadens the understanding of substrate recognition and cleavage at molecular level employed by BoNTs, provide essential information for the development of antitoxins and novel detection systems for different subtypes of BoNTs, and in addition, may throw light on the evolution trace among different serotypes and subtypes of BoNTs.

# Chapter Six: The most diverse subtype Botulinum Neurotoxin F5 with unique substrate recognition mechanism\*

## 6.1 Abstract

Botulinum Neurotoxins (BoNTs) are the causative agents of botulism via potentially inhibit the neurotransmitter release in motor neurons. In the past decade, seven serotypes of BoNTs (designated as BoNT/A-G) and about 31 *bont* gene subtypes/variants have been identified. Among the BoNT/F serotype, BoNT/F5 is the most diverse subtype which less than 50% identity in amino acid sequence to the other six subtypes. Moreover, the BoNT/F5 was reported to recognize and cleave a different scissile bond formed by L<sup>54</sup>-E<sup>55</sup> in VAMP-2. The present study firstly addressed the unique substrate recognition mechanism adopted by LC/F5 through its B1-B3 binding pockets and S2, S1' and S2' sites in the active site. Our data indicates that the optimal peptide required for efficient substrate cleavage is VAMP-2 (20-65). More interestingly, when comparing with the modeled LC/F1-VAMP-2 complex structure, in the LC/F5-VAMP-2 complex, a N-terminal four-residue shifted  $\alpha$ -helix is observed, suggesting VAMP-2 is likely to coordinate and better fit the different cleft shapes in LC/F5 and LC/F1 by changing conformation. In conclusion, the present findings may helpful in better understanding the unique substrate recognition mechanisms adopted by BoNTs, in developing antitoxin, inhibitor and detection systems.

Key words: Botulinum Neurotoxin F serotype, light chain, VAMP2, subtype, substrate recognition mechanism

Abbreviations: BoNT/F5, Botulinum Neurotoxin subtype F5; LC, light chain; VAMP2, vesicle associated membrane protein-2; SNARE, soluble NSF attachment receptor

\* Most of the work of this chapter has been done, and manuscript will be submitted soon.

## 6.2 Introduction

Botulism was named after the Latin word “*botulus*” for sausage in that it was firstly described by Justinus Kerner after a food poisoning outbreak that followed the ingestion of blood sausages (11). Botulism from food or wounds infection is caused by the most potent protein neurotoxin, Botulinum Neurotoxins (BoNTs) which are produced by *Clostridia botulinum* (5). Human botulism is serious and fatal. If prompt diagnosis and immediate treatment are not given, the mortality rate of botulism is really high, with 5-10% cases are

fatal, even though the incidence of botulism is low, and thus early detection and diagnosis is the key in preventing botulism. Moreover, due to the longevity, easy to deliver and make characteristics of BoNTs, they are treated as potential usage in biological weapons in bioterrorism attacks and listed as Category A agent by Center for Disease Control and Prevention in the United States (12,257).

BoNTs typically represent the neurotransmitters release blocker by inhibiting the release of acetylcholine (Ach) by specifically targeting and degrading the SNARE (Soluble N-ethylmaleimide sensitive fusion protein (NSF) Attachment protein Receptor) proteins at the neuromuscular junction. BoNTs belong to AB toxin family. The holotoxin is a ~ 150 kDa single polypeptide chain which can be functionally divided into two domains: an N-terminal ~ 50 kDa light chain (LC, catalytic domain) and a ~ 100 kDa C-terminal heavy chain (HC) and both of which are covalently linked through a disulfide bond until they encounter reducing conditions in the neuronal cytosol (65). The HC domain is composed of two sub-domains: translocation domain  $H_N$  which mediates translocation of LC across the endosomal membrane, and cell surface receptor-binding domain  $H_C$  (66,67). In the past almost decade, seven serotypes of BoNTs (designated as BoNT/A-G) and about 31 *bont* gene subtypes/variants have been identified (49-54,61-64). In addition, an eighth serotype, BoNT/H, was reported recently (55), however, some scientists question of the new identification and more experiments need to be performed to further prove it as a new serotype (56). And recently, BoNT/H was reported as a hybrid of serotypes F and A characterized with BoNT/A antigenicity and BoNT/F5 light chain function (266).

BoNT/F5 (122,123) is a newly reported subtype which exhibits 46-49% identity in amino acid sequence to the other six subtypes within the BoNT/F serotype. Most importantly but less surprisingly, it cleaves substrate VAMP-2 at a different scissile bond, namely  $L^{54}-E^{55}$ , whereas all the other six subtypes cleave substrate VAMP-2 at  $Q^{58}-K^{59}$ , suggesting that it belongs to a novel class of BoNTs in term of biochemical activity. The finding also shook the principle that all subtypes within a given serotype shared same cleavage site on their respective SNARE substrate. Amino acid residues near the active sites of all the seven subtypes of BoNT/F indicated that several residues immediately upstream of the active site were substituted in BoNT/F5 (122). This degree of variance may contribute to the different cleavage location recognized by BoNT/F5. However, data regarding the efficient substrate recognition and cleavage employed by LC/F5 is currently not elucidated yet.

The present study, for the first time, reported a detailed substrate recognition and cleavage mechanism employed by LC/F5, and proposed a possible LC/F5 and VAMP-2 interaction model to illustrate its unique substrate binding and recognition strategy. The findings may

broaden our understanding of the substrate recognition mechanism utilized by BoNTs, and the better understanding of the mechanism of substrate recognition and cleavage by BoNTs will be prerequisite to develop inhibitors or antidotes for BoNTs intoxication, novel therapeutic applications and rapid detection system in the future.

## **6.3 Materials and Methods**

### **6.3.1 Construct design and cloning**

To facilitate the expression of target protein, the corresponding sequence to full length LC/F5 residues 1-450 (GenBank: ADA79579.1) was codons optimized preferred in *E. coli*, synthesized by Tech Dragon (Hong Kong, China), sub-cloned into pGEX-2T vector through *SacI/BamHI* restrictive sites. In addition, the human VAMP-2 (1-97) construct was achieved as detailed previously (243). All the mutated derivatives of LC/F5 and VAMP-2 were performed by using QuickChange (Stratagene) commercial kit following the manufacturer's instruction and confirmed by sequencing in BGI (Shenzhen, China).

### **6.3.2 Protein expression and Purification**

Based on our previous study on LC/F5 (267), GST tagged full length LC/F5 (1-450) displayed the highest solubility and activity when compared with other versions of LC/F5. Thus in the present study, all the assays were carried out by using purified GST-LC/F5 (1-450) protein. The purification of GST-LC/F5 (1-450) and VAMP-2 (1-97) and all derivatives was achieved as previously described (246,267).

### **6.3.3 Molecular Modeling**

The complex structure of LC/F5-VAMP-2 was modeled by using SWISS-MODEL and refined with PyMoL software as detailed previously (245). Briefly, the structure of LC/F5 (1-450) was modeled by SWISS-MODEL by using the crystal structure of LC/F (PDB 2A8A) as searching template and the structure of VAMP-2 was extracted from the SNARE complex crystal structure (chain A, PDB 1SFC) and both structures were modified by PyMoL. The LC/F5-VAMP-2 complex structure was modeled then by aligning to the LC/A-SNAP-25 complex structure (PDB 1XTG) and refined in the PyMoL software.

### **6.3.4 Standard Linear Velocity Reaction**

Linear velocity assays were performed as previously described (246). Briefly, in 10  $\mu$ l reaction mixture, 5-10  $\mu$ M VAMP-2 or derivatives was mixed with indicated amount of LC/F5 in 10:20 buffer (10 mM Tris-HCl, pH 7.6, 20 mM NaCl). After 20min incubation at 37°C, the reactions were stopped by adding SDS-PAGE sample buffer, heated at 100°C for

5min, analyzed by SDS-PAGE. The amount of VAMP-2 cleaved was determined by densitometry.

### 6.3.5 Kinetic Parameters Determination

As described previously (262), the  $K_m$  and  $k_{cat}$  determination were almost the same as above mentioned, but the amount of LC/F5 or its derivatives was adjusted to achieve <10% cleavage of VAMP-2 which concentrations ranged from 1 to 72  $\mu$ M. Reaction velocity against substrate concentration was fitted to the Michaelis–Menten equation and kinetic constants were derived using the GraphPad program. For each protein, at least three independent assays were performed to determine the kinetic constants.

### 6.3.6 Far-UV Circular Dichroism Analysis

As detailed previously (262), LC/F5 and derivatives were analyzed by far-UV CD for the check of secondary structure change in a 10-mm path length quartz cuvette with 400  $\mu$ l volume (containing 0.1–0.4 mg/ml protein in 10:20 buffer). A JASCO J-810 spectropolarimeter was used with parameters set as: scanning speed 50 nm/min, 1s response time, 1nm data pitch, 1nm band width and accumulation times was set as 3. The wavelength range of 200-250nm was scanned, and raw CD data were converted to molar ellipticity using Yang as reference (264), and the spectrum was generated using GraphPad Prism.

## 6.4 Results

Identified as the most diverse subtype among all the seven subtypes of the BoNT/F serotype, BoNT/F5 (122,123) shares less than 50% identity in amino acid level to the other six subtypes. In addition, enzymatic analysis revealed that BoNT/F5 recognized and cleaved a different scissile bond on substrate VAMP-2 (122), which shook the principle that all subtypes within a given serotype shared same cleavage site on their respective SNARE substrate. Taken together, all of the findings indicate that, in term of biochemical activity, BoNT/F5 belongs to a novel class of BoNTs, and it is likely that BoNT/F5 employs a unique substrate recognition and cleavage strategy.

To uncover the mysterious substrate recognition mechanism of BoNT/F5, a GST tagged light chain of BoNT/F5, namely GST-LC/F5 (1-450), was purified and used to test the individual residue effect from VAMP-2 on the enzymatic activity of LC/F5. In order to achieve this goal, saturation alanine mutagenesis was carried out by using the VAMP-2 (1-97) as backbone, and at the same time, different truncations of VAMP-2 were made as well by employing mutagenesis method or other relative DNA technologies. Our data indicated that the residues within the region 20-40 of VAMP-2 contributed significantly to the

interactions between VAMP-2 and LC/F5, with the truncated VAMP-2 (40-97) deducted ~8000-fold activity of LC/F5, however, the VAMP-2 (1-65) truncation only displayed ~4-fold effect on the activity of LC/F5 (data not shown). All the data suggested that the possible minimal peptide region required for efficient substrate cleavage was VAMP-2 (20-65). In order to dissect the role of individual residue in VAMP-2, saturation alanine-scanning analysis was performed within VAMP-2 (22-66) (**Figure 6.1**). The residues that exert important contribution to interact with the corresponding residue in LC/F5 mainly locate within the region 40-60 of VAMP-2 and some other important residues locate downstream or upstream (**Figure 6.1**). Most of the residues tested with the location before 30 of VAMP-2 displayed less than 5-fold effect on the substrate cleavage by LC/F5, except N29A mutant of VAMP-2, which deducted the substrate cleavage efficiency of LC/F5 by ~20-fold. In addition, the VAMP-2 mutants, R31A, E41A, N49A, V50A, D51A, K52A, E55A, R56A and Q58A displayed ~200-, 80-, 10-, 50-, 10-, 20-, 750-, 4000- and 25-fold deductive effect respectively on the activity of LC/F5 to cleave VAMP-2 (**Figure 6.1**), most of which locate within or adjacent to the V1 motif of VAMP-2 (**Figure 6.1, inset**). Consistent with previous findings on the important role played by the P1' residue of substrate (148,243,262), for LC/F5, the VAMP-2 P1' site mutant, E55A, required about 750-fold more amount of LC/F5 to hydrolyze 50% of the mutant. The same as the R56A, the VAMP-2 P2' site mutant, which deducted the LC/F5 substrate cleavage capacity by ~4000-fold (**Figure 6.1**).

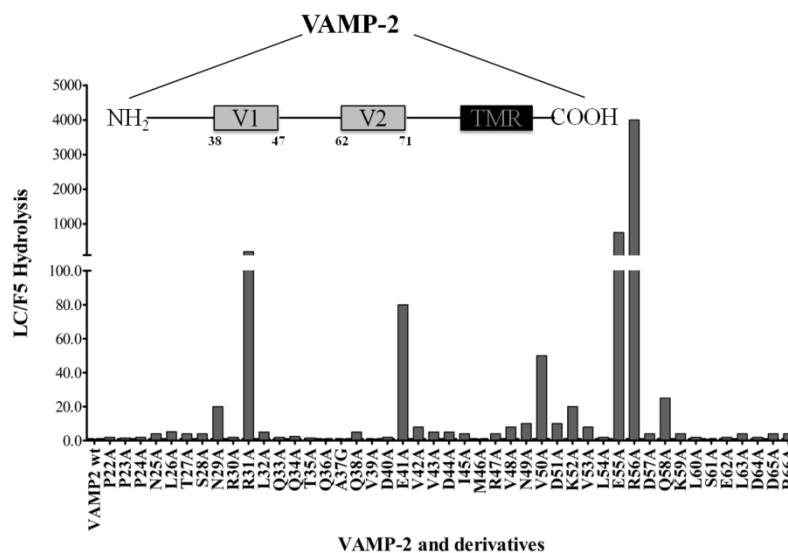


**Figure 6.1 Hydrolysis analysis LC/F5 on the cleavage of VAMP-2 and derivatives.**

Hydrolysis was measured as the ratio of the amount of LC/F5 to cleave 50% of VAMP-2 and derivatives against the amount of LC/F5 to cleave 50% of VAMP-2 wt. The dash line highlights the no effect level. In the inset, the motifs distribution within VAMP-2 is illustrated.

In order to identify the corresponding residues in LC/F5 to interact with VAMP-2, the structure of LC/F5 was firstly modeled by using SWISS MODEL based on the structure of LC/F (chain A, PDB 2A8A), and then LC/F5-VAMP-2 complex structure was modeled by aligning with the complex structure of LC/F with a peptide inhibitor (PDB 3FIE) with the help of PyMOL (**Figure 6.2**). The predicted, based on the modeled LC/F5-VAMP-2 structure, residues that may specifically interact with the corresponding residues in VAMP-2 were proved by biochemical characterization. Far-UV CD analysis were performed to probe whether the introduced mutations of LC/F5 affected the overall protein conformation and stability, with the aim to avoid the possibility that the resulted difference in substrate cleavage efficiency was arose by the different mutations of LC/F5(**Figure 6.3**). All LC/F5 mutants retain a similar secondary structure profile as wild type LC/F5 suggesting they do not likely impact the overall protein structure. Though the wavelengths at which maximal and minimal peak values observed with slight changes, the differences are too minor to take into consideration. In addition, partial trypsin digestion analysis was performed as well (data not shown), and the result indicated that all of the LC/F5 mutants had an identical digestion profile to that of wild type LC/F5. In conclusion, the introduced mutations of LC/F5 analyzed did not cause significant conformational change in the overall protein structure.

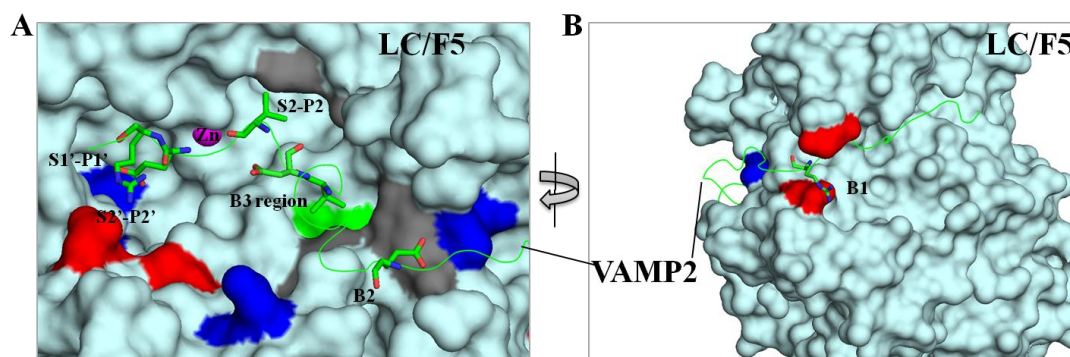


**Figure 6.2 Overall view of the modeled LC/F5-VAMP-2 complex structure.**

(A) view of the active site, B2 and B3 regions alignment; (B) view after a 90° clockwise turn, displaying the B1 region interactions. LC/F5 is shown as a surface structure, and VAMP-2 in ribbon structure. Based on prediction, the corresponding interacting sites/regions between LC/F5 and VAMP-2 are highlighted. The residues were colored based on side chain: negatively charged (red), positively charged (blue), hydrophobic (gray) polar (green) and zinc (magenta sphere).

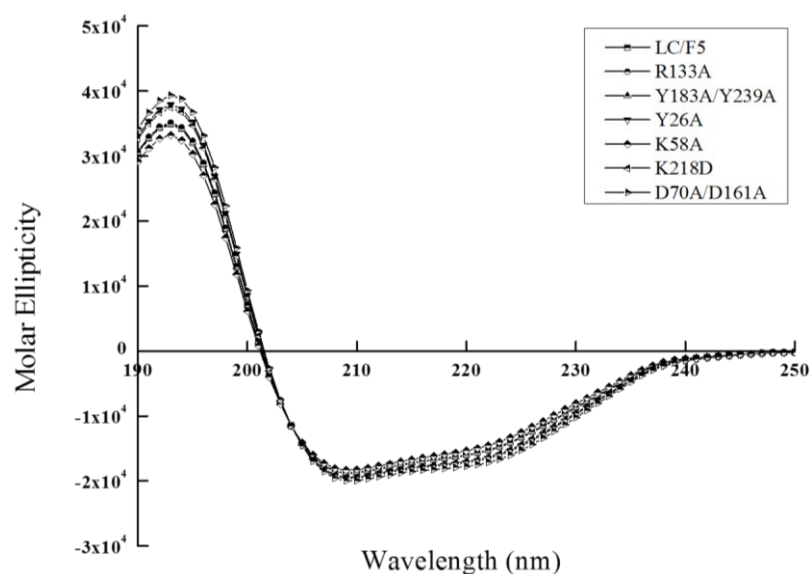


**Figure 6.3 Circular Dichroism spectroscopy analysis of LC/F5 derivatives.**

Far-UV CD (190–250 nm) data were obtained for LC/F5 and its derivatives with a JASCO J-810 spectropolarimeter at room temperature. The molar ellipticity per residue weight is shown for the representative LC/F7 derivatives and wild type, and each is labeled in different symbol.

#### 6.4.1 LC/F5 active site substrate recognition

By taking VAMP-2 alanine screening analysis and modeled LC/F5-VAMP-2 complex structure information into consideration, three active sites in LC/F5, S2', S1' and S2 (**Figure 6.2**), were identified and characterized in detail.

*The VAMP-2 P2' (R<sup>56</sup>) site interacts with the corresponding S2' pocket of LC/F5 via the mediation of salt bridge* – The S2' pocket in LC/F5 that specifically recognized the positively charged R<sup>56</sup> of VAMP-2 comprised two aspartic acids, D<sup>70</sup> and D<sup>161</sup> (**Figure 6.4A**). LC/F5 cleaved the VAMP-2 (R56A) mutant with ~4000-fold lower efficiency (**Figure 6.1**), indicating the important role played by the VAMP-2 P2' site on the hydrolysis of LC/F5. In addition, the activity of LC/F5 could be deduced by D70A and D161A mutants ~10- and ~1000-fold respectively by mainly exerting effect on  $k_{cat}$ , and the activity of LC/F5 was further abolished by the double mutation, LC/F5 (D70A/D161A) (**Table 6.1**). The data clearly proved the significant role of the salt bridge formed between R<sup>56</sup> of VAMP-2 and D<sup>70</sup>/D<sup>161</sup> of LC/F5, the interaction between the R<sup>56</sup> of VAMP-2 and D<sup>161</sup> of LC/F5 is dominant.

*Another salt bridge mediates the interaction between the P1' (E<sup>55</sup>) of VAMP-2 and the S1' pocket of LC/F5* – The P1' site in either VAMP-2 or SNAP-25 was proved to be very important to its corresponding BoNTs (145,148,150,243,262). The same rule was abided by VAMP-2 as well when hydrolyzing by LC/F5. The VAMP-2 (E55A) reduced the substrate

cleavage efficiency of LC/F5 by ~750-fold (**Figure 6.1**), indicating the very important role of the VAMP-2 P1' site in the recognition by LC/F5. The identified corresponding S1' pocket that specifically recognized the P1' site of VAMP-2 in LC/F5 was composed of a positively charged residue, K<sup>218</sup> (**Figure 6.4A**). The activity of LC/F5 was totally abolished by the alanine mutant, K218A, and the charge reversed mutant, K218D. Moreover, ~8-fold deductive effect was witnessed for the same charged residue replacement of LC/F5, K218R (**Table 6.1**). Taken together, all the findings indicated a very important role of the salt bridge formed between K<sup>218</sup> of LC/F5 and E<sup>55</sup> of VAMP-2 in orienting and stabilizing the scissile bond toward the active site of LC/F5 for efficient substrate cleavage.

**Dual recognition of the VAMP-2 P2 (V<sup>53</sup>) by the S2 pocket of LC/F5**– The P2 site of VAMP-2 plays a certain role in recognizing by LC/F5, with the VAMP-2 (V53A) mutant reduced LC/F5 hydrolysis by ~8-fold (**Figure 6.1**). In the corresponding interaction site of LC/F5, two hydrophobic residues were identified, Y<sup>183</sup> and Y<sup>239</sup> (**Figure 6.4A**). The single Alanine mutation of both Tyrosines, Y183A and Y239A exerted ~3-fold and ~8-fold effect on the LC/F5 substrate hydrolysis efficiency respectively, but the double mutant, LC/F5 (Y183A/Y239A) displayed ~1000-fold attenuated substrate cleavage efficiency, with effect mainly on *k*<sub>cat</sub> but not on *K*<sub>m</sub> (**Table 6.1**). These data indicate that the two Tyrosines work complementarily and synergetically with each other in the interaction with the VAMP-2 P2 site residue. The dual recognition strategy is proved very common in the interactions between LC/D and substrate VAMP-2 (262), the dual recognition identified in the VAMP-2 P2 site with the corresponding site of LC/F5 will undoubtedly increase the LC/F5's tolerance to mutations in nature.

#### **6.4.2 LC/F5 binding pockets interactions with VAMP-2**

Three binding pockets, designated as B1-B3, in LC/F5 were identified based on the modeled LC/F5-VAMP-2 complex structure and the VAMP-2 screening results (**Figure 6.2**).

**LC/F5 B3 pocket**– The pockets in LC/F5 that specifically recognize the B sites of VAMP-2 were designated to be B pockets. The VAMP-2 B3 region which locates adjacently to the scissile bond is composed of V<sup>50</sup> and D<sup>51</sup> (**Figure 6.4B**). The VAMP-2 alanine mutations V50A and D51A showed ~50- and ~10-fold side effect on the hydrolysis of LC/F5 on substrate VAMP-2 respectively (**Figure 6.1**). In the B3 pocket of LC/F5, two tyrosines (Y<sup>26</sup> and Y<sup>50</sup>) and one polar residue (T<sup>192</sup>) are likely interacting with the V<sup>50</sup> of VAMP-2 (**Figure 6.4B**) through hydrophobic interaction or hydrogen bond interaction, with the Y26A, Y50A and T192A attenuated the substrate cleavage efficiency of LC/F5 by ~60-, ~10- and ~3-fold respectively. The triple mutant, LC/F5 (Y26A/Y50A/T192A) could further reduced the activity of LC/F5 by ~600-fold(**Table 6.1**). One positively charged residues in the B3

pocket of LC/F5 (K<sup>58</sup>) (**Figure 6.4B**) was predicted to interact with the VAMP-2 D<sup>51</sup> residue, the corresponding alanine mutation, K58A exerted ~250-fold side effect on the substrate hydrolysis by LC/F5 (**Table 6.1**). The recognition and interactions in the B3 pocket may work in the process of orientation and tuning of scissile bond to fit the active site in LC/F5.

**LC/F5 B2 pocket**– In VAMP-2, the B2 site comprises residue E<sup>41</sup> (**Figure 6.4C**). The VAMP-2 alanine mutation E41A showed ~80-fold side effect on the hydrolysis of LC/F5 on substrate VAMP-2 (**Figure 6.1**). In the corresponding B2 pocket of LC/F5, R<sup>133</sup> (**Figure 6.4C**) was predicted to interact with the E<sup>41</sup> of VAMP-2 via salt bridge. The R133A mutation of LC/F5 displayed ~300-fold reductive effect on the activity of LC/F5 (**Table 6.1**), indicating the important interaction occurred between the E<sup>41</sup> of VAMP-2 and R<sup>133</sup> of LC/F5. In conclusion, in the B2 pocket of LC/F5, the very important salt bridge interaction between E<sup>41</sup> of VAMP-2 and R<sup>133</sup> of LC/F5 is likely stabilizing the binding of VAMP-2 with LC/F5 and orienting a further interaction between VAMP-2 and LC/F5 in the B3 pocket.

**LC/F5 B1 pocket**– The B1 site of VAMP-2, which is distal to the active site, is composed of R<sup>31</sup>, the corresponding interaction residues in the B1 pocket of LC/F5 were predicted as E<sup>147</sup> and E<sup>308</sup> (**Figure 6.4D**). The VAMP-2 mutant, R31A, could reduce the LC/F5 hydrolysis by ~200-fold (**Figure 6.1**), suggesting the important role played by the interactions with the R<sup>31</sup> of VAMP-2 in the recognition process by LC/F5. Based on the modeled LC/F5-VAMP-2 complex structure, the possible salt bridge between the R<sup>31</sup> of VAMP-2 and the E<sup>147</sup> and E<sup>308</sup> of LC/F5 plays role in substrate recognition and binding (**Figure 6.4D**). Surprisingly, the E147A and E308A mutants of LC/F5 exerted almost no effect on substrate cleavage (data not shown), so did the double mutant, LC/F5 (E147A/E308A) (**Table 6.1**). The charge reversed residue replacement of the E147 site, E147R, displayed ~80-fold reductive effect on the substrate hydrolysis by LC/F5, but the LC/F5 (E308R) charge reversed mutant did not exert obvious effect on the substrate cleavage activity (**Table 6.1**), suggesting the very important interaction occurred between the R<sup>31</sup> of VAMP-2 and the E<sup>147</sup> of LC/F5 via salt bridge. In conclusion, the interactions in the B1 pocket of LC/F5 and the corresponding B1 site of VAMP-2 are likely working in anchoring the VAMP-2 onto the LC/F5, initiating recognition and binding between VAMP-2 and LC/F5.

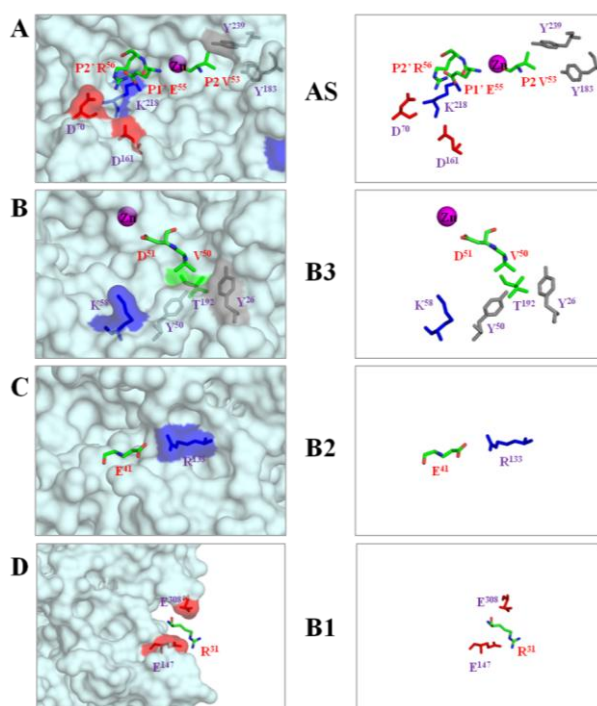


**Figure 6. 4 Specific interactions and recognition between VAMP-2 and LC/F5.**

(A) At the active site (AS), the S2' pocket in LC/F5 that specifically recognized the positively charged R<sup>56</sup> of VAMP-2 comprised two aspartic acids, D<sup>70</sup> and D<sup>161</sup> through salt bridge and the interaction between the R<sup>56</sup> of VAMP-2 and D<sup>161</sup> of LC/F5 is dominant. The identified corresponding S1' pocket that specifically recognized the P1' site of VAMP-2 (E<sup>55</sup>) in LC/F5 was composed of a positively charged residue, K<sup>218</sup>. The formed salt bridge may play role in orienting and stabilizing the scissile bond toward the active site of LC/F5 for efficient substrate cleavage. In the corresponding interaction site of LC/F5, two hydrophobic residues, Y<sup>183</sup> and Y<sup>239</sup> interact complementarily and synergetically with the P2 site of VAMP-2 (V<sup>53</sup>). (B) In the B3 pocket of LC/F5, the salt bridge between the D<sup>51</sup> of VAMP-2 and K<sup>58</sup> of LC/F5, and the hydrophobic or hydrogen bond interactions between V<sup>50</sup> of VAMP-2 and Y<sup>26</sup>, Y<sup>50</sup> and T<sup>192</sup> of LC/F5, are likely stabilizing the binding of VAMP-2 with LC/F5 and orienting the scissile bond toward the active site to prompt substrate hydrolysis. (C) Like the B3 pocket/region interactions, in the B2 site of LC/F5, another salt bridge interaction between E<sup>41</sup> of VAMP-2 and R<sup>133</sup> of LC/F5 are likely stabilizing the interactions of VAMP-2 and LC/F5 and orienting the scissile bond to prompt hydrolysis by LC/F5 as well. (D) In the B1 pocket/region interactions, the E<sup>147</sup> and E<sup>308</sup> of LC/F5 possible interact with the R<sup>31</sup> of VAMP-2 through salt bridge and with the E<sup>147</sup> plays dominant role. The interactions may initiate the recognition and binding between VAMP-2 and LC/F5. The structure of LC/F5 in the right panel is shown as surface with 40% transparency, the residues of VAMP-2 that identified interacting with the corresponding residues of LC/F5 were shown in stick. The active site recognition and binding site interactions of LC/F5 were shown in stick and highlighted based on side chain: negatively charged (red), positively charged (blue), hydrophobic (gray) polar (green) and zinc (magenta sphere).

**Table 6.1 Efficiency of VAMP-2 hydrolysis and kinetic constants of LC/F5 and derivatives.**

LC/F5 pockets	VAMP-2 site/region (residue)	LC/F5 derivatives	Activity	<i>K<sub>m</sub></i> ( $\mu$ M)	<i>K<sub>cat</sub></i> ( $s^{-1}$ )	<i>k<sub>cat</sub>/K<sub>m</sub></i> ( $s^{-1} \mu M^{-1}$ )
			reduction (-fold) <sup>a</sup>			
		LC/F5 (1-450)	1	5.13±1.75	938.90	183.02
AS <sup>b</sup> -S2'	P2'(R <sup>56</sup> )	D161A	<b>1000</b>	1.81±0.69	1.58	0.87
		D70A	<b>10</b>	4.11±1.41	131.1	31.90
		D70A/D161A	<b>ND<sup>c</sup></b>	ND	ND	ND
AS-S1'	P1' (E <sup>55</sup> )	K218A	<b>ND</b>	ND	ND	ND
		K218D	<b>ND</b>	ND	ND	ND
		K218R	8	8.27±2.65	192.8	23.31
AS-S2	P2 (V <sup>53</sup> )	Y183A	3.2	– <sup>d</sup>	–	–
		Y239A	8	–	–	–
		Y183A/Y239A	<b>1000</b>	4.91±2.41	0.85	0.17
B3	B3 region (V <sup>50</sup> , D <sup>51</sup> )	Y50A	10	14.52±7.36	402.8	27.74
		Y26A	<b>60</b>	1.29±0.25	18.43	14.29
		T192A	3	–	–	–
		Y26A/Y50A/T192A	<b>600</b>	6.55±2.33	3.2	0.49
		K58A	<b>250</b>	16.17±9.00	4.5	0.28
B2	B2 site (E <sup>41</sup> )	R133A	<b>300</b>	5.80±3.76	2.01	0.35
B1	B1 site (R <sup>31</sup> )	E147A/E308A	5	–	–	–
		E147R	<b>80</b>	6.07±2.58	23.49	3.87
		E308R	0.8	–	–	–

<sup>a</sup> The ratio of the amount of LC/F5 derivatives needed to cleave 50% of VAMP-2 wt to the amount of LC/F5 wt needed to cleave 50% of VAMP-2 wt.

<sup>b</sup> Active site.

<sup>c</sup> ND, not detectable. The mutant was too inactive to determine its kinetic constants in the present study.

<sup>d</sup> -, kinetic constants were not determined.

## 6.5 Discussion

In 2010, BoNT/F5 was reported as a new subtype of BoNT/F serotype based on phylogenetic analysis and signs of botulism in mice. The new BoNT/F5 subtype required 20 more times of antiserum to neutralize an equivalent amount of BoNT/F1 toxin (53,123). In addition, BoNT/F5 exhibits ~70% and ~47% amino acid identities at holotoxin and light chain levels respectively with BoNT/F1 (122,123). Moreover, BoNT/F5 cleaves substrate VAMP-2 at a different scissile bond from all the other six subtypes and the finding shook the principle that all subtypes within a given serotype shared same cleavage site on their respective SNARE substrate (122). Further analysis suggested that one possible reason that

led to the changed cleavage site in VAMP-2 recognized by BoNT/F5 was the substituted residues near the active sites (122).

In the present report, the detailed substrate recognition and cleavage mechanism employed by LC/F5, for the first time, was uncovered. Saturation alanine mutagenesis analysis on substrate VAMP-2 revealed that the likely minimal peptide region required for efficient substrate cleavage by LC/F5 was VAMP-2 (20-65), in which with the P1' (E<sup>55</sup>) and P2' (R<sup>56</sup>) site residues played a very significant role in interacting with LC/F5 (**Figure 6.1**). The finding is consistent with previous studies on the important role played by the P1' residue in substrate (148,243,262). In addition, most of the individual residues that found important to interact with LC/F5 are located within or adjacent to the V1 motif of VAMP-2. In the neuron cell cytosol, when the translocated LC/F5 approaches VAMP-2, the recognition between LC/F5 and VAMP-2 is initiated by the interactions between the residues in the B1 region of VAMP-2 (R<sup>31</sup>) and the corresponding residues in the B1 pocket of LC/F5 (E<sup>147</sup> and E<sup>308</sup>). After the anchor of VAMP-2 to LC/F5, the VAMP-2 is further aligned along the LC/F5 via the recognition and interactions between the B2 and B3 regions of VAMP-2 and the corresponding B2 and B3 pockets in LC/F5. In the B2 and B3 pockets of LC/F5, the two dominant salt bridge interactions between E<sup>41</sup> of VAMP-2 and R<sup>133</sup> of LC/F5 and D<sup>51</sup> of VAMP-2 and K<sup>58</sup> of LC/F5, and a third hydrophobic or hydrogen bond interactions between V<sup>50</sup> of VAMP-2 and Y<sup>26</sup>, Y<sup>50</sup> and T<sup>192</sup> of LC/F5, are likely stabilizing the binding of VAMP-2 and orienting the scissile bond toward the active site to prompt substrate hydrolysis by LC/F5. Furthermore, with the tuning and stabilization function of the P2-S2, P1'-S1' and P2'-S2' interactions and recognition (**Figure 6.4A**), the VAMP-2 scissile bond can be hydrolyzed by LC/F5 with high efficiency.

Interestingly, based on the analysis and comparison of the modeled LC/F5-VAMP-2 and the LC/F1-VAMP-2 (148) complex structures, in the later modeled structure (**Figure 6.5B**), a VAMP-2  $\alpha$ -helix was formed by residues in the region of 49-NVDKVL-54, but in the former structure(**Figure 6.5A**), a VAMP-2  $\alpha$ -helix was formed by residues in the region of 45-IMRVNV-50, there is a four-residue shift of the  $\alpha$ -helix toward N-terminal. The different conformation observed in VAMP-2 is likely to coordinate and better fit the different cleft shapes in LC/F5 and LC/F1 with the aim to achieve efficient substrate recognition and cleavage.

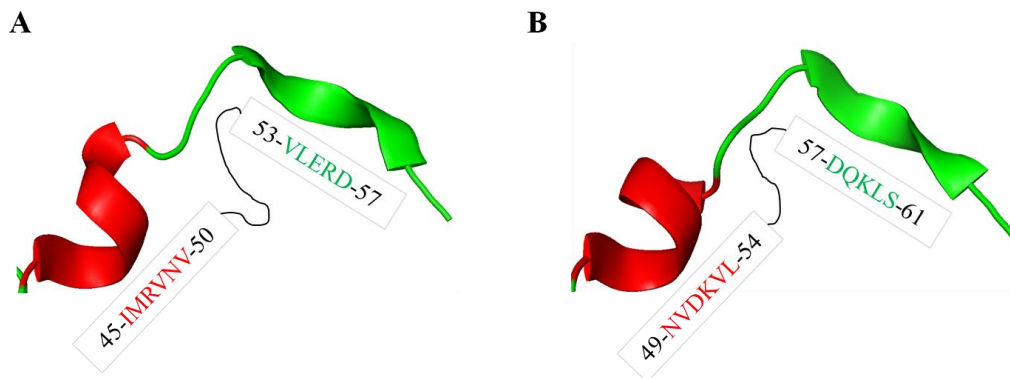


**Figure 6.5 Overall comparison of the N-terminal shifted  $\alpha$ -helix in the modeled VAMP-2.**

Comparing the LC/F5-VAMP-2 (A) and the LC/F1-VAMP-2 (B) complex structures, the VAMP-2  $\alpha$ -helix in the later shifts four residues toward the N-terminal, the shift prompts VAMP-2 to fit the cleft in the LC/F5 for efficient substrate cleavage. The modeled VAMP-2 structure is represented in cartoon with the shifted  $\alpha$ -helix colored in red, and so did the corresponding residues. The VAMP-2 structure in the modeled LC/F1-VAMP-2 complex was extracted and refined from reference (148).

To conclude, for the first time, the step by step recognition and binding between LC/F5 and VAMP-2 is dissected in the present study and the mysterious substrate recognition mechanism employed by BoNT/F5 is partially uncovered, though further studies are needed to reveal the mechanism in more detail. The present work throws light on a better understanding of the substrate recognition mechanisms adopted by BoNTs, provides more clues on the antitoxin and inhibitor development and may be helpful in developing more universal or specific detection systems.

# Chapter Seven: Substrate-based inhibitors exhibiting excellent protective and therapeutic effects against Botulinum Neurotoxin A intoxication\*

## 7.1 Abstract

Botulinum neurotoxins (BoNT), are potential biological weapon which have been classified as a category A agent by the CDC (Centers for Disease Control and Prevention) in the US. However, this group of protein is also widely used as protein-based therapeutic compounds; for instance, BoNT/A has been approved by the US FDA to treat strabismus, blepharospasm, and hemifacial spasm as early as 1989. However, with an increasing risk of human botulism and medical overdose associated with the use of BoNTs, there is an urgent need for the development of safer and more effective BoNTs therapies. Vaccine, antibodies and small compound inhibitors have attracted intense research interest during the past years. However, potent inhibitors, which can complement the lack of protective and therapeutic effects of vaccines and monoclonal antibodies in situations where BoNTs have entered the cell, are still not available. Based upon the current understanding of the substrate recognition mechanism of BoNTs, we have designed a novel class of peptide inhibitors by using the BoNT/A substrate SNAP25 as backbone. Through a combination of *in vitro*, cellular based, and *in vivo* mouse assays, several potent peptide inhibitors with about one nanomolar inhibitory strength both *in vitro* and *in vivo* have been identified. These findings validated the hypothesis that a peptide inhibitor which can interact with the two regions of BoNT responsible for substrate recognition and cleavage respectively may exhibit a synergetic inhibition effect, thereby providing insight on future development of more potent inhibitors against BoNTs.

**Keywords:** Botulinum Neurotoxin serotype A, SNAP25, inhibitor, potent, mice model

\*The work of this chapter has been done, and manuscript has been submitted.

## 7.2 Introduction

Botulinum neurotoxins (BoNTs) are the causative agents of botulism which work by specifically interfering with vesicle fusion and neurotransmitter release in nerve cells (205,207). BoNTs are synthesized as a 150 kDa single chain protein, which is subsequently cleaved into a di-chain linked by a disulfide bond between its 50 kDa light chain (LC) and 100 kDa heavy chains (HC). The typical A-B structure-function BoNTs can be further organized into three functional domains: an N-terminal catalytic domain (light chain, LC), an internal translocation domain (heavy chain, HCT), and a C-terminal receptor binding domain (heavy chain, HCR) (206). BoNTs inhibit exocytosis by specifically cleaving one of the three SNARE proteins, SNAP25, VAMP2 and syntaxin 1a, the complex formed among which is the driven force of mammalian neuronal exocytosis (208). Eight serotypes of BoNTs (termed A–H) that cleave specific residues on one of the three SNARE proteins have been identified over the past 75 years. Serotype H (BoNT/H), being a newly added member of this family, is structurally similar to the subtype F5 of BoNT/F (55,121,205,209,210,268).

It is known that muscles will regain function upon clearance of the infected neuronal cells. The reversible nature of BoNTs intoxication has made it possible to transform these deadly agents into novel therapeutics for treatment of a range of neuromuscular conditions (197,211-213,220,269-273). However, with the persistence problems of human botulism, mal-functional use and medical overdose as a result of the increased usage of BoNTs in clinical applications, efforts to develop safer and more effective BoNTs-based therapeutic approaches have intensified. Vaccines and monoclonal antibodies (154-156), including *E.coli*-based recombinant subunit vaccine (157-159) and human-derived polyclonal- and neutralizing monoclonal- antibodies that block the entry of BoNTs into nerve cells, have been developed or intensively studied. The major limitation regarding the use of vaccine and antibodies is that their effectiveness will be drastically reduced upon entry of BoNTs into nerve cells. Potent inhibitors that inactivate BoNTs activity in nerve cells are therefore urgently needed to provide therapeutic effects under such situations. Efforts have been made to develop small molecular inhibitors targeting the active site of BoNTs using various approaches, including direct compound library screening, computer-aided small molecular design, screening of natural compounds, etc. However, the most potent small molecular inhibitors that have been identified so far exhibited inhibitory effects at  $\mu\text{M}$  range. In addition, their affinity ( $K_m$ ) towards BoNTs is similar to that of BoNTs substrates; hence they have no advantage in being used as a potent inhibitor (160-165). Attempts to develop natural product-based small inhibitors that target the binding domain of BoNTs also failed (165). The difficulties of developing small molecular inhibitors for BoNTs are probably due to the unique mechanism of extended substrate recognition of BoNTs, which requires a

substrate binding and recognition regions for efficient substrate hydrolysis (133-135,145,146). Nevertheless, structural and substrate-based small peptides targeting the active site of BoNTs have been studied, with the most promising peptide inhibitors exhibiting a  $K_i$  as low as nM range. The mechanisms of inhibition of these peptide inhibitors involve interaction with BoNTs active site residues that are significant to substrate recognition (166-170). These studies therefore offer a promising possibility for the design of effective peptide-based BoNTs inhibition. However, the limited affinity of a peptide that targets only to the active site of BoNTs prohibited further development of these peptide inhibitors with higher potency.

Previous studies indicated that LC/A-SNAP25 interactions are not optimal and that the mutation at specific residues can improve both substrate binding and catalysis (133,171), supporting the hypothesis that the peptide inhibitor containing both active site and binding regions could dramatically increase its affinity and potency. In the present study, we reported the development of potent peptide inhibitors of BoNT/A which exhibited nM inhibition effect both *in vitro* and *in vivo*. Most importantly, this novel substrate based inhibitors could provide full protection against 4xLD<sub>50</sub> challenge by BoNT/A, representing the best BoNT inhibitors to date. Our findings infer that BoNT substrate-based inhibitors exhibit huge potential as effective therapeutic agents against BoNT/A intoxication.

## **7.3 Materials and Methods**

### **7.3.1 Plasmid construction and proteins purification.**

LC/A and SNAP25 were constructed and purified as described previously and description in previous chapters (133).

### **7.3.2 Development of high affinity peptides for LC/A.**

In order to produce highly potent LC/A inhibitors, site-directed mutagenesis was performed, using the SNAP25 (141-206) as backbone, to mutagenize sites which were selected based on the co-crystal structure of LC/A-SNAP25 (PDB ID: 1XTG) and previous understanding of LC/A and SNAP25 recognition mechanism (143,145). The newly created mutations were confirmed by sequencing. All the proteins were purified and subjected to activity analysis as previously described (133).

### **7.3.3 Development of potential LC/A inhibitors with high inhibition efficiency.**

Kumar *et al* reported a potential LC/A tetra-peptide inhibitor, RRGF, with an  $IC_{50}$  of 0.9  $\mu$ M and a  $K_i$  as low as 358 nM, but the substrate they used was a 17-residue synthetic peptide corresponding to residues 187-203 of SNAP25 (274). In addition, we have previously found that LC/A almost could not cleave the SNAP25 Q<sup>197</sup>C mutant (unpublished data). Based on these findings, we designed the following peptides: 1) R197C, the backbone of which is SNAP25 (80-196), with a Q<sup>197</sup>C single mutation; 2) R1, the backbone of which is SNAP25 (80-196), plus a Q<sup>197</sup>C mutation and a RRGF tetra-peptide added at the C terminal; 3) R2, the backbone of which is also SNAP25 (80-196), plus a Q<sup>197</sup>C mutation and a WTKFL penta-peptide added at the C terminal; and 4) R1-RXF, the backbone of which is R1, but with the first R deleted from the RRGF tetra-peptide at the C-terminal, and the G mutated to some other amino acids. Secondly, the sites screened above with enhanced LC/A affinity were incorporated into the first three backbones of the peptides to further analyze their *in vitro* inhibition effects on LC/A by linear velocity assays. Briefly, the reactions were performed in 10  $\mu$ l volume. Appropriate concentration of recombinant LC/A was firstly incubated with different concentrations of peptide inhibitors on ice for 20 minutes in 10 mM Tris-HCl (pH 7.6) and 20 mM NaCl. Then indicated concentration of SNAP25 was added into the reaction mixture which was incubated for another 20 min at 37°C, then stopped by adding SDS-PAGE buffer and heating for 5 min. Samples were subjected to SDS-PAGE and the amount of SNAP25 cleavage were determined by densitometry.

### **7.3.4 Cell-based inhibition of potential peptide-based inhibitors.**

In order to deliver peptide-based inhibitors into target cells, oligoarginines (R12) coupled with multiple Serine-Alanine linker sequence were directly added to the N-terminus of the most potential peptide inhibitors through recombinant DNA technology. Neuro-2a mouse neuroblastoma cells (ATCC) were maintained in DMEM medium with 10% newborn calf serum and 1% Penicillin/Streptomycin antibiotics to prevent contamination, then grown on cell-culture dishes and incubated at 37°C under 5% CO<sub>2</sub> to appropriate confluence. The pEGFP-C3-LC/A (1-425) plasmid were firstly transfected into Neuro-2a cells using Lipofectamine LTX plus (GIBCO/BRL) as suggested by manufacturer; 4h post-transfection, the cells were incubated with indicated concentrations of R12-coupled peptide inhibitors in complete DMEM medium (with 10% FBS and 1% P/S added). After 48 h incubation, cells were harvested and washed by PBS, lysed by 1x RIPA, with 1mM PMSF added, then left on ice for 10 min. Cells were scraped and spun down at 14,000 rpm for 10 min at 4°C, the total protein in the supernatant was quantified by the Bradford method (Bio-Rad). Samples were subjected to SDS-PAGE and western blotting, the cleavage of SNAP25 was

determined by probing with anti-SNAP25 antibody (SMI 81, abcam) and the amount of SNAP25 cleavage was determined by densitometry.

### **7.3.5 Evaluation of selected peptide inhibitors in mouse model.**

In order to further test the inhibition effect of the most promising peptide inhibitors, mouse model level test was performed as previously reported (275). Briefly, six-week-old female BALB/c mice were bought and maintained according to the company operation manual. For the LD<sub>50</sub> determination, raw BoNT/A holotoxin was diluted in GPB buffer (0.05 M sodium phosphate, pH 6.8, 0.2% gelatin) to a serial of challenging dose levels. The mice were divided into six groups, eight mice per group. The five experimental groups of mice were injected intraperitoneally (i.p.) by the lateral tail vein with 0.2 ml of a solution of toxin (0.875-14 ng). The toxin control group was treated only with 0.2 ml GPB buffer. Animals were observed and recorded for signs of botulism and death continuously for a period of 96 h, with 6 h interval record. The LD<sub>50</sub> was determined based on the Karber's method. The toxicity test of the selected peptide inhibitor was measured exactly the same as detailed above, but mice were randomly divided into four groups, four mice per group. The survival rate and death was recorded every 6 h during a time period of 96 h. For the *in vivo* inhibition tests, the most promising peptide inhibitor was selected based on the above mentioned cell-based assays. The mice were randomly divided into six groups, with eight mice for each group. Before i.p. injection, desired concentrations of peptide inhibitor were mixed with different amounts of the prepared BoNT/A samples (ranged from 1 x LD<sub>50</sub> to 16 x LD<sub>50</sub>), incubated at 37°C for 30 min, then 0.2 ml of the mixture was injected into mice. The control group of mice was treated with 0.2 ml GPB buffer. All mice were examined for several days and the survival, behavior, breath and signs of expression of botulism symptoms were recorded at the interval of 6 h.

## **7.4 Results**

LC/A substrate recognition involves multi-step substrate binding and catalysis, in which substrate binding distal to the active site contributes significantly to substrate affinity (143,145,171,235). In addition to substrate recognition, our previous study showed that LC/A could also bind to another region of SNAP25, namely SNAP25(80-110), facilitating the recognition and cleavage of SANP25 on neuronal cell membrane (235). Based on these findings and our data on saturation mutagenesis mapping of SNAP25, we set to develop potent substrate based inhibitor for BoNT/A since small molecule inhibitors lacking the distal binding site did not show a promising level of potency. In our design, we used

SNAP25(80-196), which included both binding sites to LC/A as backbone for development of various forms of inhibitors.

#### 7.4.1 Screening for SNAP25 sites that contribute to higher binding to LC/A

Previous studies indicated that the LC/A-SNAP25 interactions were not optimal and that mutation at specific residues can improve both the substrate binding and catalysis (133,171). In this work, we identified some potential SNAP25 sites (amino acids) that may contribute to high affinity substrate binding to LC/A based on both the co-crystal structure of LC/A-SNAP25 (PDB ID: 1XTG) and our previous understanding of the mechanisms of substrate recognition of LC/A (143,145). Several residues were identified, including H<sup>162</sup>, R<sup>180</sup>, E<sup>183</sup>, D<sup>186</sup>, T<sup>190</sup>, E<sup>194</sup> and M<sup>202</sup>. These residues can potentially interact with LC/A in a format of SNAP25/LCA: H<sup>162</sup>/K<sup>340</sup>, R<sup>180</sup>/Y<sup>144</sup>, E<sup>183</sup>/P<sup>25</sup>, D<sup>186</sup>/O atom of P<sup>25</sup> and N<sup>26</sup>, T<sup>190</sup>/F<sup>168</sup>, E<sup>194</sup>/P<sup>239</sup> and M<sup>202</sup>/L<sup>200</sup>, Y<sup>250</sup>/F<sup>369</sup>. These interactions may not be optimal and may affect the binding of SNAP25 to LC/A. We therefore created different substitutions in these residues with the hope of achieving optimal interactions at these sites. In order to screen the effect of SNAP25 substitution on LC/A binding affinity, we used a LC/A activity assay to screen for the mutations that resulted in higher binding affinity to LC/A. The idea is that, with the LC/A-SNAP25 active site recognition efficiency unchanged, an increase in binding affinity of SNAP25 to LC/A could subsequently result in an increase in the efficiency of LC/A cleavage of SNAP25. By the use of this assay, we observed that mutations at various site of SNAP25 could enhance the cleavage efficiency of LC/A by 10~20 folds, with SNAP25 (H<sup>162</sup>D) and (R<sup>180</sup>L) being the most efficient mutations (**Table 7.1**). In the LC/A-SNAP25 complex structure, the H<sup>162</sup> of SNAP25 is likely interacting with the K<sup>340</sup> of LC/A (**Figure 7.1A, left panel**), both residues are positively charged, they may repel to each other in the real situation, but in the SNAP25 (H<sup>162</sup>D) mutant (**Figure 7.1A, right panel**), the Aspartic acid may interact with the K<sup>340</sup> of LC/A via salt bridge, thus enhance the binding affinity between SNAP25 and LC/A. For the R<sup>180</sup> of SNAP25, the possible interacting residues in LC/A are S<sup>143</sup> and Y<sup>144</sup> (**Figure 7.1B, left panel**), which forms a hydrophobic pocket, the preferred corresponding residue in SNAP25 is hydrophobic as well, Leucine, for example (**Figure 7.1B, right panel**). Our data proved that the SNAP25 (R<sup>180</sup>L) derivative could increase the LC/A substrate cleavage efficiency. Further incorporated double mutants of SNAP25, for example, SNAP25 (H<sup>162</sup>D, R<sup>180</sup>L) and SNAP25 (T<sup>190</sup>V, M<sup>202</sup>F), however, did not enhance the cleavage efficiency by LC/A, suggesting that optimizing interaction at multiple sites simultaneously did not have a synergistic effect (**Table 7.1**).

**Table 7.1 Cleavage of SNAP25 and its derivatives by LC/A (1-425).**

SNAP25 and its derivatives	LC/A needed for 90% cleavage of SNAP25/derivatives (ng)	Ratio of LC/A activity (SNAP25 derivative/wt SNAP25)
wt SNAP25 (141-206)	10	1
SNAP25 (T <sup>190</sup> V)	1	10
SNAP25 (T <sup>190</sup> F)	1	10
SNAP25 (H <sup>162</sup> D)	0.5	20
SNAP25 (R <sup>180</sup> L)	0.5	20
SNAP25 (R <sup>180</sup> F)	1	10
SNAP25 (M <sup>202</sup> F)	1	10
SNAP25 (H <sup>162</sup> D, R <sup>180</sup> L)	1	10
SNAP25 (E <sup>183</sup> L)	1	10
SNAP25 (E <sup>183</sup> F)	1	10
SNAP25 (E <sup>194</sup> L)	1	10
SNAP25 (E <sup>194</sup> F)	1	10
SNAP25 (D <sup>186</sup> N)	1	10
SNAP25 (D <sup>186</sup> H)	1	10
SNAP25 (T <sup>190</sup> V, M <sup>202</sup> F)	1	10

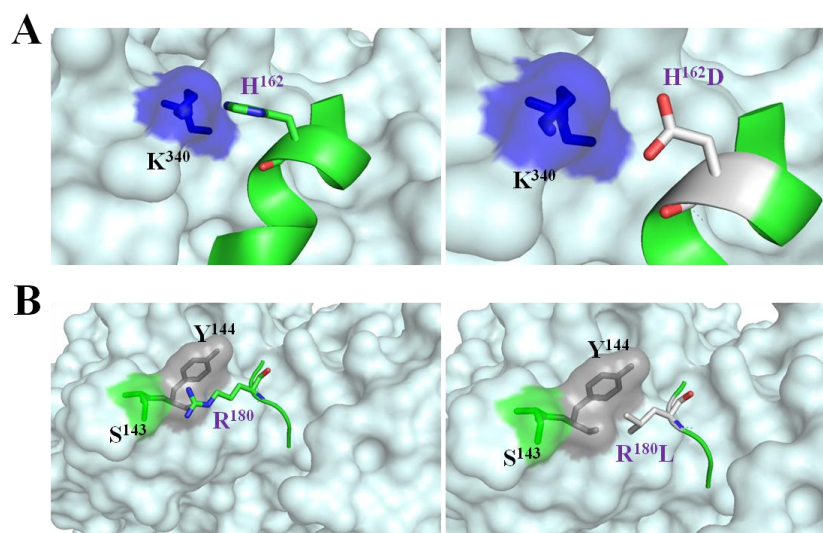


**Figure 7. 1 The two examples illustrate the enhanced interactions between SNAP25 and LC/A.**

(A) The originally possible interacting residues at the 162 site of SNAP25 and the corresponding site in LC/A (left panel) and the modified residue in SNAP25 to illustrate a possibly optimized interactions at the same sites (right panel). (B) The comparison between the original (left panel) and modified (right panel) interactions at the 180 site of SNAP25 and the corresponding sites in LC/A.

The LC/A-SNAP25 complex structure was extracted from the PDB bank (ID: 1XTG) with modifications by using PyMOL software. The LC/A structure was displayed in surface in palecyan color with the specific residues showed in sticks, and the SNAP25 was showed in cartoon in green with the specific residues showed in sticks as well. The residues were colored based on side chain: negatively charged (red), positively charged (blue), hydrophobic (gray) and polar (green).

#### **7.4.2 Development of inhibitors using SNAP25 based peptides with enhanced affinity**

The tetra-peptide RRGF was reported to exhibit an  $IC_{50}$  of 0.9  $\mu$ M and a  $K_i$  as low as 358 nM (274) when using SNAPtide as substrate (a 17-residue synthetic peptide corresponding to the residues 187-203 of SNAP25). However, when using SNAP25(141-206) as substrate, the  $IC_{50}$  was about 1000-fold higher, suggesting that RRGF could effectively inhibit the binding of SNAPtide to the active site of LC/A, whereas its inhibition to SNAP25(141-206) was not effective due to the presence of a binding site of SNAP25 to LC/A. However, this tetra-peptide is still the best peptide to constitute the C-terminus part of our peptide inhibitor. Therefore, SNAP25(80-197-RRGF) and SNAP25(80-197- WTKFL) were used as the backbone of the inhibitor and designated as R1 and R2 respectively. In addition, our previous study also showed that substituting the P1' site of VAMP2 by Cys residue could covert BoNT substrate into a weak inhibitor. Therefore, SNAP25 (80~196-C) was also used as another peptide inhibitor backbone and designated as R197C. The  $IC_{50}$  of these three inhibitors, R1, R2 and R197C, were determined to be 17.15 $\mu$ M, 15.71 $\mu$ M and 2.22 $\mu$ M

respectively and the  $K_i$  were 13.52 $\mu$ M, 12.39 $\mu$ M and 1.75 $\mu$ M respectively. We then incorporated different substitutions that could enhance the binding of SNAP25 peptides into these three inhibitors, including H<sup>162</sup>D, R<sup>180</sup>L, E<sup>183</sup>L, D<sup>186</sup>H, T<sup>190</sup>V, H<sup>162</sup>D/T<sup>190</sup>V. Inhibitor R1 (R<sup>180</sup>L) displayed the highest inhibition effect, with a  $IC_{50}$  of 0.28  $\mu$ M and  $K_i$  of 0.22  $\mu$ M. Inhibitor, R1 (H<sup>162</sup>D) and R1 (H<sup>162</sup>D, T<sup>190</sup>V) had a slightly higher  $IC_{50}$  and  $K_i$  than R1(R<sup>180</sup>L). Inhibitor R2 (H<sup>162</sup>D) exhibited  $IC_{50}$  of 1.11  $\mu$ M and  $K_i$  of 0.88  $\mu$ M and R2 (T<sup>190</sup>V) exhibited almost the same inhibitory effect. However, inhibitor R2 (R<sup>180</sup>L), did not enhance the inhibitory effect. For the R197C type of inhibitor, R197C (D<sup>186</sup>H) exhibited  $IC_{50}$  of 0.28  $\mu$ M and  $K_i$  of 0.22  $\mu$ M.

Further analysis of the modeled complex structures of LC/A-R1 and LC/A-R2 showed that replacing RRGF at the C-terminus of the inhibitor by RGF could fit these inhibitors better in LC/A (**Figure 7.2**), particularly the active site. Additional inhibitors, such as SNAP25(80-196-RGF), which was designated as R1-RGF, plus other derivatives, were generated. Inhibitor R1-RGF exhibited a very low  $IC_{50}$  of 0.0021 $\mu$ M and a  $K_i$  of 0.0017  $\mu$ M. Inhibitor R1-RLF exhibited an  $IC_{50}$  of 0.93 $\mu$ M and a  $K_i$  of 0.83 $\mu$ M (**Table 7.2**). The more potent inhibition of these inhibitors than the one with RRGF as C-terminus may be due to the better fit of the C-terminus of inhibitor into the active site of LC/A, which was evidenced by the examination of the structure of LC/A-RRGF (PDB ID: 3QW5).

**Table 7. 2 IC<sub>50</sub> and K<sub>i</sub> of peptide inhibitors of LC/A (1-425).**

Peptide inhibitors	IC <sub>50</sub> ( $\mu$ M) <sup>†</sup>	K <sub>i</sub> ( $\mu$ M) <sup>†</sup>
	0.9	0.358 <sup>Δ</sup>
RRGF	912.5 $\pm$ 0.19	719.57 $\pm$ 0.15*
R1	17.15 $\pm$ 0.83	13.52 $\pm$ 0.17
R1 (H <sup>162</sup> D)	0.64 $\pm$ 0.17	0.5 $\pm$ 0.13
R1 (R <sup>180</sup> L)	0.28 $\pm$ 0.44	0.22 $\pm$ 0.35
R1 (E <sup>183</sup> L)	20.40 $\pm$ 0.03	16.08 $\pm$ 0.02
R1 (D <sup>186</sup> H)	17.69 $\pm$ 0.09	13.95 $\pm$ 0.07
R1 (T <sup>190</sup> V)	14.72 $\pm$ 0.06	11.61 $\pm$ 0.04
R1 (H <sup>162</sup> D, T <sup>190</sup> V)	0.60 $\pm$ 0.29	0.48 $\pm$ 0.23
R2	15.71 $\pm$ 0.05	12.39 $\pm$ 0.04
R2 (H <sup>162</sup> D)	1.11 $\pm$ 0.44	0.88 $\pm$ 0.35
R2 (R <sup>180</sup> L)	13.96 $\pm$ 0.30	11.01 $\pm$ 0.24
R2 (E <sup>183</sup> L)	60.86 $\pm$ 1.29	47.99 $\pm$ 1.02
R2 (D <sup>186</sup> H)	14.47 $\pm$ 0.004	11.41 $\pm$ 0.003
R2 (T <sup>190</sup> V)	1.13 $\pm$ 0.20	0.89 $\pm$ 0.16
R2 (R <sup>180</sup> L, T <sup>190</sup> V)	54.40 $\pm$ 0.48	42.90 $\pm$ 0.38
R197C	2.22 $\pm$ 0.31	1.75 $\pm$ 0.24
R197C (H <sup>162</sup> D)	5.24 $\pm$ 0.28	4.13 $\pm$ 0.22
R197C (R <sup>180</sup> F)	27.09 $\pm$ 0.34	25.71 $\pm$ 0.32
R197C (R <sup>180</sup> L)	4.78 $\pm$ 0.49	3.77 $\pm$ 0.39
R197C (E <sup>183</sup> L)	18.75 $\pm$ 0.72	14.78 $\pm$ 0.55
R197C (D <sup>186</sup> H)	0.28 $\pm$ 0.39	0.22 $\pm$ 0.32
R197C (T <sup>190</sup> V)	6.36 $\pm$ 0.18	6.04 $\pm$ 0.17
R1-RGF	0.0021 $\pm$ 0.002	0.0017 $\pm$ 0.0012
R1-RAF	20.42 $\pm$ 0.09	16.10 $\pm$ 0.71
R1-RFF	57.73 $\pm$ 1.02	45.52 $\pm$ 0.80
R1-RIF	26.88 $\pm$ 0.76	21.20 $\pm$ 0.60
R1-RLF	0.93 $\pm$ 1.02	0.73 $\pm$ 0.80
R1-RPF	13.01 $\pm$ 2.11	10.26 $\pm$ 1.67
R1-RWF	3.72 $\pm$ 0.16	2.93 $\pm$ 0.12

<sup>†</sup> Average of at least three measurements.

<sup>‡</sup> The equation used in the calculation is:  $K_i = IC_{50} / (1 + [S]/KM)$ , and the KM of LCA (1-425) is 16 $\mu$ M (133).

<sup>Δ</sup> Data from reference (274).

\* Data of the present work.

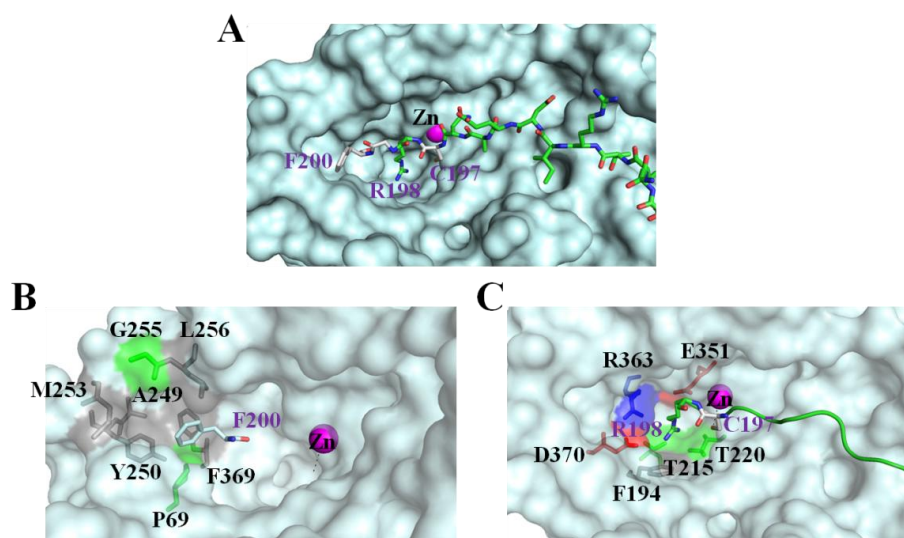


**Figure 7.2 Molecular interactions of the modeled complex structure of inhibitor and LC/A.**

(A) An overall view of the interactions between C197, R198 and F200 of peptide inhibitor with LC/A. (B) The predicted interactions between the F200 from RGF based peptide inhibitors with LC/A. (C) The predicted interactions between the C197 and R198 from RGF based peptide inhibitors with LC/A. The structure of RGF based peptide inhibitors with LC/A was modeled with reference to the crystal structures of LC/A-SNAP25 (PDB 1XTG) and RRGF-LC/A (PDB 3QW5) by using PyMOL software. The LC/A structure was displayed in surface in palecyan color with the specific residues showed in sticks, and the SNAP25 was showed in cartoon in green with the specific residues showed in sticks as well. The residues were colored based on side chain: negatively charged (red), positively charged (blue), hydrophobic (gray) polar (green). and zinc (magenta sphere).

### 7.4.3 Inhibition of LC/A by SNAP25 based inhibitors in cell model

In order to further investigate the *in vivo* inhibitory effects of developed peptide inhibitors, we coupled oligoarginines (R12) with the four most promising peptide inhibitors, namely R1 (R<sup>180</sup>L), R2 (T<sup>190</sup>V), R197C and R1-RGF to perform the cell-based inhibition assays. Consistent with our *in vitro* results, these four peptide inhibitors showed high LC/A inhibition effect *in vivo* as well. About 0.7  $\mu$ M R12-R1 (R<sup>180</sup>L) and R12-R197C inhibited >60% activity of LC/A, with the latter exhibiting slightly higher inhibitory effects on LC/A *in vivo* (**Figure 7.3A and 7.3C**); however, the *in vitro* inhibition effect of R1 (R<sup>180</sup>L) was about 10-fold higher than that of R197C (**Table 7.2**). More than 80% LC/A activity was inhibited by about 1.3  $\mu$ M R12-R2 (T<sup>190</sup>V) (**Figure 7.3B**), and for R12-R1-RGF, the concentration decreased to about 0.4  $\mu$ M to inhibit >80% LC/A activity (**Figure 7.3D**).

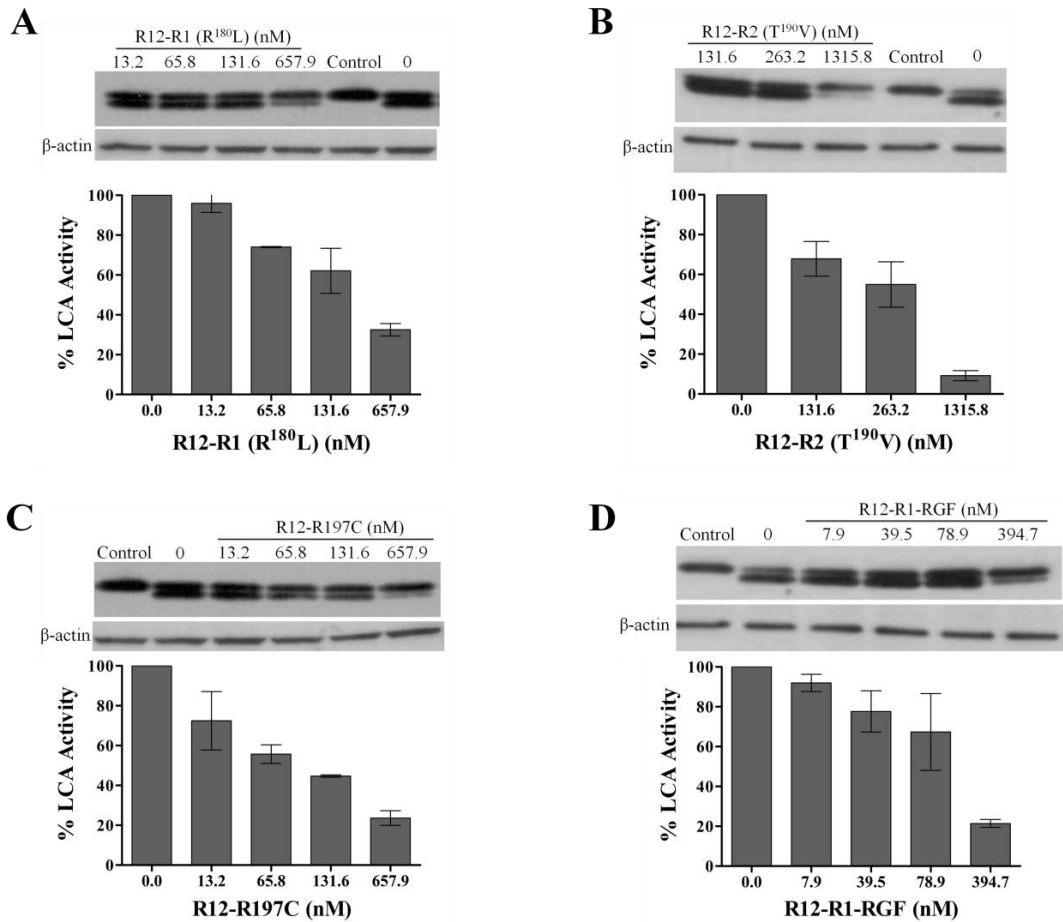


**Figure 7.3** Neuro-2a cell based *in vivo* inhibition effect of inhibitors.

(A) R12-R1 (R<sup>180</sup>L), (B) R12-R2 (T<sup>190</sup>V), (C) R12-R197C and (D) R12-R1-RGF.

#### 7.4.4 Full protection of BoNT/A intoxication by SNAP25 inhibitors in mice

To further test the inhibitory effect of SNAP25 based inhibitors to BoNT/A intoxication *in vivo*, we performed protection assays using inhibitor R1-RGF. Our data showed that a dose of 2 $\mu$ g R1-RGF or higher could fully protect the challenge of 2 x LD<sub>50</sub> of BoNT/A (**Figure 7.4A**), a dose of 10 $\mu$ g or higher could protect 4 x LD<sub>50</sub> challenge by BoNT/A (**Figure 7.4B**). At higher doses (8 x LD<sub>50</sub> and 16 x LD<sub>50</sub>) of BoNT/A challenge, the protective effects of R1-RGF were not apparent, but the application of inhibitors at 10 $\mu$ g or higher could delay the killing of mice by BoNT/A (**Figure 7.4C, D**).

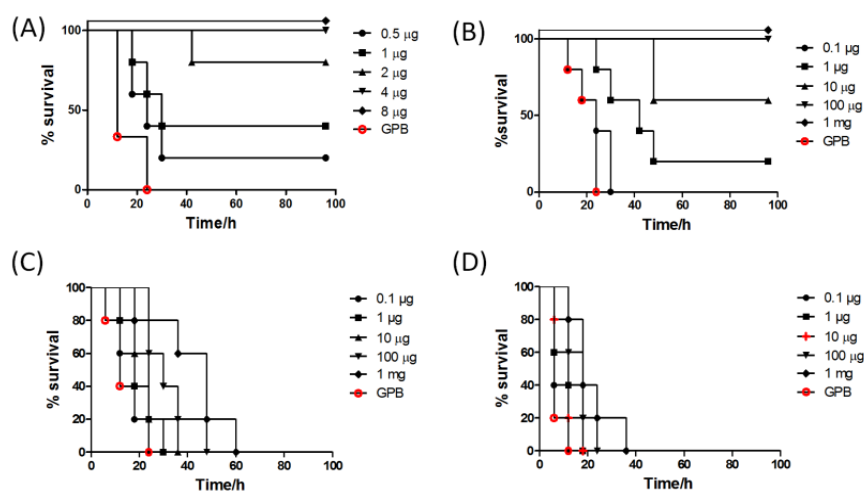


**Figure 7.4 Protection of mice against dosages of BoNT/A challenge by SNAP25-based inhibitor.**

Different amounts of BoNT/A, 2 x LD<sub>50</sub> (A), 4 x LD<sub>50</sub> (B), 8 x LD<sub>50</sub> (C) and 16 x LD<sub>50</sub> (D), were mixed with different amounts of peptide-based inhibitors, R12-R1-RGF, for 30min before inoculation of mice. The lethal rate of mice were recorded overtime. GPB refers to control group.

## 7.5 Discussion

The dual status of Botulinum Neurotoxin as causative agent of human botulism and bioterrorism weapon, as well as the most widely used protein therapeutic agent for neuromuscular disorders, has greatly promoted the development of small molecule inhibitors in the past decade. However, due to the unique substrate recognition mechanism of these classes of toxins, small molecular inhibitors that specifically bind to the active site of Botulinum neurotoxin are still not available. The interaction between the toxin and its substrate at the distal site renders active site inhibition ineffective. This is especially evidenced from our data that the tetra-peptide RRGF and its derivatives exhibited very potent inhibitory effects on LC/A cleavage of SNAPtide, whereas their ability to inhibit LC/A cleavage of SNAP25 (141-206) decreased by 1000 folds due to the presence of an additional LC/A binding site in region 141-180 of SNAP25. Therefore, development of peptide inhibitors that constitute both the binding and substrate recognition site of SNAP25 may offer the most effective inhibition.

Another unique feature of BoNT/A substrate interaction is that it can recognize an additional binding site at region of SNAP25 (80-110), thereby facilitating LC/A to bind to SNAP25 in neuronal cells. This additional binding may offer LC/A an advantage to compete with syntaxin to initiate its substrate recognition process since in syntaxin-SNAP25 or SNARE complex, LC/A substrate region SNAP25(141-206), is occupied to form the SNARE complex. Therefore the free region SNAP25(80-110) in the complex form of

SNAP25 becomes the first target when LC/A comes into contact with SNAP25, which is then followed by further substrate recognition and cleavage. This binding site could also contribute to high affinity binding of LC/A to SNAP25. Therefore, region of SNAP25(80-196) was selected as the backbone of the inhibitor.

In addition to the binding site, the active site architecture of the inhibitor is also very important. The incorporation of known active site inhibitor RRGF and its derivatives dramatically increased the inhibitory effect. Structural analysis of inhibitors with R1 and R2 with LC/A showed that the C-terminal RRGF may not fit the active site well. Therefore we replaced the C-terminal part with RGF and its derivatives (**Figure 7.2**). R1-RLF increased its potency to  $IC_{50}$  of  $0.93\mu M$  and R1-RGF dramatically improved its potency to  $IC_{50}$  of  $0.0021\mu M$ . These inhibitors are the most potent inhibitors that have been reported so far. Most importantly, R1-RGF not only exhibited potent inhibition of LC/A activity in cell model, but also displayed full protection against  $4 \times LD_{50}$  LC/A challenge in mice, suggesting the huge potential of this inhibitor on BoNT/A intoxication treatment. Most importantly, this inhibitor is the first to display full protection to LC/A challenge; the fact that it is derived from the substrate SNAP25, suggests that it offers great advantage as protein therapy development. SNAP25 is one of human neuronal cell protein; hence inhibitors derived from it probably do not exhibit toxicity to human and would not trigger immune response during therapy. These characteristics render SNAP25-based inhibitors a promising candidate for future development.

**Acknowledgements** This work was supported by the General Research Fund from Hong Kong University Grant Council for SC (560211).

## Chapter Eight: Conclusion and summary

The most potent protein toxins identified so far, CNTs, have been approved as effective therapeutic usage in numerous neuronal disorders and cosmetics. And our knowledge of them has been and will be in increase with the development of more advanced and new technologies in the fields of microbiology, molecular and structural biology. Moreover, it is undoubtedly that intensive investigations from diverse aspects, especially the basic studies, in the future will enhance our knowledge on the powerful molecule of CNTs as well.

It is well known that CNTs are a public health hazard and potential bioterrorism agent, many different approaches have been utilized to discover new drugs against CNTs, unfortunately, no satisfied drug is commercially available till now. A better and more comprehensive understanding of the substrate recognition mechanisms employed by CNTs will provide valuable information to develop countermeasures for them. Previously detailed dissection of the LC/A-SNAP25 interactions indicate that the interactions between LC/A and SNAP25 are optimizable, mutation at specific residues can improve both substrate binding and catalysis. In addition, structural and substrate-based small peptides targeting the active site of BoNTs have been studied and displayed promising inhibition effect, but the limited affinity of the developed peptide inhibitors to BoNTs prevent their further development with higher potency. All these studies prompted the hypothesis that peptide inhibitor containing both active site and binding regions could dramatically increase its affinity and potency. In the chapter seven of the thesis, we reported the development of potent peptide inhibitors of BoNT/A which exhibited nM inhibition effect both in vitro and in vivo. Most importantly, this novel substrate based inhibitors could provide full protection against 4xLD<sub>50</sub> challenge by BoNT/A, representing the best BoNT inhibitors to date.

In addition, in terms of the CNTs detection aspect, the understanding of the substrate recognition and specificity of CNTs will help to design high through, rapid and sensitive systems for CNTs detection from environment samples. Large complexes of different size and composition and increasingly identified variants of CNTs challenge the development of efficient detection of CNTs. In the chapter three of the thesis, a VAMP-2 based FRET assay based on the understanding of the VAMP-2 and LC/B interactions was developed. The designed FVP-B FRET peptide, constituting the shortest and optimal peptide, VAMP-2 (63-85), with FRET dyes (EDAN and Dabcyl) labeled at position 76 and 85, respectively, showed minimal effect on VAMP-2 substrate catalysis by LC/B and displayed a detection sensitivity as low as ~20 pM in 2 h. Importantly, FVP-B showed the potential to be scaled up and used in high throughput screening of LC/B inhibitor.

BoNTs are the most widely used protein therapeutic agents. In most therapeutic usages of BoNTs or derivatives, repeated injections or high dose are necessary. In some patients, neutralizing antibodies against the corresponding toxin used have been detected and thus reducing the beneficial effects or rendering the patient completely unresponsive to further treatment. And recently, increasing cases have been reported about the immunoresistance of BoNT therapies in patients. One possible factor that leads to patient immune response is the relatively high dosage used, engineer BoNTs with elevated substrate catalysis efficiency is one way to overcome the immunoresistance problem in BoNTs or derivatives therapies by reducing dosage needed. In the chapter two of the thesis, based on the thorough understanding of the substrate recognition and specificity of LC/B and LC/T, a LC/T mutant, LC/T (K168E, L230I), was engineered with ~100-fold increased catalytic activity toward substrate. And for LC/B, the LC/B (S201P) mutant increased LC/B activity by more than 10-fold. The reported LC/B and LC/T derivatives with elevated activity could be developed into novel therapy that may minimize the immune resistance issue of BoNTs therapy.

To conclude, a better and more comprehensive understanding of the substrate recognition and interaction mechanisms employed by CNTs is the key in the development of inhibitors or antidotes against BoNTs intoxication, in engineering CNTs with elevated activity which may be applied to reduce immune resistance issue of BoNTs therapy in the future, in broadening and developing novel therapeutic applications and rapid, sensitive detection system development. With the same purposes of a thorough understanding of CNTs, the substrate recognition and interaction mechanisms employed by BoNT/D, BoNT/F7 and BoNT/F5 were dissected in detail in chapters four, five and six respectively. We believe that these studies will provide helpful information in the future to fight against CNTs by minimizing the disadvantage and amplifying the advantage of CNTs, thus making them service human beings more efficiently and better.

## References

1. Kiernan, M. C., Isbister, G. K., Lin, C. S., Burke, D., and Bostock, H. (2005) Acute tetrodotoxin-induced neurotoxicity after ingestion of puffer fish. *Ann Neurol* **57**, 339-348
2. Haghdoost-Yazdi, H., Faraji, A., Fraidouni, N., Movahedi, M., Hadibeygi, E., and Vaezi, F. (2011) Significant effects of 4-aminopyridine and tetraethylammonium in the treatment of 6-hydroxydopamine-induced Parkinson's disease. *Behav Brain Res* **223**, 70-74
3. DeBin, J. A., Maggio, J. E., and Strichartz, G. R. (1993) Purification and characterization of chlorotoxin, a chloride channel ligand from the venom of the scorpion. *Am J Physiol* **264**, C361-369
4. McCleskey, E. W., Fox, A. P., Feldman, D. H., Cruz, L. J., Olivera, B. M., Tsien, R. W., and Yoshikami, D. (1987) Omega-conotoxin: direct and persistent blockade of specific types of calcium channels in neurons but not muscle. *Proc Natl Acad Sci U S A* **84**, 4327-4331
5. Bruggemann H, G. G. e. (ed) (2009) *Clostridia: Molecular Biology in the post-genomic era*, Norwich, UK: Caister Academic Press, UK
6. Arriagada, S. D., Wilhelm, B. J., and Donoso, F. A. (2009) [Infant botulism: case report and review]. *Rev Chilena Infectol* **26**, 162-167
7. Davies, A. H., Roberts, A. K., Shone, C. C., and Acharya, K. R. (2011) Super toxins from a super bug: structure and function of Clostridium difficile toxins. *Biochem J* **436**, 517-526
8. Sakurai, J., Nagahama, M., and Oda, M. (2004) Clostridium perfringens alpha-toxin: characterization and mode of action. *J Biochem* **136**, 569-574
9. Facchiano, F., Deloye, F., Doussau, F., Innamorati, G., Ashton, A. C., Dolly, J. O., Beninati, S., Facchiano, A., Luini, A., Poulain, B., and Benfenati, F. (2010) Transglutaminase participates in the blockade of neurotransmitter release by tetanus toxin: evidence for a novel biological function. *Amino Acids* **39**, 257-269
10. Meites, E., Zane, S., Gould, C., and Investigators, C. s. (2010) Fatal Clostridium sordellii infections after medical abortions. *The New England journal of medicine* **363**, 1382-1383
11. Erbguth, F. J. (2004) Historical notes on botulism, Clostridium botulinum, botulinum toxin, and the idea of the therapeutic use of the toxin. *Movement disorders : official journal of the Movement Disorder Society* **19 Suppl 8**, S2-6
12. Arnon, S. S., Schechter, R., Inglesby, T. V., Henderson, D. A., Bartlett, J. G., Ascher, M. S., Eitzen, E., Fine, A. D., Hauer, J., Layton, M., Lillibridge, S., Osterholm, M. T., O'Toole, T., Parker, G., Perl, T. M., Russell, P. K., Swerdlow, D. L., Tonat, K., and Working Group on Civilian, B. (2001) Botulinum toxin as a biological weapon: medical and public health management. *Jama* **285**, 1059-1070
13. Sobel, J. (2005) Botulism. *Clinical infectious diseases : an official publication of the Infectious Diseases Society of America* **41**, 1167-1173
14. Sollner, T., Whiteheart, S. W., Brunner, M., Erdjument-Bromage, H., Geromanos, S., Tempst, P., and Rothman, J. E. (1993) SNAP receptors implicated in vesicle targeting and fusion. *Nature* **362**, 318-324
15. Sollner, T., Bennett, M. K., Whiteheart, S. W., Scheller, R. H., and Rothman, J. E. (1993) A protein assembly-disassembly pathway in vitro that may correspond to sequential steps of synaptic vesicle docking, activation, and fusion. *Cell* **75**, 409-418
16. Chapman, E. R. (2002) Synaptotagmin: a Ca(2+) sensor that triggers exocytosis? *Nature reviews. Molecular cell biology* **3**, 498-508
17. Malsam, J., and Sollner, T. H. (2011) Organization of SNAREs within the Golgi stack. *Cold Spring Harbor perspectives in biology* **3**, a005249
18. Rothman, J. E. (1994) Mechanisms of intracellular protein transport. *Nature* **372**, 55-63

19. Fernandez, I., Ubach, J., Dulubova, I., Zhang, X., Sudhof, T. C., and Rizo, J. (1998) Three-dimensional structure of an evolutionarily conserved N-terminal domain of syntaxin 1A. *Cell* **94**, 841-849
20. Lerman, J. C., Robblee, J., Fairman, R., and Hughson, F. M. (2000) Structural analysis of the neuronal SNARE protein syntaxin-1A. *Biochemistry* **39**, 8470-8479
21. Sutton, R. B., Fasshauer, D., Jahn, R., and Brunger, A. T. (1998) Crystal structure of a SNARE complex involved in synaptic exocytosis at 2.4 Å resolution. *Nature* **395**, 347-353
22. Fasshauer, D. (2003) Structural insights into the SNARE mechanism. *Biochimica et biophysica acta* **1641**, 87-97
23. Sudhof, T. C. (2012) Calcium control of neurotransmitter release. *Cold Spring Harbor perspectives in biology* **4**, a011353
24. Raptis, A., Torrejon-Escribano, B., Gomez de Aranda, I., and Blasi, J. (2005) Distribution of synaptobrevin/VAMP 1 and 2 in rat brain. *Journal of chemical neuroanatomy* **30**, 201-211
25. Schoch, S., Deak, F., Konigstorfer, A., Mozhayeva, M., Sara, Y., Sudhof, T. C., and Kavalali, E. T. (2001) SNARE function analyzed in synaptobrevin/VAMP knockout mice. *Science* **294**, 1117-1122
26. Gronborg, M., Pavlos, N. J., Brunk, I., Chua, J. J., Munster-Wandowski, A., Riedel, D., Ahnert-Hilger, G., Urlaub, H., and Jahn, R. (2010) Quantitative comparison of glutamatergic and GABAergic synaptic vesicles unveils selectivity for few proteins including MAL2, a novel synaptic vesicle protein. *The Journal of neuroscience : the official journal of the Society for Neuroscience* **30**, 2-12
27. Becher, A., Drenckhahn, A., Pahner, I., Margittai, M., Jahn, R., and Ahnert-Hilger, G. (1999) The synaptophysin-synaptobrevin complex: a hallmark of synaptic vesicle maturation. *The Journal of neuroscience : the official journal of the Society for Neuroscience* **19**, 1922-1931
28. Yelamanchili, S. V., Reisinger, C., Becher, A., Sikorra, S., Bigalke, H., Binz, T., and Ahnert-Hilger, G. (2005) The C-terminal transmembrane region of synaptobrevin binds synaptophysin from adult synaptic vesicles. *European journal of cell biology* **84**, 467-475
29. Antonin, W., Holroyd, C., Fasshauer, D., Pabst, S., Von Mollard, G. F., and Jahn, R. (2000) A SNARE complex mediating fusion of late endosomes defines conserved properties of SNARE structure and function. *The EMBO journal* **19**, 6453-6464
30. Rose, A. J., Jeppesen, J., Kiens, B., and Richter, E. A. (2009) Effects of contraction on localization of GLUT4 and v-SNARE isoforms in rat skeletal muscle. *American journal of physiology. Regulatory, integrative and comparative physiology* **297**, R1228-1237
31. Sherry, D. M., Yang, H., and Standifer, K. M. (2001) Vesicle-associated membrane protein isoforms in the tiger salamander retina. *The Journal of comparative neurology* **431**, 424-436
32. Rizo, J., and Sudhof, T. C. (2002) Snares and Munc18 in synaptic vesicle fusion. *Nature reviews. Neuroscience* **3**, 641-653
33. Chapman, E. R., An, S., Barton, N., and Jahn, R. (1994) SNAP-25, a t-SNARE which binds to both syntaxin and synaptobrevin via domains that may form coiled coils. *The Journal of biological chemistry* **269**, 27427-27432
34. Nagy, G., Milosevic, I., Fasshauer, D., Muller, E. M., de Groot, B. L., Lang, T., Wilson, M. C., and Sorensen, J. B. (2005) Alternative splicing of SNAP-25 regulates secretion through nonconservative substitutions in the SNARE domain. *Molecular biology of the cell* **16**, 5675-5685
35. Bark, I. C., Hahn, K. M., Ryabinin, A. E., and Wilson, M. C. (1995) Differential expression of SNAP-25 protein isoforms during divergent vesicle fusion events of neural development. *Proc Natl Acad Sci U S A* **92**, 1510-1514

36. Bark, C., Bellinger, F. P., Kaushal, A., Mathews, J. R., Partridge, L. D., and Wilson, M. C. (2004) Developmentally regulated switch in alternatively spliced SNAP-25 isoforms alters facilitation of synaptic transmission. *The Journal of neuroscience : the official journal of the Society for Neuroscience* **24**, 8796-8805
37. Bragina, L., Candiracci, C., Barbaresi, P., Giovedi, S., Benfenati, F., and Conti, F. (2007) Heterogeneity of glutamatergic and GABAergic release machinery in cerebral cortex. *Neuroscience* **146**, 1829-1840
38. Pan, P. Y., Cai, Q., Lin, L., Lu, P. H., Duan, S., and Sheng, Z. H. (2005) SNAP-29-mediated modulation of synaptic transmission in cultured hippocampal neurons. *The Journal of biological chemistry* **280**, 25769-25779
39. Holt, M., Varoqueaux, F., Wiederhold, K., Takamori, S., Urlaub, H., Fasshauer, D., and Jahn, R. (2006) Identification of SNAP-47, a novel Qbc-SNARE with ubiquitous expression. *The Journal of biological chemistry* **281**, 17076-17083
40. Bennett, M. K., Garcia-Araras, J. E., Elferink, L. A., Peterson, K., Fleming, A. M., Hazuka, C. D., and Scheller, R. H. (1993) The syntaxin family of vesicular transport receptors. *Cell* **74**, 863-873
41. Pevsner, J., Hsu, S. C., Braun, J. E., Calakos, N., Ting, A. E., Bennett, M. K., and Scheller, R. H. (1994) Specificity and regulation of a synaptic vesicle docking complex. *Neuron* **13**, 353-361
42. Dulubova, I., Sugita, S., Hill, S., Hosaka, M., Fernandez, I., Sudhof, T. C., and Rizo, J. (1999) A conformational switch in syntaxin during exocytosis: role of munc18. *The EMBO journal* **18**, 4372-4382
43. Misura, K. M., Scheller, R. H., and Weis, W. I. (2000) Three-dimensional structure of the neuronal-Sec1-syntaxin 1a complex. *Nature* **404**, 355-362
44. Burkhardt, P., Hattendorf, D. A., Weis, W. I., and Fasshauer, D. (2008) Munc18a controls SNARE assembly through its interaction with the syntaxin N-peptide. *The EMBO journal* **27**, 923-933
45. Han, G. A., Malintan, N. T., Collins, B. M., Meunier, F. A., and Sugita, S. (2010) Munc18-1 as a key regulator of neurosecretion. *Journal of neurochemistry* **115**, 1-10
46. Gerber, S. H., Rah, J. C., Min, S. W., Liu, X., de Wit, H., Dulubova, I., Meyer, A. C., Rizo, J., Arancillo, M., Hammer, R. E., Verhage, M., Rosenmund, C., and Sudhof, T. C. (2008) Conformational switch of syntaxin-1 controls synaptic vesicle fusion. *Science* **321**, 1507-1510
47. Watson, R. T., and Pessin, J. E. (2001) Transmembrane domain length determines intracellular membrane compartment localization of syntaxins 3, 4, and 5. *American journal of physiology. Cell physiology* **281**, C215-223
48. Karvar, S., Zhu, L., Crothers, J., Jr., Wong, W., Turkoz, M., and Forte, J. G. (2005) Cellular localization and stimulation-associated distribution dynamics of syntaxin-1 and syntaxin-3 in gastric parietal cells. *Traffic* **6**, 654-666
49. van Ermengem, E. (1979) Classics in infectious diseases. A new anaerobic bacillus and its relation to botulism. E. van Ermengem. Originally published as "Ueber einen neuen anaeroben Bacillus und seine Beziehungen zum Botulismus" in *Zeitschrift für Hygiene und Infektionskrankheiten* 26: 1-56, 1897. *Reviews of infectious diseases* **1**, 701-719
50. Burke, G. S. (1919) Notes on Bacillus botulinus. *Journal of bacteriology* **4**, 555-570 551
51. Bengtson, I. A. (1921) Standardization of Botulism Antitoxins. *American journal of public health* **11**, 352-357
52. Moller, V., and Scheibel, I. (1960) Preliminary report on the isolation of an apparently new type of CI. botulinum. *Acta pathologica et microbiologica Scandinavica* **48**, 80
53. Gimenez, D. F., and Ciccarelli, A. S. (1968) Clostridium botulinum type F in the soil of Argentina. *Appl Microbiol* **16**, 732-734

54. Gimenez, D. F., and Ciccarelli, A. S. (1970) Another type of *Clostridium botulinum*. *Zentralblatt für Bakteriologie, Parasitenkunde, Infektionskrankheiten und Hygiene. I. Abt. Medizinisch-hygienische Bakteriologie, Virusforschung und Parasitologie. Originale* **215**, 221-224
55. Dover, N., Barash, J. R., Hill, K. K., Xie, G., and Arnon, S. S. (2013) Molecular Characterization of a Novel Botulinum Neurotoxin Type H Gene. *Journal of Infectious Diseases*
56. Johnson, E. A. (2014) Validity of botulinum neurotoxin serotype H. *The Journal of infectious diseases* **210**, 992-993; discussion 993
57. Barash, J. R., and Arnon, S. S. (2014) A novel strain of *Clostridium botulinum* that produces type B and type H botulinum toxins. *The Journal of infectious diseases* **209**, 183-191
58. Franciosa, G., Floridi, F., Maugliani, A., and Aureli, P. (2004) Differentiation of the gene clusters encoding botulinum neurotoxin type A complexes in *Clostridium botulinum* type A, Ab, and A(B) strains. *Appl Environ Microbiol* **70**, 7192-7199
59. Franciosa, G., Ferreira, J. L., and Hatheway, C. L. (1994) Detection of type A, B, and E botulinum neurotoxin genes in *Clostridium botulinum* and other *Clostridium* species by PCR: evidence of unexpressed type B toxin genes in type A toxigenic organisms. *J Clin Microbiol* **32**, 1911-1917
60. Hill, K. K., Smith, T. J., Helma, C. H., Ticknor, L. O., Foley, B. T., Svensson, R. T., Brown, J. L., Johnson, E. A., Smith, L. A., Okinaka, R. T., Jackson, P. J., and Marks, J. D. (2007) Genetic diversity among Botulinum Neurotoxin-producing clostridial strains. *Journal of bacteriology* **189**, 818-832
61. Carter, A. T., Paul, C. J., Mason, D. R., Twine, S. M., Alston, M. J., Logan, S. M., Austin, J. W., and Peck, M. W. (2009) Independent evolution of neurotoxin and flagellar genetic loci in proteolytic *Clostridium botulinum*. *BMC Genomics* **10**, 115
62. Smith, T. J., Lou, J., Geren, I. N., Forsyth, C. M., Tsai, R., Laporte, S. L., Tepp, W. H., Bradshaw, M., Johnson, E. A., Smith, L. A., and Marks, J. D. (2005) Sequence variation within botulinum neurotoxin serotypes impacts antibody binding and neutralization. *Infect Immun* **73**, 5450-5457
63. Arndt, J. W., Jacobson, M. J., Abola, E. E., Forsyth, C. M., Tepp, W. H., Marks, J. D., Johnson, E. A., and Stevens, R. C. (2006) A structural perspective of the sequence variability within botulinum neurotoxin subtypes A1-A4. *J Mol Biol* **362**, 733-742
64. Hill, K. K., and Smith, T. J. (2013) Genetic diversity within *Clostridium botulinum* serotypes, botulinum neurotoxin gene clusters and toxin subtypes. *Current topics in microbiology and immunology* **364**, 1-20
65. Montecucco, C., and Schiavo, G. (1995) Structure and function of tetanus and botulinum neurotoxins. *Q Rev Biophys* **28**, 423-472
66. Turton, K., Chaddock, J. A., and Acharya, K. R. (2002) Botulinum and tetanus neurotoxins: structure, function and therapeutic utility. *Trends Biochem Sci* **27**, 552-558
67. Lacy, D. B., Tepp, W., Cohen, A. C., DasGupta, B. R., and Stevens, R. C. (1998) Crystal structure of botulinum neurotoxin type A and implications for toxicity. *Nat Struct Biol* **5**, 898-902
68. Kumaran, D., Eswaramoorthy, S., Furey, W., Navaza, J., Sax, M., and Swaminathan, S. (2009) Domain organization in *Clostridium botulinum* neurotoxin type E is unique: its implication in faster translocation. *J Mol Biol* **386**, 233-245
69. Swaminathan, S., and Eswaramoorthy, S. (2000) Structural analysis of the catalytic and binding sites of *Clostridium botulinum* neurotoxin B. *Nat Struct Biol* **7**, 693-699
70. Sakaguchi, G. (1982) *Clostridium botulinum* toxins. *Pharmacol Ther* **19**, 165-194
71. Collins, M. D., and East, A. K. (1998) Phylogeny and taxonomy of the food-borne pathogen *Clostridium botulinum* and its neurotoxins. *J Appl Microbiol* **84**, 5-17

72. Gu, S., Rumpel, S., Zhou, J., Strotmeier, J., Bigalke, H., Perry, K., Shoemaker, C. B., Rummel, A., and Jin, R. (2012) Botulinum neurotoxin is shielded by NTNHA in an interlocked complex. *Science* **335**, 977-981
73. Fujii, N., Kimura, K., Yokosawa, N., Yashiki, T., Tsuzuki, K., and Oguma, K. (1993) The complete nucleotide sequence of the gene encoding the nontoxic component of *Clostridium botulinum* type E progenitor toxin. *J Gen Microbiol* **139**, 79-86
74. East, A. K., and Collins, M. D. (1994) Conserved structure of genes encoding components of botulinum neurotoxin complex M and the sequence of the gene coding for the nontoxic component in nonproteolytic *Clostridium botulinum* type F. *Curr Microbiol* **29**, 69-77
75. Lin, G., Tepp, W. H., Pier, C. L., Jacobson, M. J., and Johnson, E. A. (2010) Expression of the *Clostridium botulinum* A2 neurotoxin gene cluster proteins and characterization of the A2 complex. *Appl Environ Microbiol* **76**, 40-47
76. Ito, H., Sagane, Y., Miyata, K., Inui, K., Matsuo, T., Horiuchi, R., Ikeda, T., Suzuki, T., Hasegawa, K., Kouguchi, H., Oguma, K., Niwa, K., Ohyama, T., and Watanabe, T. (2011) HA-33 facilitates transport of the serotype D botulinum toxin across a rat intestinal epithelial cell monolayer. *FEMS Immunol Med Microbiol* **61**, 323-331
77. Inoue, K., Fujinaga, Y., Honke, K., Yokota, K., Ikeda, T., Ohyama, T., Takeshi, K., Watanabe, T., and Oguma, K. (1999) Characterization of haemagglutinin activity of *Clostridium botulinum* type C and D 16S toxins, and one subcomponent of haemagglutinin (HA1). *Microbiology* **145** ( Pt 9), 2533-2542
78. Poulain, B., Lonchamp, E., Jover, E., Popoff, M. R., and Molgo, J. (2009) [Mechanisms of action of botulinum toxins and neurotoxins]. *Ann Dermatol Venereol* **136 Suppl 4**, S73-76
79. Bhandari, M., Campbell, K. D., Collins, M. D., and East, A. K. (1997) Molecular characterization of the clusters of genes encoding the botulinum neurotoxin complex in *Clostridium botulinum* (*Clostridium argentinense*) type G and nonproteolytic *Clostridium botulinum* type B. *Curr Microbiol* **35**, 207-214
80. Yao, G., Lee, K., Gu, S., Lam, K. H., and Jin, R. (2014) Botulinum neurotoxin A complex recognizes host carbohydrates through its hemagglutinin component. *Toxins (Basel)* **6**, 624-635
81. Turner, J. R. (2009) Intestinal mucosal barrier function in health and disease. *Nat Rev Immunol* **9**, 799-809
82. Woodley, J. F. (1994) Enzymatic barriers for GI peptide and protein delivery. *Crit Rev Ther Drug Carrier Syst* **11**, 61-95
83. Ohishi, I., Sugii, S., and Sakaguchi, G. (1977) Oral toxicities of *Clostridium botulinum* toxins in response to molecular size. *Infect Immun* **16**, 107-109
84. Sugii, S., Ohishi, I., and Sakaguchi, G. (1977) Correlation between oral toxicity and in vitro stability of *Clostridium botulinum* type A and B toxins of different molecular sizes. *Infect Immun* **16**, 910-914
85. Lam, T. I., Stanker, L. H., Lee, K., Jin, R., and Cheng, L. W. (2015) Translocation of botulinum neurotoxin serotype A and associated proteins across the intestinal epithelia. *Cell Microbiol*
86. Maksymowych, A. B., and Simpson, L. L. (2004) Structural features of the botulinum neurotoxin molecule that govern binding and transcytosis across polarized human intestinal epithelial cells. *J Pharmacol Exp Ther* **310**, 633-641
87. Maksymowych, A. B., and Simpson, L. L. (1998) Binding and transcytosis of botulinum neurotoxin by polarized human colon carcinoma cells. *The Journal of biological chemistry* **273**, 21950-21957
88. Couesnon, A., Molgo, J., Connan, C., and Popoff, M. R. (2012) Preferential entry of botulinum neurotoxin A Hc domain through intestinal crypt cells and targeting to cholinergic neurons of the mouse intestine. *PLoS Pathog* **8**, e1002583
89. Couesnon, A., Shimizu, T., and Popoff, M. R. (2009) Differential entry of botulinum neurotoxin A into neuronal and intestinal cells. *Cell Microbiol* **11**, 289-308

90. Fujinaga, Y. (2010) Interaction of botulinum toxin with the epithelial barrier. *J Biomed Biotechnol* **2010**, 974943
91. Matsumura, T., Jin, Y., Kabumoto, Y., Takegahara, Y., Oguma, K., Lencer, W. I., and Fujinaga, Y. (2008) The HA proteins of botulinum toxin disrupt intestinal epithelial intercellular junctions to increase toxin absorption. *Cell Microbiol* **10**, 355-364
92. Ahsan, C. R., Hajnoczky, G., Maksymowych, A. B., and Simpson, L. L. (2005) Visualization of binding and transcytosis of botulinum toxin by human intestinal epithelial cells. *J Pharmacol Exp Ther* **315**, 1028-1035
93. Couesnon, A., Pereira, Y., and Popoff, M. R. (2008) Receptor-mediated transcytosis of botulinum neurotoxin A through intestinal cell monolayers. *Cell Microbiol* **10**, 375-387
94. Jin, Y., Takegahara, Y., Sugawara, Y., Matsumura, T., and Fujinaga, Y. (2009) Disruption of the epithelial barrier by botulinum haemagglutinin (HA) proteins - differences in cell tropism and the mechanism of action between HA proteins of types A or B, and HA proteins of type C. *Microbiology* **155**, 35-45
95. Sugawara, Y., Matsumura, T., Takegahara, Y., Jin, Y., Tsukasaki, Y., Takeichi, M., and Fujinaga, Y. (2010) Botulinum hemagglutinin disrupts the intercellular epithelial barrier by directly binding E-cadherin. *J Cell Biol* **189**, 691-700
96. Fujinaga, Y., Sugawara, Y., and Matsumura, T. (2013) Uptake of botulinum neurotoxin in the intestine. *Current topics in microbiology and immunology* **364**, 45-59
97. Schiavo, G., Matteoli, M., and Montecucco, C. (2000) Neurotoxins affecting neuroexocytosis. *Physiol Rev* **80**, 717-766
98. Restani, L., Novelli, E., Bottari, D., Leone, P., Barone, I., Galli-Resta, L., Strettoi, E., and Caleo, M. (2012) Botulinum neurotoxin A impairs neurotransmission following retrograde transsynaptic transport. *Traffic* **13**, 1083-1089
99. Bercsenyi, K., Giribaldi, F., and Schiavo, G. (2013) The elusive compass of clostridial neurotoxins: deciding when and where to go? *Current topics in microbiology and immunology* **364**, 91-113
100. Bullens, R. W., O'Hanlon, G. M., Wagner, E., Molenaar, P. C., Furukawa, K., Furukawa, K., Plomp, J. J., and Willison, H. J. (2002) Complex gangliosides at the neuromuscular junction are membrane receptors for autoantibodies and botulinum neurotoxin but redundant for normal synaptic function. *The Journal of neuroscience : the official journal of the Society for Neuroscience* **22**, 6876-6884
101. Peng, L., Tepp, W. H., Johnson, E. A., and Dong, M. (2011) Botulinum neurotoxin D uses synaptic vesicle protein SV2 and gangliosides as receptors. *PLoS Pathog* **7**, e1002008
102. Dong, M., Tepp, W. H., Liu, H., Johnson, E. A., and Chapman, E. R. (2007) Mechanism of botulinum neurotoxin B and G entry into hippocampal neurons. *J Cell Biol* **179**, 1511-1522
103. Dong, M., Liu, H., Tepp, W. H., Johnson, E. A., Janz, R., and Chapman, E. R. (2008) Glycosylated SV2A and SV2B mediate the entry of botulinum neurotoxin E into neurons. *Molecular biology of the cell* **19**, 5226-5237
104. Ginalska, K., Venclovas, C., Lesyng, B., and Fidelis, K. (2000) Structure-based sequence alignment for the beta-trefoil subdomain of the clostridial neurotoxin family provides residue level information about the putative ganglioside binding site. *FEBS letters* **482**, 119-124
105. Rummel, A. (2013) Double receptor anchorage of botulinum neurotoxins accounts for their exquisite neurospecificity. *Current topics in microbiology and immunology* **364**, 61-90
106. Lam, K. H., Yao, G., and Jin, R. (2015) Diverse binding modes, same goal: The receptor recognition mechanism of botulinum neurotoxin. *Progress in biophysics and molecular biology*
107. Gambale, F., and Montal, M. (1988) Characterization of the channel properties of tetanus toxin in planar lipid bilayers. *Biophysical journal* **53**, 771-783

108. Finkelstein, A. (1990) Channels formed in phospholipid bilayer membranes by diphtheria, tetanus, botulinum and anthrax toxin. *Journal de physiologie* **84**, 188-190
109. Fischer, A., and Montal, M. (2007) Crucial role of the disulfide bridge between botulinum neurotoxin light and heavy chains in protease translocation across membranes. *The Journal of biological chemistry* **282**, 29604-29611
110. Fischer, A., and Montal, M. (2007) Single molecule detection of intermediates during botulinum neurotoxin translocation across membranes. *Proc Natl Acad Sci U S A* **104**, 10447-10452
111. Galloux, M., Vitrac, H., Montagner, C., Raffestin, S., Popoff, M. R., Chenal, A., Forge, V., and Gillet, D. (2008) Membrane Interaction of botulinum neurotoxin A translocation (T) domain. The belt region is a regulatory loop for membrane interaction. *The Journal of biological chemistry* **283**, 27668-27676
112. Fischer, A., Sambashivan, S., Brunger, A. T., and Montal, M. (2012) Beltless translocation domain of botulinum neurotoxin A embodies a minimum ion-conductive channel. *The Journal of biological chemistry* **287**, 1657-1661
113. Koriazova, L. K., and Montal, M. (2003) Translocation of botulinum neurotoxin light chain protease through the heavy chain channel. *Nat Struct Biol* **10**, 13-18
114. Fu, F. N., Busath, D. D., and Singh, B. R. (2002) Spectroscopic analysis of low pH and lipid-induced structural changes in type A botulinum neurotoxin relevant to membrane channel formation and translocation. *Biophysical chemistry* **99**, 17-29
115. Sun, S., Suresh, S., Liu, H., Tepp, W. H., Johnson, E. A., Edwardson, J. M., and Chapman, E. R. (2011) Receptor binding enables botulinum neurotoxin B to sense low pH for translocation channel assembly. *Cell host & microbe* **10**, 237-247
116. Mushrush, D. J., Koteiche, H. A., Sammons, M. A., Link, A. J., McHaourab, H. S., and Lacy, D. B. (2011) Studies of the mechanistic details of the pH-dependent association of botulinum neurotoxin with membranes. *The Journal of biological chemistry* **286**, 27011-27018
117. Fischer, A. (2013) Synchronized chaperone function of botulinum neurotoxin domains mediates light chain translocation into neurons. *Current topics in microbiology and immunology* **364**, 115-137
118. Kistner, A., and Habermann, E. (1992) Reductive cleavage of tetanus toxin and botulinum neurotoxin A by the thioredoxin system from brain. Evidence for two redox isomers of tetanus toxin. *Naunyn Schmiedebergs Arch Pharmacol* **345**, 227-234
119. Schiavo, G., Rossetto, O., Santucci, A., DasGupta, B. R., and Montecucco, C. (1992) Botulinum neurotoxins are zinc proteins. *The Journal of biological chemistry* **267**, 23479-23483
120. Schiavo, G., Poulain, B., Rossetto, O., Benfenati, F., Tauc, L., and Montecucco, C. (1992) Tetanus toxin is a zinc protein and its inhibition of neurotransmitter release and protease activity depend on zinc. *The EMBO journal* **11**, 3577-3583
121. Schiavo, G., Benfenati, F., Poulain, B., Rossetto, O., Poverino de Laureto, P., DasGupta, B. R., and Montecucco, C. (1992) Tetanus and botulinum-B neurotoxins block neurotransmitter release by proteolytic cleavage of synaptobrevin. *Nature* **359**, 832-835
122. Kalb, S. R., Baudys, J., Webb, R. P., Wright, P., Smith, T. J., Smith, L. A., Fernandez, R., Raphael, B. H., Maslanka, S. E., Pirkle, J. L., and Barr, J. R. (2012) Discovery of a novel enzymatic cleavage site for botulinum neurotoxin F5. *FEBS letters* **586**, 109-115
123. Raphael, B. H., Choudoir, M. J., Luquez, C., Fernandez, R., and Maslanka, S. E. (2010) Sequence diversity of genes encoding botulinum neurotoxin type F. *Appl Environ Microbiol* **76**, 4805-4812
124. Williamson, L. C., Halpern, J. L., Montecucco, C., Brown, J. E., and Neale, E. A. (1996) Clostridial neurotoxins and substrate proteolysis in intact neurons: botulinum neurotoxin C acts on synaptosomal-associated protein of 25 kDa. *The Journal of biological chemistry* **271**, 7694-7699

125. Schiavo, G., Shone, C. C., Bennett, M. K., Scheller, R. H., and Montecucco, C. (1995) Botulinum neurotoxin type C cleaves a single Lys-Ala bond within the carboxyl-terminal region of syntaxins. *The Journal of biological chemistry* **270**, 10566-10570
126. Doellgast, G. J., Triscott, M. X., Beard, G. A., Bottoms, J. D., Cheng, T., Roh, B. H., Roman, M. G., Hall, P. A., and Brown, J. E. (1993) Sensitive enzyme-linked immunosorbent assay for detection of Clostridium botulinum neurotoxins A, B, and E using signal amplification via enzyme-linked coagulation assay. *J Clin Microbiol* **31**, 2402-2409
127. Ekong, T. A., Feavers, I. M., and Sesardic, D. (1997) Recombinant SNAP-25 is an effective substrate for Clostridium botulinum type A toxin endopeptidase activity in vitro. *Microbiology* **143** ( Pt 10), 3337-3347
128. Vaidyanathan, V. V., Yoshino, K., Jahnz, M., Dorries, C., Bade, S., Nauenburg, S., Niemann, H., and Binz, T. (1999) Proteolysis of SNAP-25 isoforms by botulinum neurotoxin types A, C, and E: domains and amino acid residues controlling the formation of enzyme-substrate complexes and cleavage. *Journal of neurochemistry* **72**, 327-337
129. Yamasaki, S., Baumeister, A., Binz, T., Blasi, J., Link, E., Cornille, F., Roques, B., Fykse, E. M., Sudhof, T. C., Jahn, R., and et al. (1994) Cleavage of members of the synaptobrevin/VAMP family by types D and F botulinum neurotoxins and tetanus toxin. *The Journal of biological chemistry* **269**, 12764-12772
130. Yamasaki, S., Binz, T., Hayashi, T., Szabo, E., Yamasaki, N., Eklund, M., Jahn, R., and Niemann, H. (1994) Botulinum neurotoxin type G proteolyzes the Ala81-Ala82 bond of rat synaptobrevin 2. *Biochem Biophys Res Commun* **200**, 829-835
131. Rossetto, O., Schiavo, G., Montecucco, C., Poulain, B., Deloye, F., Lozzi, L., and Shone, C. C. (1994) SNARE motif and neurotoxins. *Nature* **372**, 415-416
132. Washbourne, P., Pellizzari, R., Baldini, G., Wilson, M. C., and Montecucco, C. (1997) Botulinum neurotoxin types A and E require the SNARE motif in SNAP-25 for proteolysis. *FEBS letters* **418**, 1-5
133. Chen, S., and Barbieri, J. T. (2006) Unique substrate recognition by botulinum neurotoxins serotypes A and E. *The Journal of biological chemistry* **281**, 10906-10911
134. Chen, S., Hall, C., and Barbieri, J. T. (2008) Substrate recognition of VAMP-2 by botulinum neurotoxin B and tetanus neurotoxin. *The Journal of biological chemistry* **283**, 21153-21159
135. Sikorra, S., Henke, T., Galli, T., and Binz, T. (2008) Substrate recognition mechanism of VAMP/synaptobrevin-cleaving clostridial neurotoxins. *The Journal of biological chemistry* **283**, 21145-21152
136. Jin, R., Sikorra, S., Stegmann, C. M., Pich, A., Binz, T., and Brunger, A. T. (2007) Structural and biochemical studies of botulinum neurotoxin serotype C1 light chain protease: implications for dual substrate specificity. *Biochemistry* **46**, 10685-10693
137. Silvaggi, N. R., Boldt, G. E., Hixon, M. S., Kennedy, J. P., Tzipori, S., Janda, K. D., and Allen, K. N. (2007) Structures of Clostridium botulinum Neurotoxin Serotype A Light Chain complexed with small-molecule inhibitors highlight active-site flexibility. *Chem Biol* **14**, 533-542
138. Arndt, J. W., Chai, Q., Christian, T., and Stevens, R. C. (2006) Structure of botulinum neurotoxin type D light chain at 1.65 Å resolution: repercussions for VAMP-2 substrate specificity. *Biochemistry* **45**, 3255-3262
139. Agarwal, R., Binz, T., and Swaminathan, S. (2005) Structural analysis of botulinum neurotoxin serotype F light chain: implications on substrate binding and inhibitor design. *Biochemistry* **44**, 11758-11765
140. Arndt, J. W., Yu, W., Bi, F., and Stevens, R. C. (2005) Crystal structure of botulinum neurotoxin type G light chain: serotype divergence in substrate recognition. *Biochemistry* **44**, 9574-9580
141. Agarwal, R., Binz, T., and Swaminathan, S. (2005) Analysis of active site residues of botulinum neurotoxin E by mutational, functional, and structural studies: Glu335Gln is an apoenzyme. *Biochemistry* **44**, 8291-8302

142. Breidenbach, M. A., and Brunger, A. T. (2005) 2.3 A crystal structure of tetanus neurotoxin light chain. *Biochemistry* **44**, 7450-7457
143. Breidenbach, M. A., and Brunger, A. T. (2004) Substrate recognition strategy for botulinum neurotoxin serotype A. *Nature* **432**, 925-929
144. Agarwal, R., Schmidt, J. J., Stafford, R. G., and Swaminathan, S. (2009) Mode of VAMP substrate recognition and inhibition of Clostridium botulinum neurotoxin F. *Nat Struct Mol Biol* **16**, 789-794
145. Chen, S., Kim, J. J., and Barbieri, J. T. (2007) Mechanism of substrate recognition by botulinum neurotoxin serotype A. *The Journal of biological chemistry* **282**, 9621-9627
146. Chen, S., and Barbieri, J. T. (2007) Multiple pocket recognition of SNAP25 by botulinum neurotoxin serotype E. *The Journal of biological chemistry* **282**, 25540-25547
147. Hanson, M. A., and Stevens, R. C. (2000) Cocystal structure of synaptobrevin-II bound to botulinum neurotoxin type B at 2.0 Å resolution. *Nat Struct Biol* **7**, 687-692
148. Chen, S., and Wan, H. Y. (2011) Molecular mechanisms of substrate recognition and specificity of botulinum neurotoxin serotype F. *Biochem J* **433**, 277-284
149. Chen, S., Karalewitz, A. P., and Barbieri, J. T. (2012) Insights into the Different Catalytic Activities of Clostridium Neurotoxins. *Biochemistry*
150. Chen, S., Karalewitz, A. P., and Barbieri, J. T. (2012) Insights into the different catalytic activities of Clostridium neurotoxins. *Biochemistry* **51**, 3941-3947
151. Sikorra, S., Henke, T., Swaminathan, S., Galli, T., and Binz, T. (2006) Identification of the amino acid residues rendering TI-VAMP insensitive toward botulinum neurotoxin B. *J Mol Biol* **357**, 574-582
152. Cornille, F., Martin, L., Lenoir, C., Cussac, D., Roques, B. P., and Fournie-Zaluski, M. C. (1997) Cooperative exosite-dependent cleavage of synaptobrevin by tetanus toxin light chain. *The Journal of biological chemistry* **272**, 3459-3464
153. Chen, S. (2014) Clostridial neurotoxins: mode of substrate recognition and novel therapy development. *Current protein & peptide science* **15**, 490-503
154. Smith, L. A. (1998) Development of recombinant vaccines for botulinum neurotoxin. *Toxicon* **36**, 1539-1548
155. Smith, L. A., Jensen, M. J., Montgomery, V. A., Brown, D. R., Ahmed, S. A., and Smith, T. J. (2004) Roads from vaccines to therapies. *Movement disorders : official journal of the Movement Disorder Society* **19 Suppl 8**, S48-52
156. Smith, L. A., and Rusnak, J. M. (2007) Botulinum neurotoxin vaccines: past, present, and future. *Crit Rev Immunol* **27**, 303-318
157. Baldwin, M. R., Tepp, W. H., Przedpelski, A., Pier, C. L., Bradshaw, M., Johnson, E. A., and Barbieri, J. T. (2008) Subunit vaccine against the seven serotypes of botulism. *Infect Immun* **76**, 1314-1318
158. Yu, Y. Z., Li, N., Zhu, H. Q., Wang, R. L., Du, Y., Wang, S., Yu, W. Y., and Sun, Z. W. (2009) The recombinant Hc subunit of Clostridium botulinum neurotoxin serotype A is an effective botulism vaccine candidate. *Vaccine* **27**, 2816-2822
159. Dux, M. P., Huang, J., Barent, R., Inan, M., Swanson, S. T., Sinha, J., Ross, J. T., Smith, L. A., Smith, T. J., Henderson, I., and Meagher, M. M. (2010) Purification of a Recombinant Heavy Chain Fragment C Vaccine Candidate against Botulinum Serotype C Neurotoxin [rBoNTC(H(c))] Expressed in Pichia pastoris. *Protein Expr Purif*
160. Pang, Y. P., Davis, J., Wang, S., Park, J. G., Nambiar, M. P., Schmidt, J. J., and Millard, C. B. (2010) Small molecules showing significant protection of mice against botulinum neurotoxin serotype A. *PLoS One* **5**, e10129

161. Roxas-Duncan, V., Enyedy, I., Montgomery, V. A., Eccard, V. S., Carrington, M. A., Lai, H., Gul, N., Yang, D. C., and Smith, L. A. (2009) Identification and biochemical characterization of small-molecule inhibitors of Clostridium botulinum neurotoxin serotype A. *Antimicrob Agents Chemother* **53**, 3478-3486
162. Hermone, A. R., Burnett, J. C., Nuss, J. E., Tressler, L. E., Nguyen, T. L., Solaja, B. A., Vennerstrom, J. L., Schmidt, J. J., Wipf, P., Bavari, S., and Gussio, R. (2008) Three-dimensional database mining identifies a unique chemotype that unites structurally diverse botulinum neurotoxin serotype A inhibitors in a three-zone pharmacophore. *ChemMedChem* **3**, 1905-1912
163. Tang, J., Park, J. G., Millard, C. B., Schmidt, J. J., and Pang, Y. P. (2007) Computer-aided lead optimization: improved small-molecule inhibitor of the zinc endopeptidase of botulinum neurotoxin serotype A. *PLoS One* **2**, e761
164. Lai, H., Feng, M., Roxas-Duncan, V., Dakshanamurthy, S., Smith, L. A., and Yang, D. C. (2009) Quinolinol and peptide inhibitors of zinc protease in botulinum neurotoxin A: effects of zinc ion and peptides on inhibition. *Arch Biochem Biophys* **491**, 75-84
165. Silhar, P., Capkova, K., Salzameda, N. T., Barbieri, J. T., Hixon, M. S., and Janda, K. D. (2010) Botulinum neurotoxin A protease: discovery of natural product exosite inhibitors. *J Am Chem Soc* **132**, 2868-2869
166. Zuniga, J. E., Hammill, J. T., Drory, O., Nuss, J. E., Burnett, J. C., Gussio, R., Wipf, P., Bavari, S., and Brunger, A. T. (2010) Iterative structure-based peptide-like inhibitor design against the botulinum neurotoxin serotype A. *PLoS ONE* **5**, e11378
167. Kumaran, D., Rawat, R., Ludivico, M. L., Ahmed, S. A., and Swaminathan, S. (2008) Structure- and substrate-based inhibitor design for Clostridium botulinum neurotoxin serotype A. *The Journal of biological chemistry* **283**, 18883-18891
168. Burnett, J. C., Ruthel, G., Stegmann, C. M., Panchal, R. G., Nguyen, T. L., Hermone, A. R., Stafford, R. G., Lane, D. J., Kenny, T. A., McGrath, C. F., Wipf, P., Stahl, A. M., Schmidt, J. J., Gussio, R., Brunger, A. T., and Bavari, S. (2007) Inhibition of metalloprotease botulinum serotype A from a pseudo-peptide binding mode to a small molecule that is active in primary neurons. *The Journal of biological chemistry* **282**, 5004-5014
169. Schmidt, J. J., Stafford, R. G., and Bostian, K. A. (1998) Type A botulinum neurotoxin proteolytic activity: development of competitive inhibitors and implications for substrate specificity at the S1' binding subsite. *FEBS letters* **435**, 61-64
170. Zuniga, J. E., Schmidt, J. J., Fenn, T., Burnett, J. C., Arac, D., Gussio, R., Stafford, R. G., Badie, S. S., Bavari, S., and Brunger, A. T. (2008) A potent peptidomimetic inhibitor of botulinum neurotoxin serotype A has a very different conformation than SNAP-25 substrate. *Structure* **16**, 1588-1597
171. Ahmed, S. A., Olson, M. A., Ludivico, M. L., Gilsdorf, J., and Smith, L. A. (2008) Identification of residues surrounding the active site of type A botulinum neurotoxin important for substrate recognition and catalytic activity. *Protein J* **27**, 151-162
172. Arnon, S. S. (2001) Botulinum toxin as a biological weapon: Medical and public health management (vol 285, pg 1059, 2001). *Jama-Journal of the American Medical Association* **285**, 2081-2081
173. Ohishi, I., and Sakaguchi, G. (1980) ORAL TOXICITIES OF CLOSTRIDIUM-BOTULINUM TYPE-C AND TYPE-D TOXINS OF DIFFERENT MOLECULAR SIZES. *Infection and Immunity* **28**, 303-309
174. Sharma, S. K., Ferreira, J. L., Eblen, B. S., and Whiting, R. C. (2006) Detection of type A, B, E, and F Clostridium botulinum neurotoxins in foods by using an amplified enzyme-linked immunosorbent assay with digoxigenin-labeled antibodies. *Applied and Environmental Microbiology* **72**, 1231-1238
175. Kautter, D. A., and Solomon, H. M. (1977) COLLABORATIVE STUDY OF A METHOD FOR DETECTION OF CLOSTRIDIUM-BOTULINUM AND ITS TOXINS IN FOODS. *Journal of the Association of Official Analytical Chemists* **60**, 541-545

176. Fach, P., Hauser, D., Guillou, J. P., and Popoff, M. R. (1993) POLYMERASE CHAIN-REACTION FOR THE RAPID IDENTIFICATION OF CLOSTRIDIUM-BOTULINUM TYPE-A STRAINS AND DETECTION IN FOOD SAMPLES. *Journal of Applied Bacteriology* **75**, 234-239
177. Saiki, R. K., Gelfand, D. H., Stoffel, S., Scharf, S. J., Higuchi, R., Horn, G. T., Mullis, K. B., and Erlich, H. A. (1988) PRIMER-DIRECTED ENZYMATIC AMPLIFICATION OF DNA WITH A THERMOSTABLE DNA-POLYMERASE. *Science* **239**, 487-491
178. Kirchner, S., Kraemer, K. M., Schulze, M., Pauly, D., Jacob, D., Gessler, F., Nitsche, A., Dorner, B. G., and Dorner, M. B. (2010) Pentaplexed Quantitative Real-Time PCR Assay for the Simultaneous Detection and Quantification of Botulinum Neurotoxin-Producing Clostridia in Food and Clinical Samples. *Applied and Environmental Microbiology* **76**, 4387-4395
179. Fach, P., Micheau, P., Mazuet, C., Perelle, S., and Popoff, M. (2009) Development of real-time PCR tests for detecting botulinum neurotoxins A, B, E, F producing *Clostridium botulinum*, *Clostridium baratii* and *Clostridium butyricum*. *Journal of Applied Microbiology* **107**, 465-473
180. van Baar, B. L. M., Hulst, A. G., de Jong, A. L., and Wils, E. R. J. (2002) Characterisation of botulinum toxins type A and B, by matrix-assisted laser desorption ionisation and electrospray mass spectrometry. *Journal of Chromatography A* **970**, 95-115
181. van Baar, B. L. M., Hulst, A. G., de Jong, A. L., and Wils, E. R. J. (2004) Characterisation of botulinum toxins type C, D, E, and F by matrix-assisted laser desorption ionisation and electrospray mass spectrometry. *Journal of Chromatography A* **1035**, 97-114
182. Kalb, S. R., Moura, H., Boyer, A. E., McWilliams, L. G., Pirkle, J. L., and Barr, J. R. (2006) The use of Endopep-MS for the detection of botulinum toxins A, B, E, and F in serum and stool samples. *Analytical Biochemistry* **351**, 84-92
183. Kalb, S. R., Smith, T. J., Moura, H., Hill, K., Lou, J., Geren, I. N., Garcia-Rodriguez, C., Marks, J. D., Smith, L. A., Pirkle, J. L., and Barr, J. R. (2008) The use of Endopep-MS to detect multiple subtypes of botulinum neurotoxins A, B, E, and F. *International Journal of Mass Spectrometry* **278**, 101-108
184. Barr, J. R., Kalb, S. R., and Pirkle, J. L. (2011) Detection, Differentiation and Subtyping of Botulinum Neurotoxins in Clinical Samples with Mass Spectrometry. *Rapid Characterization of Microorganisms by Mass Spectrometry* **1065**, 83-97
185. Kalb, S. R., Baudys, J., Rees, J. C., Smith, T. J., Smith, L. A., Helma, C. H., Hill, K., Kull, S., Kirchner, S., Dorner, M. B., Dorner, B. G., Pirkle, J. L., and Barr, J. R. (2012) De novo subtype and strain identification of botulinum neurotoxin type B through toxin proteomics. *Analytical and Bioanalytical Chemistry* **403**, 215-226
186. Kohler, G., and Milstein, C. (2005) Continuous cultures of fused cells secreting antibody of predefined specificity (Reprinted from Nature, vol 256, 1975). *Journal of Immunology* **174**, 2453-2455
187. Ferreira, J. L., Maslanka, S., Johnson, E., and Goodnough, M. (2003) Detection of botulinum neurotoxins A, B, E, and F by amplified enzyme-linked immunosorbent assay: Collaborative study. *Journal of Aoac International* **86**, 314-331
188. Kozaki, S., Dufrenne, J., Hagenaaars, A. M., and Notermans, S. (1979) ENZYME LINKED IMMUNOSORBENT ASSAY (ELISA) FOR DETECTION OF CLOSTRIDIUM-BOTULINUM TYPE-B TOXIN. *Japanese Journal of Medical Science & Biology* **32**, 199-205
189. Notermans, S., Dufrenne, J., and Kozaki, S. (1979) ENZYME-LINKED IMMUNOSORBENT ASSAY FOR DETECTION OF CLOSTRIDIUM-BOTULINUM TYPE-E TOXIN. *Applied and Environmental Microbiology* **37**, 1173-1175
190. Schiavo, G., Rossetto, O., Catsicas, S., Delaureto, P. P., Dasgupta, B. R., Benfenati, F., and Montecucco, C. (1993) IDENTIFICATION OF THE NERVE-TERMINAL TARGETS OF BOTULINUM

- NEUROTOXIN SEROTYPE-A, SEROTYPE-D, AND SEROTYPE-E. *Journal of Biological Chemistry* **268**, 23784-23787
191. Anne, C., Cornille, F., Lenoir, C., and Roques, B. P. (2001) High-throughput fluorogenic assay for determination of botulinum type B neurotoxin protease activity. *Analytical Biochemistry* **291**, 253-261
  192. Ruge, D. R., Dunning, F. M., Piazza, T. M., Molles, B. E., Adler, M., Zeytin, F. N., and Tucker, W. C. (2011) Detection of six serotypes of botulinum neurotoxin using fluorogenic reporters. *Analytical Biochemistry* **411**, 200-209
  193. Guo, J., Xu, C., Li, X., and Chen, S. (2014) A simple, rapid and sensitive FRET assay for botulinum neurotoxin serotype B detection. *PLoS One* **9**, e114124
  194. Klein, A. W. (2004) The therapeutic potential of botulinum toxin. *Dermatol Surg* **30**, 452-455
  195. Davletov, B., Bajohrs, M., and Binz, T. (2005) Beyond BOTOX: advantages and limitations of individual botulinum neurotoxins. *Trends in Neurosciences* **28**, 446-452
  196. Chen, S. (2012) Clinical Uses of Botulinum Neurotoxins: Current Indications, Limitations and Future Developments. *Toxins* **4**, 913-939
  197. Glogau, R. G. (2002) Review of the use of botulinum toxin for hyperhidrosis and cosmetic purposes. *Clin J Pain* **18**, S191-197
  198. Bertolasi, L., Frasson, E., Cappelletti, J. Y., Vicentini, S., Bordinon, M., and Graziottin, A. (2009) Botulinum neurotoxin type A injections for vaginismus secondary to vulvar vestibulitis syndrome. *Obstet Gynecol* **114**, 1008-1016
  199. Fageeh, W. M. K. (2011) Different Treatment Modalities for Refractory Vaginismus in Western Saudi Arabia. *J Sex Med* **8**, 1735-1739
  200. Patti, R., Almasio, P. L., Muggeo, V. M., Buscemi, S., Arcara, M., Matranga, S., and Di Vita, G. (2005) Improvement of wound healing after hemorrhoidectomy: a double-blind, randomized study of botulinum toxin injection. *Dis Colon Rectum* **48**, 2173-2179
  201. Brashear, A. (2001) Botulinum toxin type B: a new injectable treatment for cervical dystonia. *Expert Opin Investig Drugs* **10**, 2191-2199
  202. (2001) Neurotoxins licensed as treatment for neck neuromuscular disorder. *Am J Health Syst Pharm* **58**, 200, 202
  203. Figgitt, D. P., and Noble, S. (2002) Botulinum toxin B: a review of its therapeutic potential in the management of cervical dystonia. *Drugs* **62**, 705-722
  204. Chen, S. (2012) Clinical uses of botulinum neurotoxins: current indications, limitations and future developments. *Toxins (Basel)* **4**, 913-939
  205. Montecucco, C., and Schiavo, G. (1994) Mechanism of action of tetanus and botulinum neurotoxins. *Mol Microbiol* **13**, 1-8
  206. Davletov, B., Bajohrs, M., and Binz, T. (2005) Beyond BOTOX: advantages and limitations of individual botulinum neurotoxins. *Trends Neurosci* **28**, 446-452
  207. Montecucco, C., and Schiavo, G. (1993) Tetanus and botulism neurotoxins: a new group of zinc proteases. *Trends Biochem Sci* **18**, 324-327
  208. Brunger, A. T. (2005) Structure and function of SNARE and SNARE-interacting proteins. *Q Rev Biophys* **38**, 1-47
  209. Schiavo, G., Malizio, C., Trimble, W. S., Polverino de Laureto, P., Milan, G., Sugiyama, H., Johnson, E. A., and Montecucco, C. (1994) Botulinum G neurotoxin cleaves VAMP/syntaxin at a single Ala-Ala peptide bond. *The Journal of biological chemistry* **269**, 20213-20216

210. Schiavo, G., Rossetto, O., Benfenati, F., Poulain, B., and Montecucco, C. (1994) Tetanus and botulinum neurotoxins are zinc proteases specific for components of the neuroexocytosis apparatus. *Ann N Y Acad Sci* **710**, 65-75
211. Benedetto, A. V. (2004) Commentary: Botulinum toxin in clinical medicine: part II. *Clin Dermatol* **22**, 1-2
212. Ascher, B., and Rossi, B. (2004) [Botulinum toxin and wrinkles: few side effects and effective combining procedures with other treatments]. *Ann Chir Plast Esthet* **49**, 537-552
213. Cheng, C. M., Chen, J. S., and Patel, R. P. (2006) Unlabeled uses of botulinum toxins: a review, part 2. *Am J Health Syst Pharm* **63**, 225-232
214. Abrams, S. B., and Hallett, M. (2013) Clinical utility of different botulinum neurotoxin preparations. *Toxicon* **67**, 81-86
215. Naumann, M., Dressler, D., Hallett, M., Jankovic, J., Schiavo, G., Segal, K. R., and Truong, D. (2013) Evidence-based review and assessment of botulinum neurotoxin for the treatment of secretory disorders. *Toxicon* **67**, 141-152
216. Hallett, M., Albanese, A., Dressler, D., Segal, K. R., Simpson, D. M., Truong, D., and Jankovic, J. (2013) Evidence-based review and assessment of botulinum neurotoxin for the treatment of movement disorders. *Toxicon* **67**, 94-114
217. Esquenazi, A., Albanese, A., Chancellor, M. B., Elovic, E., Segal, K. R., Simpson, D. M., Smith, C. P., and Ward, A. B. (2013) Evidence-based review and assessment of botulinum neurotoxin for the treatment of adult spasticity in the upper motor neuron syndrome. *Toxicon* **67**, 115-128
218. Chancellor, M. B., Elovic, E., Esquenazi, A., Naumann, M., Segal, K. R., Schiavo, G., Smith, C. P., and Ward, A. B. (2013) Evidence-based review and assessment of botulinum neurotoxin for the treatment of urologic conditions. *Toxicon* **67**, 129-140
219. Goschel, H., Wohlfarth, K., Frevert, J., Dengler, R., and Bigalke, H. (1997) Botulinum A toxin therapy: neutralizing and nonneutralizing antibodies--therapeutic consequences. *Exp Neurol* **147**, 96-102
220. Atassi, M. Z. (2004) Basic immunological aspects of botulinum toxin therapy. *Movement disorders : official journal of the Movement Disorder Society* **19 Suppl 8**, S68-84
221. Jankovic, J. (2006) Botulinum toxin therapy for cervical dystonia. *Neurotox Res* **9**, 145-148
222. Brashear, A., Lew, M. F., Dykstra, D. D., Comella, C. L., Factor, S. A., Rodnitzky, R. L., Trosch, R., Singer, C., Brin, M. F., Murray, J. J., Wallace, J. D., Willmer-Hulme, A., and Koller, M. (1999) Safety and efficacy of NeuroBloc (botulinum toxin type B) in type A-responsive cervical dystonia. *Neurology* **53**, 1439-1446
223. Swope, D., and Barbano, R. (2008) Treatment recommendations and practical applications of botulinum toxin treatment of cervical dystonia. *Neurol Clin* **26 Suppl 1**, 54-65
224. Comella, C. L. (2008) The treatment of cervical dystonia with botulinum toxins. *J Neural Transm* **115**, 579-583
225. Dasgupta, B. R., and Sugiyama, H. (1972) Isolation and characterization of a protease from Clostridium botulinum type B. *Biochimica et biophysica acta* **268**, 719-729
226. Powell, H. R. (1999) The Rossmann Fourier autoindexing algorithm in MOSFLM. *Acta Crystallogr D Biol Crystallogr* **55**, 1690-1695
227. (2008) Molecular replacement. Proceedings of the CCP4 study weekend, University of Reading, United Kingdom. *Acta Crystallogr D Biol Crystallogr* **64**, 1-140
228. Potterton, E., Briggs, P., Turkenburg, M., and Dodson, E. (2003) A graphical user interface to the CCP4 program suite. *Acta Crystallogr D Biol Crystallogr* **59**, 1131-1137

229. Emsley, P., and Cowtan, K. (2004) Coot: model-building tools for molecular graphics. *Acta Crystallogr D Biol Crystallogr* **60**, 2126-2132
230. Dolimbek, B. Z., Aoki, K. R., Steward, L. E., Jankovic, J., and Atassi, M. Z. (2007) Mapping of the regions on the heavy chain of botulinum neurotoxin A (BoNT/A) recognized by antibodies of cervical dystonia patients with immunoresistance to BoNT/A. *Mol Immunol* **44**, 1029-1041
231. Atassi, M. Z., Dolimbek, B. Z., Jankovic, J., Steward, L. E., and Aoki, K. R. (2008) Molecular recognition of botulinum neurotoxin B heavy chain by human antibodies from cervical dystonia patients that develop immunoresistance to toxin treatment. *Mol Immunol* **45**, 3878-3888
232. Atassi, M. Z., Jankovic, J., Steward, L. E., Aoki, K. R., and Dolimbek, B. Z. (2012) Molecular immune recognition of botulinum neurotoxin B. The light chain regions that bind human blocking antibodies from toxin-treated cervical dystonia patients. Antigenic structure of the entire BoNT/B molecule. *Immunobiology* **217**, 17-27
233. Dolimbek, B. Z., Aoki, K. R., and Atassi, M. Z. (2011) Reduction of antibody response against botulinum neurotoxin A by synthetic monomethoxypolyethylene glycol-peptide conjugates. *Immunol Lett* **137**, 46-52
234. Foster, K. A. (2009) Engineered toxins: new therapeutics. *Toxicon* **54**, 587-592
235. Chen, S., and Barbieri, J. T. (2011) Association of botulinum neurotoxin serotype A light chain with plasma membrane-bound SNAP-25. *The Journal of biological chemistry* **286**, 15067-15072
236. Hill, K. K., Smith, T. J., Helma, C. H., Ticknor, L. O., Foley, B. T., Svensson, R. T., Brown, J. L., Johnson, E. A., Smith, L. A., Okinaka, R. T., Jackson, P. J., and Marks, J. D. (2007) Genetic diversity among botulinum neurotoxin-producing clostridial strains. *Journal of Bacteriology* **189**, 818-832
237. Montecucco, C., and Schiavo, G. (1994) MECHANISM OF ACTION OF TETANUS AND BOTULINUM NEUROTOXINS. *Molecular Microbiology* **13**, 1-8
238. Schiavo, G., Rossetto, O., Benfenati, F., Poulain, B., and Montecucco, C. (1994) TETANUS AND BOTULINUM NEUROTOXINS ARE ZINC PROTEASES SPECIFIC FOR COMPONENTS OF THE NEUROEXOCYTOSIS APPARATUS. *Toxins and Exocytosis* **710**, 65-75
239. Maksymowych, A. B., and Simpson, L. L. (1998) Binding and transcytosis of botulinum neurotoxin by polarized human colon carcinoma cells. *Journal of Biological Chemistry* **273**, 21950-21957
240. Maksymowych, A. B., and Simpson, L. L. (2004) Structural features of the botulinum neurotoxin molecule that govern binding and transcytosis across polarized human intestinal epithelial cells. *Journal of Pharmacology and Experimental Therapeutics* **310**, 633-641
241. Fujinaga, Y. (2010) Interaction of Botulinum Toxin with the Epithelial Barrier. *Journal of Biomedicine and Biotechnology*
242. Brunger, A. T. (2005) Structure and function of SNARE and SNARE-interacting proteins. *Quarterly Reviews of Biophysics* **38**, 1-47
243. Chen, S., Hall, C., and Barbieri, J. T. (2008) Substrate recognition of VAMP-2 by botulinum neurotoxin B and tetanus neurotoxin. *Journal of Biological Chemistry* **283**, 21153-21159
244. Chen, S., Kim, J.-J. P., and Barbieri, J. T. (2007) Mechanism of substrate recognition by botulinum neurotoxin serotype A. *Journal of Biological Chemistry* **282**, 9621-9627
245. Chen, S., and Barbieri, J. T. (2007) Multiple pocket recognition of SNAP25 by botulinum neurotoxin serotype E. *Journal of Biological Chemistry* **282**, 25540-25547
246. Chen, S., and Wan, H. Y. (2011) Molecular mechanisms of substrate recognition and specificity of botulinum neurotoxin serotype F. *Biochemical Journal* **433**, 277-284

247. Wang, G. T., Matayoshi, E., Huffaker, H. J., and Krafft, G. A. (1990) DESIGN AND SYNTHESIS OF NEW FLUOROGENIC HIV PROTEASE SUBSTRATES BASED ON RESONANCE ENERGY-TRANSFER. *Tetrahedron Letters* **31**, 6493-6496
248. Scotcher, M. C., Cheng, L. W., and Stanker, L. H. (2010) Detection of Botulinum Neurotoxin Serotype B at Sub Mouse LD50 Levels by a Sandwich Immunoassay and Its Application to Toxin Detection in Milk. *Plos One* **5**
249. Dunning, F. M., Ruge, D. R., Piazza, T. M., Stanker, L. H., Zeytin, F. N., and Tucker, W. C. (2012) Detection of Botulinum Neurotoxin Serotype A, B, and F Proteolytic Activity in Complex Matrices with Picomolar to Femtomolar Sensitivity. *Applied and Environmental Microbiology* **78**, 7687-7697
250. Wictome, M., Newton, K., Jameson, K., Hallis, B., Dunnigan, P., Mackay, E., Clarke, S., Taylor, R., Gaze, J., Foster, K., and Shone, C. (1999) Development of an in vitro bioassay for Clostridium botulinum type B neurotoxin in foods that is more sensitive than the mouse bioassay. *Applied and Environmental Microbiology* **65**, 3787-3792
251. Liu, W., Montana, V., Chapman, E. R., Mohideen, U., and Parpura, V. (2003) Botulinum toxin type B micromechanosensor. *Proceedings of the National Academy of Sciences of the United States of America* **100**, 13621-13625
252. Salzameda, N. T., Barbieri, J. T., and Janda, K. D. (2009) Synthetic substrate for application in both high and low throughput assays for botulinum neurotoxin B protease inhibitors. *Bioorganic & Medicinal Chemistry Letters* **19**, 5848-5850
253. Boldt, G. E., Kennedy, J. P., Hixon, M. S., McAllister, L. A., Barbieri, J. T., Tzipori, S., and Janda, K. D. (2006) Synthesis, characterization and development of a high-throughput methodology for the discovery of botulinum neurotoxin A inhibitors. *Journal of Combinatorial Chemistry* **8**, 513-521
254. Joshi, S. G. (2012) Detection of biologically active botulinum neurotoxin-A in serum using high-throughput FRET-assay. *Journal of Pharmacological and Toxicological Methods* **65**, 8-12
255. Feltrup, T. M., and Singh, B. R. (2012) Development of a Fluorescence Internal Quenching Correction Factor to Correct Botulinum Neurotoxin Type A Endopeptidase Kinetics Using SNAPtide. *Analytical Chemistry* **84**, 10549-10553
256. Jankovic, J., and Brin, M. F. (1991) Therapeutic uses of botulinum toxin. *The New England journal of medicine* **324**, 1186-1194
257. Bossi, P., and Bricaire, F. (2003) [Botulism toxin, bioterrorist weapon]. *Presse Med* **32**, 463-465
258. Arnon, S. S., Schechter, R., Inglesby, T. V., Henderson, D. A., Bartlett, J. G., Ascher, M. S., Eitzen, E., Fine, A. D., Hauer, J., Layton, M., Lillibridge, S., Osterholm, M. T., O'Toole, T., Parker, G., Perl, T. M., Russell, P. K., Swerdlow, D. L., and Tonat, K. (2001) Botulinum toxin as a biological weapon: medical and public health management. *Jama* **285**, 1059-1070
259. Pearce, L. B., First, E. R., MacCallum, R. D., and Gupta, A. (1997) Pharmacologic characterization of botulinum toxin for basic science and medicine. *Toxicon* **35**, 1373-1412
260. Smith, T. J., Hill, K. K., Xie, G., Foley, B. T., Williamson, C. H., Foster, J. T., Johnson, S. L., Chertkov, O., Teshima, H., Gibbons, H. S., Johnsky, L. A., Karavis, M. A., and Smith, L. A. (2014) Genomic sequences of six botulinum neurotoxin-producing strains representing three clostridial species illustrate the mobility and diversity of botulinum neurotoxin genes. *Infect Genet Evol* **30C**, 102-113
261. Blasi, J., Chapman, E. R., Link, E., Binz, T., Yamasaki, S., De Camilli, P., Sudhof, T. C., Niemann, H., and Jahn, R. (1993) Botulinum neurotoxin A selectively cleaves the synaptic protein SNAP-25. *Nature* **365**, 160-163
262. Guo, J., and Chen, S. (2013) Unique Substrate Recognition Mechanism of the Botulinum Neurotoxin D Light Chain. *Journal of Biological Chemistry* **288**, 27881-27887

263. Kalb, S. R., Baudys, J., Egan, C., Smith, T. J., Smith, L. A., Pirkle, J. L., and Barr, J. R. (2011) Different substrate recognition requirements for cleavage of synaptobrevin-2 by *Clostridium baratii* and *Clostridium botulinum* type F neurotoxins. *Appl Environ Microbiol* **77**, 1301-1308
264. Yang, J. T., Wu, C. S., and Martinez, H. M. (1986) Calculation of protein conformation from circular dichroism. *Methods Enzymol* **130**, 208-269
265. Wang, D., Krilich, J., Pellett, S., Baudys, J., Tepp, W. H., Barr, J. R., Johnson, E. A., and Kalb, S. R. (2013) Comparison of the catalytic properties of the botulinum neurotoxin subtypes A1 and A5. *Biochimica et biophysica acta* **1834**, 2722-2728
266. Kalb, S. R., Baudys, J., Raphael, B. H., Dykes, J. K., Luquez, C., Maslanka, S. E., and Barr, J. R. (2015) Functional Characterization of Botulinum Neurotoxin Serotype H as a Hybrid of Known Serotypes F and A (BoNT F/A). *Anal Chem*
267. Guo, J., and Chen, S. (2015) Expression and biochemical characterization of light chains of Botulinum neurotoxin subtypes F5 and F7. *Protein Expr Purif* **111**, 87-90
268. Barash, J. R., and Arnon, S. S. (2013) A Novel Strain of *Clostridium botulinum* That Produces Type B and Type H Botulinum Toxins. *Journal of Infectious Diseases*
269. Atassi, M. Z., and Oshima, M. (1999) Structure, activity, and immune (T and B cell) recognition of botulinum neurotoxins. *Crit Rev Immunol* **19**, 219-260
270. Bell, K. R., and Williams, F. (2003) Use of botulinum toxin type A and type B for spasticity in upper and lower limbs. *Phys Med Rehabil Clin N Am* **14**, 821-835
271. Mahajan, S. T., and Brubaker, L. (2007) Botulinum toxin: from life-threatening disease to novel medical therapy. *Am J Obstet Gynecol* **196**, 7-15
272. Mahant, N., Clouston, P. D., and Lorentz, I. T. (2000) The current use of botulinum toxin. *J Clin Neurosci* **7**, 389-394
273. Thant, Z. S., and Tan, E. K. (2003) Emerging therapeutic applications of botulinum toxin. *Med Sci Monit* **9**, RA40-48
274. Kumar, G., Kumaran, D., Ahmed, S. A., and Swaminathan, S. (2012) Peptide inhibitors of botulinum neurotoxin serotype A: design, inhibition, cocrystal structures, structure-activity relationship and pharmacophore modeling. *Acta Crystallographica Section D-Biological Crystallography* **68**, 511-520
275. Singh, P., Singh, M. K., Chaudhary, D., Chauhan, V., Bharadwaj, P., Pandey, A., Upadhyay, N., and Dhaked, R. K. (2012) Small-Molecule Quinololinol Inhibitor Identified Provides Protection against BoNT/A in Mice. *Plos One* **7**